AIAA ELECTRIC PROPULSION CONFERENCE
BROADMOOR HOTEL, COLORADO SPRINGS, COLO. MARCH 11-13, 1963

(II, a)

SURFACE IONIZATION OF CESIUM WITH POROUS TUNGSTEN IONIZERS

by
R. G. Wilson
G. D. Seele
J. F. Hon
Rocketdyne,
A Division of North American Aviation, Inc.
Canoga Park, California
63017

DISCLAIMER

THIS PAGE

WAS INTENTIONALLY

LEFT BLANK

ABSTRACT

The surface ionization properties of porous tungsten ionizers which have been sintered from powders with diameters of 0.1, 0.9, 5, 8, 12 to 18, and 44 to 74 microns and with densities from 60 to 80 percent have been determined experimentally with a neutral atom and ion detector for through-fed cesium.

CONTENTS

1. INTRODUCTION

The phenomenon of surface ionization is being used for the generation of ions in one of the several types of electrostatic thrustors under development. The over-all power efficiency, propellant utilization efficiency, and thrustor lifetime are dependent upon the fundamentals of surface ionization. Most thrustors utilizing surface ionization are of the through-fed type employing porous tungsten for the ionizer. It is desirable to use porous tungsten ionizers which have properties that optimize the current-producing and propellant-utilization characteristics. The relationships between porous tungsten properties and current-producing characteristics and propellant utilization have been under investigation since the onset of experimental work in electrical propulsion. However, the relationships are not yet resolved to the point that permits ionizer design optimization.

This paper presents the results of experiments performed for the cesium-tungsten system with ionizers having different porous properties. While the work reported here does not determine unequivocably all of the characteristics of this system, it does show directions and dependencies of current production and propellant utilization as functions of the properties of porous tungsten ionizers and of operating conditions.

THIS PAGE

WAS INTENTIONALLY

LEFT BLANK

2. SUMMARY AND CONCLUSIONS

The surface ionization properties of porous tungsten ionizers which have been sintered from powders with diameters of 0.1, 0.9, 5, 8, 12 to 18, and 44 to 74 microns, and with densities from 60 to 80 percent have been determined experimentally with a neutral atom and ion detector for through-fed cesium. The neutral- and ion-current producing characteristics, the ionization efficiencies, and the critical temperatures for ion production were obtained as functions of ionizer temperature, the ion-accelerating electrostatic field, the cesium vapor pressure at the rear of the ionizer (as calculated from the vapor temperature), the particle fluxes from the ionizing surface (neutral, ion, and total), and the basic tungsten powder diameter. The values of the variables in the ranges studied are: ionizing surface temperature, 900 to 1600 K; cesium vapor temperature, 360 to 600 K; and corresponding cesium vapor pressure at the rear of the ionizer, 4×10^{-4} to 3 mm Hg; ion-accelerating electrostatic field (nominal), 0 to 3.6×10^{3} v/cm; particle fluxes (current densities), 0 to 3×10^{16} particles/sq cm-sec (0 to 5 ma/sq cm); and ionizer powder diameters and porosities, as above. The background pressure was maintained in the 10^{-6} mm Hg range, with data obtained occasionally in the high 10^{-7} range.

The experimental apparatus used separates and measures independently the ion and neutral currents. Grid electron suppression and liquid-nitrogen cooling are employed. The neutral atom current is measured by ionization with a hot tungsten filament inside an isolated chamber. A neutral-beam interrupter is employed to provide background filament current readings for all neutral-current measurements. A process believed to be cesium gettering was used to clean the ionizing surfaces before data were taken. All data were obtained by the decreasing accelerating field technique described herein.

To make correlations between the surface ionization properties of these ionizers and their porous structure parameters, the results of gas-flow

measurements with these same ionizers, and of metallographic studies of identically fabricated compacts, are presented. The porous structure parameters reported are the basic powder diameter, the density (porosity), the mean pore diameter, the mean grain diameter, the mean interpore spacing, the viscous flow permeability, the specific surface, and the specific periphery (defined herein). The effects of the original powder size and porosity on parameters important for application to the electrical propulsion program are discussed, and it is shown that the trends are not always compatible. It is pointed out that improvements in the sintering fabrication techniques will be required for powder diameters less than a few microns if long-term operation at optimum conditions is to be attained.

The theory and equations for patchy surface ionization are summarized. The differences between the application of the equations to filament ionizers and to porous ionizers are outlined. Simplifications of the theory and equations for the special case of the cesium-tungsten system in the region of the normal and anomalous Schottky effects are discussed. The experimentally observed influence of the applied electric field, E, on the current density is illustrated and discussed. The mode most commonly observed was that in which a decrease in current density with E is followed by an increase. The conclusion is drawn that the influence of the normal Schottky effect is being observed at high values of applied voltage when the ion current increases with E, and that the anomalous Schottky effect may be causing the decrease in the ion current at values of E in the weak field region. The minimum in the ion current (vs E) occurs at successively higher values of the electric field as the magnitude of the emission-limited ion current is increased.

The apparent perveance increases with the ion current density. Differences are noted depending upon whether the cesium vapor pressure or the ionizer temperature is used to increase the ion current density. Experimental perveances at comparable conditions of cesium vapor pressure and ionizer temperature are tabulated. Results reported here show that the perveance increases with decreasing powder size.

The 0.1-micron ionizer showed little porous structure and developed numerous well-defined cracks under even mild heat treatment, and therefore could not be used for surface ionization measurements. For the ionizer of 0.9-micron powder diameter, the ionization efficiency increased uniformly, while the current-producing capabilities decreased severely with accrued operating time, particularly at high ionizer temperatures (1400 to 1600 K).

The various modes for the passage of gases through porous media are considered. The validity of the basic assumptions underlying their applications to the case of alkali metals and refractory porous metal ionizers for surface ionization systems are examined, and comparable equations governing the flow of the cesium through the porous ionizers are displayed for the various modes. Consideration of the basic assumptions for these equations and the dependence upon vapor pressure, ionizer temperature, and porous structure, compared with the experimental results, indicate that the cesium transport occurs primarily as simple (monolayer or less) surface diffusion or migration, with the possibility of some free molecular flow, particularly at the higher flowrates. It is also indicated that viscous flow, turbulent flow, multilayer adsorptive flow, and flow by capillary condensation are, at most, secondary modes of transport. This conclusion is consistent with the ionization efficiencies that are observed for these ionizers.

The dependences of the four variables which influence the flow of cesium through the porous tungsten ionizers (the cesium vapor pressure at the rear ionizer surface, the ionizer temperature, the porous ionizer permeability, and the electric field at the front surface of the ionizer and the resulting rate of ion formation and extraction) are illustrated and discussed. For all of the ionizers studied, a linear relationship is exhibited between the neutral flux and the cesium vapor pressure when the latter is the only variable influencing the flow. The ion flux, n_+ or J_+, is also observed to increase with the vapor pressure, though not necessarily linearly. An interesting relationship between the ratio of total particle flux for emission-limited (EL) ion production to the

total particle flux for E = 0 (no ion emission) and the ionizer powder size, and therefore the influence of E on the cesium flowrate, is observed. This ratio decreases consistently with increasing powder size, having a value of unity at about 15 microns and being less than unity for larger powder sizes. The ratio n_+ (EL)/n_0 (E = 0) is as high as 2.5.

Data which show how the neutral and ion fluxes, n_0 and J_+, increase with the ionizer temperature, T, are presented. When ln J_+ vs 1/T is plotted, fairly straight lines are observed for all ionizers with rather constant slopes which result in an average exponential coefficient of ~0.68 eV/atom. Several possible significances for this observation are discussed.

Data showing the dependence of the ionization efficiency upon the extracted cesium ion flux or current density produced by the variation of both the cesium vapor pressure and the ionizer temperature for the porous tungsten ionizers of various initial powder sizes are presented. These data are compared to the results reported by other workers for porous tungsten ionizers. The results of this work support the conclusion that the ionization efficiency decreases with increasing J_+ at constant T, with some exceptions. The data are consistent in leading to two new conclusions. In every case where J_+ was increased by increasing T at constant vapor pressure, the ionization efficiency was observed to increase with increasing J_+. The second observation is that the ionization efficiency decreases with J_+ more rapidly as the ionizer powder size increases. The details and explanations of the dependences are discussed.

Two critical temperatures are distinguished: the lower critical temperature, defined as the ionizer temperature at which ion formation first occurs, and the upper critical temperature, defined as the temperature at which the emission-limited ion current is first drawn. The concepts of critical temperature, T_C, for both filament and porous ionizers are discussed and compared. The most reliable data obtained in this work for the variation of T_C with J_+, together with most of the other published data for porous tungsten ionizers and cesium, are plotted on a common graph. For the data

of this work, the range of J_+ is extended to lower values. The lower critical temperatures fall within the range of 1123±5 K. The values of the upper critical temperature for the higher J_+ fall among the data reported by other workers. It was observed in this work, that if T_C was obtained from simple plots of J_+ vs T at some arbitrary value of applied voltage (electric field) the points for T_C vs J_+ fell with a great deal of scatter, much as do the points reported by all investigators. A technique was discovered and is discussed for which the points fell more nearly on a smooth curve and fairly close to the empirical curve for filament ionizers, although still toward higher values of T. Several possible reasons for the scatter of the data from all sources are considered. The rate of increase of the difference between the lower and upper critical temperatures with J_+ was observed to fit a straight line on a log-log plot. An extrapolation of these data to J_+ values one decade higher allowed the empirical curve of T_C vs J_+ for porous ionizers to be extended to 10 ma/sq cm. It was observed that the maximum ionization efficiency occurs at temperatures above T_C.

The theory for porous ionizers predicts that little or no critical temperature hysteresis effect should exist for porous ionizers, and that the single critical temperature which does occur, should be the critical temperature obtained for a decrease of ionizer temperature in the case of filament ionizers. An experiment was performed with the 5-micron porous tungsten ionizer to measure experimentally the upper limit for this effect for porous tungsten ionizers (for cesium). The technique used was the standard one employed throughout this work to obtain emission-limited ion current densities as a function of ionizer temperature. The results of this experiment, which show that the magnitude of the critical temperature hysteresis is ≤ 5 K, are presented in detail.

The largest-powder-size ionizer studied (44 to 74 microns) yielded some characteristics which were different from the smaller-sized powders studied in this work and by other investigators, particularly at a high cesium vapor

pressure. Low ionization efficiencies and sharp drops in ion current with ionizer temperature are examples. These observations are discussed in detail.

If high values of ionization efficiency and ion current density are simultaneously desirable, and if J_+ is to be increased by increasing the vapor pressure at constant T, then this work leads to the conclusion that as small a powder size as possible (within the lower limit imposed by sintering changes) and as high an ionizer temperature as possible (within the limit imposed by power efficiency--higher T results in higher radiated power loses) are required. The observation that T_C increases with J_+ is consistent with this desirability of a high T, because T must exceed T_C, but a strong contradiction occurs when the relationship between J_+ and powder size is examined. In that case, the permeability to cesium flow decreases significantly with decreasing ionizer powder size at constant porosity, and hence high J_+ and smaller powder size are incompatible. One method for partially correcting for the inhibition of J_+ by small powder size may exist in the observation that the ionizer permeability increases with increasing porosity at constant powder size. Thus, a benefit is gained for J_+ by combining small powder size and high ionizer porosity at no apparent loss in ionization efficiency, according to the results of this work. The optimum relationship among powder size (probably between 2 and 20 microns), porosity, ionizer temperature, and vapor pressure must be found for each specific application of porous ionizers, depending upon the system limitations on the ion-current density, the ionizer temperature (from power considerations), and the ionization efficiency (from charge-exchange electrode sputtering considerations). That is, a higher ionization efficiency can be had at fixed T, although a sacrifice in J_+ may be required; or a greater ion-current density (subject to other system limitations) can be had if a sacrifice in ionization efficiency can be tolerated. In any case, high porosity ($\geq 1/3$) seems to be valuable in increasing ion current density with no sacrifice in ionization efficiency.

3. PHYSICAL AND METALLURGICAL PROPERTIES OF THE POROUS TUNGSTEN IONIZERS*

3.1 IONIZER FABRICATION

The porous tungsten ionizers used in this study are 0.030-inch thick and 0.25 inch in diameter. They were fabricated by the compaction of tungsten powders of single-sized grains for the 0.1-, 0.9-, 5-, and 8-micron ionizers and of the indicated ranges of grain sizes for the 12- to 18- and 44- to 74-micron ionizers. Compaction was followed by sintering to bulk densities of from 60 to 80 percent of the theoretical density (19.3 gm/cu cm) as listed in Table 1. Examples of sintering conditions are: 2350 C for 2 hours for the 5- and 8-micron specimens, and 1300 C for 15 minutes for the 0.9-micron ionizer.

3.2 SINTERING EXPERIMENTS

Further long-term sintering experiments with the 0.9-, 5-, and 8-micron samples (100 hours at 800 C, followed by 100 hours at 1200 C, followed by 100 hours at 1600 C) showed (Ref. 1 and 2) a decrease in ionizer porosity in all three cases, following the 1600 C test, but little or none following the 800 C and 1200 C runs for the 5- and 8-micron specimens. The data for the 0.9-micron ionizer at 1200 C were inconclusive but later flowrate measurements with cesium (section 5.5) prove that a significant decrease in permeability (and porosity) occured with operat-time in the range of 1200 to 1300 C. The 0.1-micron specimen exhibited cracks and signs of pore shrinkage even after 100 hours at 800 C, while the 1200 and 1600 C conditions showed increasing tendencies for grain

*The gas-flow and metallographic studies described in this section were performed by Dr. Peter Schwarzkopf of Materials Research, and the results reported here were communicated through his kindness.

TABLE 1

SUMMARY OF AIR-FLOW CALCULATIONS AND METALLOGRAPHIC ANALYSES OF SINTERED POROUS TUNGSTEN IONIZERS

The information presented for the sequence of 8-micron ionizers of varying density was obtained before the specimens were operated as cesium ionizers. For the varying grain-size sequence, the information was obtained after considerable use at elevated temperatures as cesium ionizers.

Unsintered Powder Diameter, microns Quoted	Percent of Theoretical Density Density Measurement	Mean Pore Diameter (d), microns		Mean Grain Diameter (D), microns		Mean Inter-Pore Spacing (S), microns		Viscous Flow Permeability (k), sq cm Air Flow	Specific Surface (S_V), sq cm/cu cm (Knudsen) Air Flow	Specific Periphery[a] (P_S), microns/sq microns $3.6\ d/S^2$
		Air Flow	Metallographic	(Poiseulle) Air Flow	Metallographic	Air Flow	Metallographic			
0.1	This ionizer exhibited numerous cracks and no definite pore structure.									
0.9	76	1.1	1.3	0.9	3.4	5.4	4.2	8.7×10^{-12}	9.6×10^{5}	0.13
5	80		2.8[c]		5.5[d]		12[d]	3×10^{-10}[d]		0.070
8	68	5.9[e]	6.0[e]				17[e]	2×10^{-9}[d]		0.062
12 to 18	68	16	9.7	13	23	27	27	2.1×10^{-8}	2.9×10^{4}	0.064
44 to 74	63	35	40	40	58	61	77	9.3×10^{-8}	8.3×10^{4}	0.027
8	60	6.6	6.4	3.9	8.8	28	17	7.2×10^{-9}	2.5×10^{4}	0.081
8[b]	70	5.9	6.0	5.0	10	32	17	3.7×10^{-9}	2.1×10^{4}	0.073
8[b]	80	6.2	6.6	8.3	14	42	19	2.3×10^{-9}	1.4×10^{4}	0.064
8[b]	90	4.8	5.4	19	16	35	17	1.2×10^{-9}	4.5×10^{3}	0.063

[a] From Table 2, section 5.4

[b] Not Studied with the neutral atom detector

[c] From reference 1 or 2

[d] Determined from comparisons with cesium flow characteristics

[e] Assumed from 8 (70 percent) values

coalescence and disappearance of the smaller pores, resulting in an increase in the mean pore size and decreases in the porosity and permeability. After the 1600 C run, the surface of the specimen was so ruptured and so few pores remained, that its use as an ionizer was impossible. Data presented in section 5.5 show that for the 0.9-micron ionizer, significant decreases occurred in both the neutral cesium flowrate through the ionizer and in the perveance, or ion-current producing capabilities, with operating time and temperature. This indicates that the permeability and number of active pores decrease for the temperatures and times to be indicated. This deterioration observed in both the 0.1- and 0.9-micron ionizers made it clear that an upper limit on ionizer temperature should be observed if changes in structure and operating characteristics were to be prevented for all of the ionizers. For this reason, experimental data were obtained for all specimens measured at ionizer temperatures limited to less than 1250 C, except for a few short-term experiments up to 1350 C.

This information for the 0.1- and 0.9-micron ionizers also clearly indicates that powders of less than 1 or 2 microns in diameter cannot be used to fabricate satisfactory sintered porous tungsten ionizers unless significant advances are made in the techniques of power metallurgy and sintering.

3.3 POROUS IONIZER PARAMETERS

The pores formed by the voids between neighboring tungsten particles act as capillary channels through the body of the ionizer. These channels are not straight, may change irregularly in cross section along their length, and may be distributed in a nonuniform manner throughout the bulk of the porous structure. Isolated, noninterconnecting porosity and dead-end channels are possible. The porous tungsten ionizers used in the surface ionization studies, and the compacts formed and sintered under identical conditions, were subjected to density measurements, gas-flow testing, and metallographic examination to determine a group of parameters for comparison of their porous structure.

The permeability, k, is a measure of the ease with which a fluid flows through a porous medium under the influence of a pressure gradient. It is defined using Darcy's law (an empirical relation). If v is the volume of fluid crossing a unit area per unit time under the pressure gradient (dP/dx) (for small v), Darcy's relation is:

$$k' \frac{dP}{dx} = v \tag{1}$$

where k' is a constant dependent upon both the fluid and the porous medium. Because it is desirable to have the permeability be essentially a function of the porous structure and not the fluid, k, the permeability is defined as

$$k \equiv \eta k' = \frac{\eta v}{dP/dx} \quad \text{(sq cm)} \tag{2}$$

where

η = coefficient of shear viscosity of the fluid

The units of permeability are sq cm. Another frequently used quantity, the conductance, F, is related to the permeability through F = vA (in cu cm/sec) where A is the flow area of the porous medium. The permeability and conductance are then related by

$$k = \left(\frac{\eta\, dx}{A\, dP}\right) F \tag{3}$$

From gas-flow measurements, the following parameters were determined: F, the conductance; S_v, the specific internal surface area per unit volume; k, the permeability to viscous flow; D, the mean grain diameter; d, the mean pore diameter; and s, the mean interpore spacing. The metallographic examinations yielded the statistical distributions of the interpore spacings, the grain sizes, and the pore sizes, from which the mean interpore spacings, the mean pore sizes, and the mean grain sizes were determined. A brief summary of these studies is presented here, together with Table 1, which tabulates the combined results.

3.4 GAS FLOW ANALYSES

The treatment of gas flow, due to Adzumi (Ref. 3), was used to calculate the mean pore size and pore density. Similar considerations were used to calculate the specific internal surface area of the porous microstructures according to treatments of Kozeny (Ref. 4) and Deryagin (Ref. 5) for viscous and molecular flow, respectively. Assuming a series-parallel capillary arrangement to exist in the porous plug, the total conductance was obtained from.

$$F = \frac{\pi}{8\eta}\,\alpha\,\overline{P} + \frac{8}{3}\,\beta\,Z\sqrt{\frac{\pi R_G T}{2M}} \qquad (4)$$

where

η = gas viscosity

M = gas molecular weight

T = plug temperature

R_G = universal gas constant

Z = a semi-empirical constant related to the mean free path of the gas molecule and gives the fraction of molecular flow

$\overline{P}$ = mean pressure across the plug

α and β = equivalent conductances of the series-parallel capillary arrangement

The values α and β are related to R, the mean pore radius, and to N, the pore density by

$$R = \frac{\alpha}{\beta}$$

$$N = \frac{\beta^4}{\alpha^3}\,\frac{L}{A} \qquad (5)$$

L = plug thickness

A = cross-sectional flow area

Experimentally F was measured as a function of $\overline{P}$. The data fell on a straight line:

$$F = C\overline{P} + b$$

$$R = \frac{64\,\eta}{3\,\pi}\,\frac{C}{b}\,Z\,\sqrt{\frac{\pi R_G T}{2\,M}} \quad \text{(mean pore radius)} \tag{6}$$

and

$$N = \frac{3}{8}\,\frac{d}{ZA}\,\frac{b}{R^3}\,\sqrt{\frac{2M}{\pi R_G T}} \quad \text{(pore density)} \tag{7}$$

Similarly, the specific surface area per unit volume, S_V, was written in terms of the straight line parameters corresponding to each pure flow regime. For viscous flow:

$$S_V^2 = \frac{3}{5\eta(1-\epsilon)^2}\,\frac{A}{L}\,\frac{1}{C} \tag{8}$$

where

ϵ = bulk plug porosity

For molecular flow:

$$S_V = \frac{24}{13}\,\frac{\epsilon^2}{(1-\epsilon)}\,Z\,\frac{A}{L}\,\frac{2\,R_G T}{\pi M}\,\frac{1}{b} \tag{9}$$

The permeability of the plug to viscous flow was obtained from

$$k = \frac{F_V L \eta}{\overline{P}\,A} \tag{10}$$

where

F_V = conductance for viscous flow

It has been shown experimentally (Ref. 6) that the mean grain diameter is given by

$$D = \frac{6}{(S_V)_p} \tag{11}$$

where

$(S_V)_p$ = specific surface area calculated from the viscous permeability

The ionizers were experimentally tested with dry air, hydrogen, and argon to obtain a range of viscosities and molecular weights. The results of air flow as a function of pressure drop through the specimens is plotted in Fig. 1. The slope of this log-log plot is unity, i.e., the equation is linear, which is characteristic of Knudsen molecular flow. A slight increase in slope at high values of ΔP for some specimens indicates a transition to Poiseulle viscous flow. From these and other data, plots of the conductance as a function of average pressure were drawn. From the resulting slopes and zero pressure intercepts, the various microstructural properties of the porous plugs were calculated. A summary of the results is presented in Table 1.

3.5 METALLOGRAPHIC ANALYSES

The problems posed by metallographic analyses of porous microstructures are twofold. First, for an analysis to be reliable, a large number (>600) of grains or pores must be measured on a representative metallographic section. Secondly, the pore and grain size measurements made on a two-dimensional cross section must be related to the actual volume distribution in the specimen.

The grain and pore size distributions were determined with a semi-automatic measuring and counting instrument, the Zeiss TGZ-3 Particle Size Analyzer.

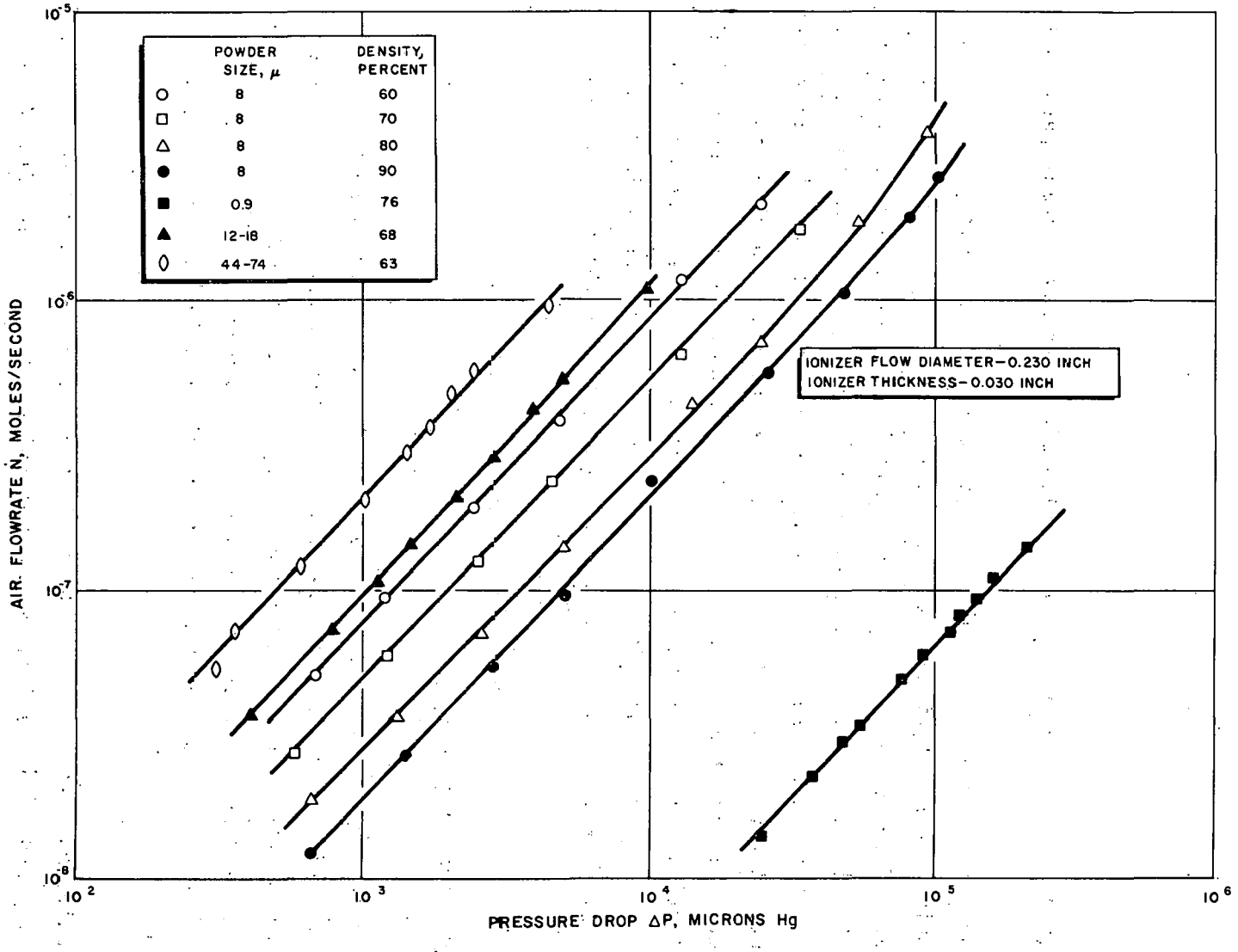

Figure 1. Air Flowrates vs Pressure Drop for Porous Tungsten Ionizers

The ionizers were first infiltrated with a copper/2-percent nickel alloy. Photomicrographs were then made of polished representative sections of each ionizer. The magnifications were chosen for easy use with the Zeiss Particle Size Analyzer in that the minimum diameter measured was not less than 1 millimeter. The pore size distribution curves were plotted in cumulative form, and a few of them are shown in Fig. 2. The mean pore size occurs at 50 percent.

3.6 COMPARISON OF AIR FLOW AND METALLOGRAPHIC RESULTS

A comparison of the metallographic and air flow results of pore and grain sizes is, in most cases, quite good. However, the values for the interpore spacing are in all cases lower for air flow than when observed directly by metallography. Two explanations are possible. First, the low values could be a shortcoming of the gas-flow method, attributable to the nature of the assumptions made concerning the capillary nature of the flow channels. Secondly, they could be an indication that not all of the pores observed by direct metallography are active, i.e., open. From the experimental results, it would seem that the effective free area to gas flow is much less than observed by metallography. This observation may be the result of a restriction of gas flow through a relatively small number of high-conductance channels formed by the bulk pore structure of the material. The previously mentioned decreases in permeability and porosity with operating time with cesium for the small grain sizes tend to support this theory. The values for mean grain diameter of the sintered ionizers obtained from gas-flow analysis were in agreement with the quoted initial particle sizes, but were smaller than the metallographic values (Table 1). This result is probably because of the technique of measurement of initial grain size. Irregularly shaped particles, with surface areas larger than the same-diameter sphere, would register a smaller mean diameter than the average rounded metallographic size.

The gas-flow permeability is related to the transport rate by Eq. 3. The transport uniformity for ionizers of the same permeability increases as the

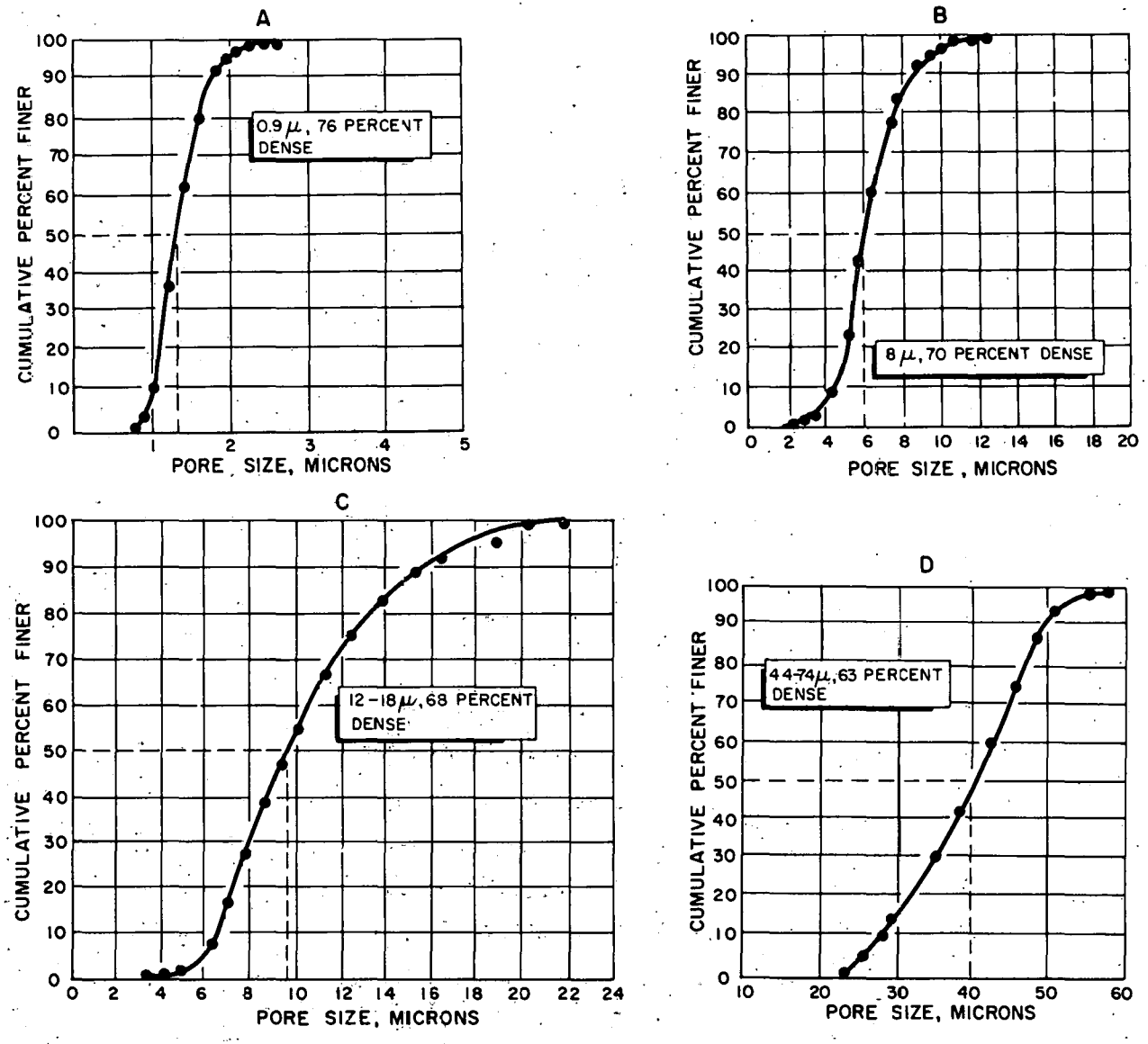

Figure 2. Pore Size Distributions for the Sintered Tungsten Ionizers

total number of channelways, measured by the specific surface, increases. The permeability is affected by the porosity, pore size, and plug thickness, increasing as the first two increase, and decreasing as the last one increases. The permeability shown in Table 1 for the 0.9-micron ionizer is seen to be much lower than any others. It should be pointed out that the value reported for this ionizer was measured after the ionizer had been used in the neutral atom detector as a cesium ionizer at temperatures as high as 1300 C. As pointed out above, the 0.1-micron ionizer permeability was essentially zero after sintering even at temperatures below or comparable to the critical temperature for ion production ($\sim$1150 K).

3.7 POROSITY AND SINTERING EFFECTS

The data for the 8-micron porosity sequence (Table 1), obtained by variation of the sintering time, show the following: (1) the mean pore diameter and the mean interpore spacing remain relatively unchanged for decreases in porosity (very small changes in the opposite direction account for a change in the specific periphery P_S, defined in Section 5.4); (2) the mean grain diameter, D, increases significantly with decreases in porosity, particularly the gas-flow values which tend to be a better measure of the internal structure than the metallographic values measured on the surface (the metallographic values are, in turn, more significant in relation to surface properties such as the specific periphery); (3) the permeability decreases with decreases in porosity; and (4) the specific periphery increases slightly, but significantly, with increasing porosity. The increase in D is seen to be accelerated with increasing sintered density, roughly 4, 5, 8, and 19 microns for densities of 60, 70, 80, and 90 percent, respectively. The permeability, on the other hand, is observed to accelerate with increasing porosity (1 minus the density), very nearly as $k_{20} = 2k_{10}$, $k_{30} = 3k_{10}$, and $k_{40} = 6k_{10}$. There is more than a 25-percent increase in ion-emitting area, which is proportional to P_S (within a given range of surface coverage), between 10- and 40-percent porosity. Because 3 and 4 above are favorable to the attainment of high J_+ with no apparent reduction in ionization efficiency, a higher ionizer porosity, at any given powder size, is expected to be desirable for electrical propulsion applications.

THIS PAGE

WAS INTENTIONALLY

LEFT BLANK

4. EXPERIMENTAL APPARATUS AND TECHNIQUES

4.1 INTRODUCTION

The experimental device used in these studies measures directly and independently the charged and neutral particle fluxes (current densities) extracted and evaporated, respectively, from the porous ionizers. The ion flux is measured by collecting and recording the entire extracted ion current. The neutral flux is determined by selecting and isolating a portion emitted through a known solid angle, ionizing it with a hot tungsten filament, measuring the resulting electron current in this auxiliary ionizer, and calculating the corresponding total emitted neutral flux from knowledge of the geometry and the solid angle, and from the assumption of a cosine distribution of neutral atom emission from the ionizer. This method is far superior to those in which the neutral particle currents are obtained as the difference between two measured ion currents or are calculated from the measured depleted propellant mass and the time-integrated ion current.

4.2 ELECTRON SUPPRESSION

Suppression of all kinds of electron emission from all ion-collecting surfaces is accomplished with highly transparent grids maintained at a negative potential and properly spaced. The suppressed electrons are primarily secondary electrons resulting from ion impact, photo-electrons resulting from the absorption of radiation from the hot ionizer, and thermionic electrons resulting from heating of the surface because of ion impacts. The last process is also inhibited by the low temperatures produced by liquid-nitrogen cooling of the entire ion collector-neutral atom detector assembly. This grid suppression technique is much more reliable than that of creating a magnetic field parallel to the collecting surface.

4.3 NEUTRAL FLUX

A shutter in the neutral particle beam path is employed to ensure accurate measurement of the neutral flux by providing recordings of both the total (shutter open) and background (shutter closed) electron currents in the ionizing filament of the neutral atom detector for each set of experimental conditions. This allows correction for any electron current contributions arising from thermionic emission from the filament, photoelectric emission from the detector body to the filament caused by the absorption of electromagnetic radiation from the hot filament, or ionization in the background vacuum gas in the detector volume. Secondary emission from the filament is negligible because the impinging neutral atoms have only thermal energies.

Contrary to the cases of surface ionization by the bulb and the molecular beam methods, the neutral particle current and, hence, the effective neutral flux, n_o, reaching the ionizer can be measured for a porous ionizer by electrically shorting the ionizer to the entire surrounding environment (reducing the surface electric field to zero) and measuring the subsequent equilibrium rate of evaporated neutrals, which is equal to the flowrate of neutrals through the ionizer. The effective incident neutral flux is then obtained by dividing by the total ionizer area.

4.4 VACUUM CONDITIONS

The apparatus used for these measurements is located in a vacuum chamber (8 inches in diameter and 24 inches long) in which was maintained a vacuum, during source operation, of from 2×10^{-7} to 3×10^{-6} millimeters Hg. A particular value depends upon ionizer temperature and beam current, with 1×10^{-6} millimeters Hg being a normal value. A schematic of the entire system is shown in Fig. 3 and a photograph of the device and ionizer housing in Fig. 4. Porous ionizers, 0.25 inch in diameter and 0.030 inch thick, and similar to the one shown in Fig. 5, were employed. Sustained currents of 1 milliampere could easily be drawn from these. Currents

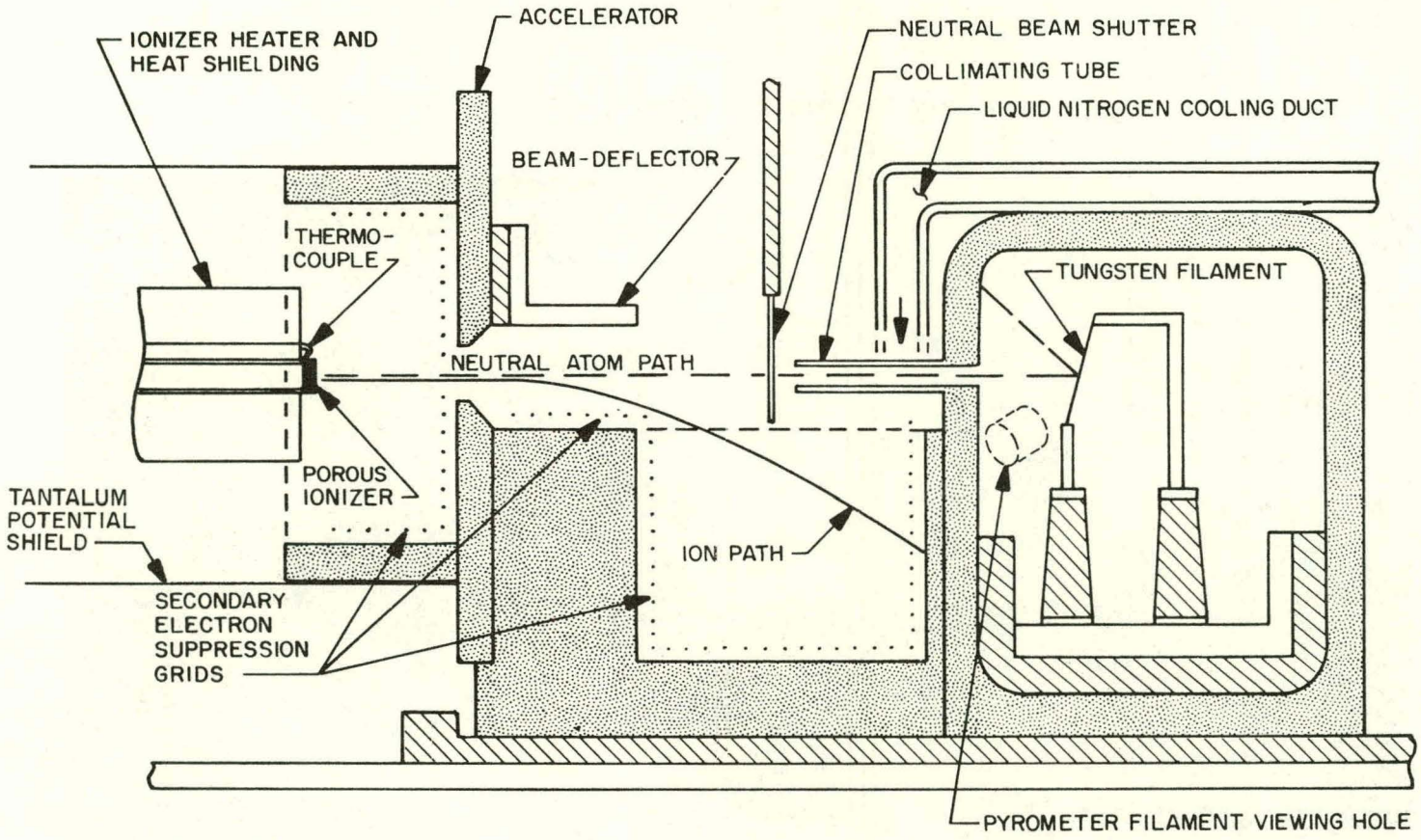

Figure 3. Schematic of Neutral Atom Detector

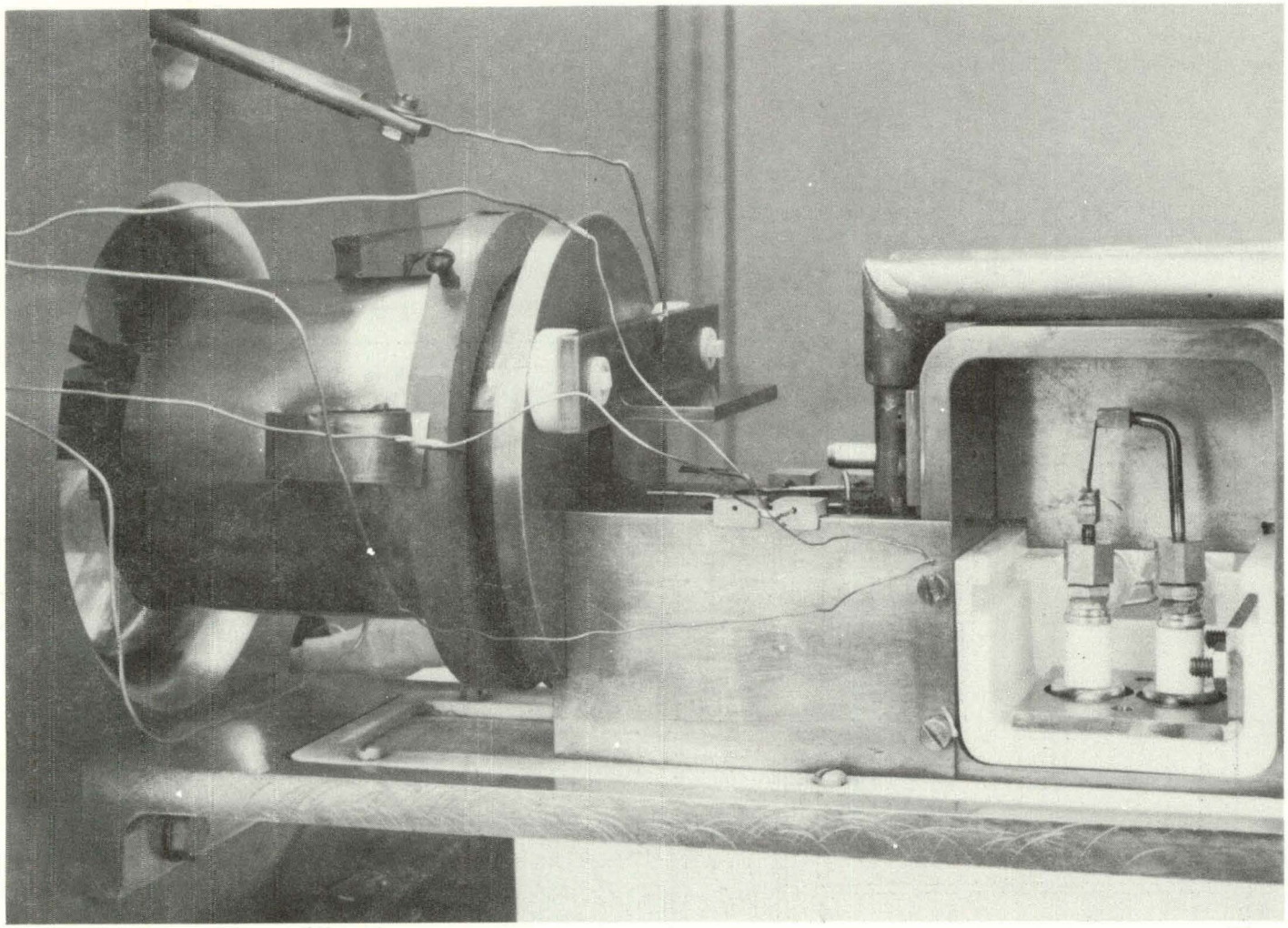

Figure 4. Ionizer Housing and Neutral Atom Detector

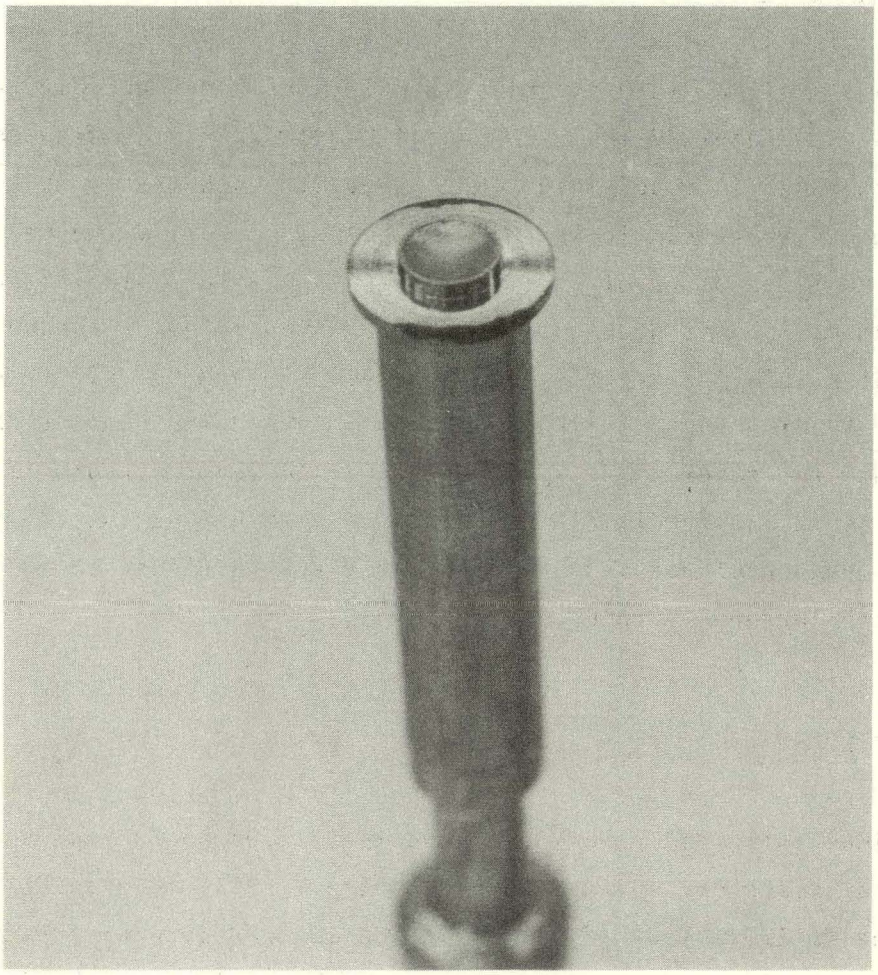

Figure 5. 1/4-Inch Porous Tungsten Ionizer

higher than about 1.5 milliamperes could be drawn but tended to cause the vacuum and electrical breakdown properties of the system to deteriorate with operating time. A 1-milliampere current corresponds to a current density of 3.17 ma/sq cm.

4.5 CESIUM STORAGE

The cesium is stored in a stainless-steel reservoir, the temperature of which can be maintained in the range of 80 to 350 C by a Nichrome heating element embedded in Sauereisen. The reservoir capacity is about 1 gram of cesium. A thermocouple is inserted into the body of the reservoir to monitor the temperature of the cesium vapor. To maintain the purity of the cesium at a level as high as possible, the cesium is loaded from 1-gram ampules into the reservoir in an argon atmosphere, after the reservoir and other loading equipment have been in an evacuated chamber adjoining the dry box for several hours. The sealed, loaded reservoir is mounted, with the ionizer assembly, as quickly as possible, onto an end plate to minimize leakage of air into the reservoir and is placed in the vacuum system with the neutral-atom detector.

4.6 STRUCTURE

A mechanical valve and a molybdenum delivery tube serve as the link between the reservoir and the porous ionizer, which is joined to the end of the delivery tube (Fig. 5). The ionizer is heated radiatively by an adjacent tungsten heating element. The ionizer and heating unit are entirely surrounded by many layers of 0.001-inch tantalum heat shielding. The ionizer temperature is monitored by a platinum, platinum-rhodium thermocouple attached at the junction of the ionizer surface and the lip of the delivery tube (Fig. 5). Downstream from the ionizer is a large copper structure which serves as the accelerating electrode, the beam collector, the neutral beam collimating tube, the housing for the

neutral atom detector, and the support for the ion beam deflector. This entire structure is cooled by liquid nitrogen flow which enhances the vacuum conditions as well as serving to condense the neutral cesium vapor from the detector volume.

4.7 SEPARATION OF NEUTRAL AND ION BEAMS

The charged portion of the beam, which passes through the hole in the accelerator-collector, is deflected from its initial path into a deep, Faraday collecting cup (Fig. 3) by means of an electrostatic field which must be maintained between 0.5 and 0.7 of the accelerating voltage to ensure direction of the entire ion beam into the cup. The beam of neutral particles continues along its original path and passes through a collimating tube 0.125 inch in diameter and 1.5 inches long. The neutral atoms which pass through this collimating tube impinge upon a tungsten filament, 3/4 inch long and 0.25 inch wide, which is maintained at a temperature of 1325 K. A hole in the neutral atom detector housing allows this temperature to be monitored continuously by means of an optical pyrometer, and corrections are made as needed to maintain it to within the accuracy of the pyrometer.

4.8 MEASUREMENT OF NEUTRAL FLUX

Ionization of cesium on tungsten, for low incident fluxes, is close to 100 percent and almost constant between 1200 and 1500 K (Ref. 7). Because of this plateau of constant ionization efficiency, and because the background current (a function of the filament temperature) is measured before each data point is recorded, the accuracy with which the temperature of this filament is maintained is not a critical factor in the performance of the instrument. The cesium atoms, after being ionized at the hot tungsten surface, are attracted by a negative 90-volt potential to the main body of the detector. Each atom which is ionized at

the filament and drawn to the body of the detector, leaves an electron at the filament, and the resulting electron current is measured and used to calculate the ionization efficiency of the ionizer being examined. The magnitudes of these currents were measured with a Kiethley micro-microammeter. Typical value ranges are 3×10^{-10} to 5×10^{-9} amperes for the background, and 4×10^{-10} to 2×10^{-7} for the total current depending upon the ionizer temperature, beam current, and ionization efficiency. Neutral current values are read to three significant figures with an error of about three in the third place. The values obtained are then corrected for the solid angle seen by the filament and for an assumed cosine distribution of neutral atom emission from the ionizer.

4.9 SUPPRESSION GRIDS AND ION DEFLECTOR

Grids constructed of parallel 0.005-inch-diameter nickel wires with about 1/8-inch gridwire spacings exist in both collecting cups where the beam strikes the copper of the detector body (Fig. 3). These grids are maintained at a negative potential of between 100 and 150 volts for the purpose of suppression of elcctrons. The ion beam deflector is a stainless-steel plate insulated from the accelerating electrode structure above the exit aperture.

4.10 LIQUID-NITROGEN COOLING

To maintain the cesium vapor pressure in the vacuum system at a value as low as possible, the neutral atom detector is cooled to near the temperature of liquid nitrogen by circulating liquid nitrogen through a cooling coil attached to the body of the detector. Excellent heat conduction is ensured because the narrowest heat path anywhere in the detector is 1/4 inch, the detector is made of copper, and copper screws are used wherever parts are joined. The temperature of the body of the detector is monitored during operation by means of a thermocouple. Typical values range between 90 and 120 K.

4.11 NEUTRAL BEAM INTERRUPTER

The shutter for interrupting the neutral beam is suspended from the vacuum tank wall and operates at the upstream end of the collimating tube. This beam interrupter is a strip of 0.005-inch-thick tantalum foil 0.25 inch wide. A cylindrical insulator, which extends to 1 inch above the neutral beam and which may be rotated by means external to the vacuum system, supports the tantalum foil. The foil is mounted on the edge of the cylindrical rod so that a 90-degree rotation of the rod in either direction will move the foil from a position in which it completely blocks the measured neutral flux to a position completely out of, and parallel to, the neutral beam. Thus, both the background filament current and the actual neutral flux are measured and recorded at each data point.

4.12 IONIZER CHARACTERISTICS

With this device, it is possible to measure the ionization efficiency and current-voltage characteristics of each porous ionizer as a function of the ion accelerating potential, the ionizer temperature, the vapor pressure (temperature), and time. The experimental perveance of the ionizers studied was as high as 3×10^{-9} amp/volt$^{3/2}$ allowing a current of 1 milliampere to be produced at an accelerating potential of about 4.5 kilovolts for a reservoir temperature of about 300 C and an ionizer temperature of 1100 C. Greater space-charge-limited currents can be drawn by increasing either the ionizer or reservoir temperature, but currents in excess of 1-1/2 milliamperes tend to cause problems in the reliable operation of the neutral atom detector.

4.13 NEUTRAL EMISSION DISTRIBUTION

The theory of surface ionization with porous ionizers (Ref. 8), which differs significantly from that for filament ionizers because either the bulb or molecular beam method of presentation must be employed in the

latter, indicates qualitatively that the emission of neutral atoms from porous ionizers should not be a cosine distribution except for sufficiently large flowrates in the absence of any ion-extracting electric field and subsequent ion emission (Fig. 6). As the magnitude of the electric field is increased and the extracted space-charge-limited current consequently increases, the neutral emission distribution should become more of an overcosine, i.e., represented by larger values of n in $\cos^n \psi$ (where ψ is measured from the normal and $n>1$ corresponds to over overcosine, and $n<1$ corresponds to undercosine), until the extreme is reached for the emission-limited current condition.

The theory also predicts that this effect will vary inversely as the magnitude of the emission-limited current, i.e., as the emission-limited current increases, n should approach unity. The details of this theory are presented in Ref. 8 . A quantitative description of the effect is difficult unless the details of the geometry of the pore openings and surface structure are known.

The same theory predicts that the experimental ionizer perveance should increase with the magnitude of the emission-limited ion current and that the ionization efficiency should decrease with the magnitude of the emission-limited current, i.e., with the current density. Both of these last predictions have been verified experimentally, the first, in this work, and the second, in this work as well as in other laboratories, e.g., Ref. 9 and 10 .

Because the total neutral emission is determined from the normal direction only, the total calculated neutral emission, assuming a cosine distribution, will be too large if the actual distribution is an overcosine. Therefore, the ionization efficiency values reported here are lower limits for the true values, although no large deviations are expected for sintered powder ionizers. If β was 98 percent, a 10-percent error in the calculated total neutral emission would change β by only 0.2 percent. If n was

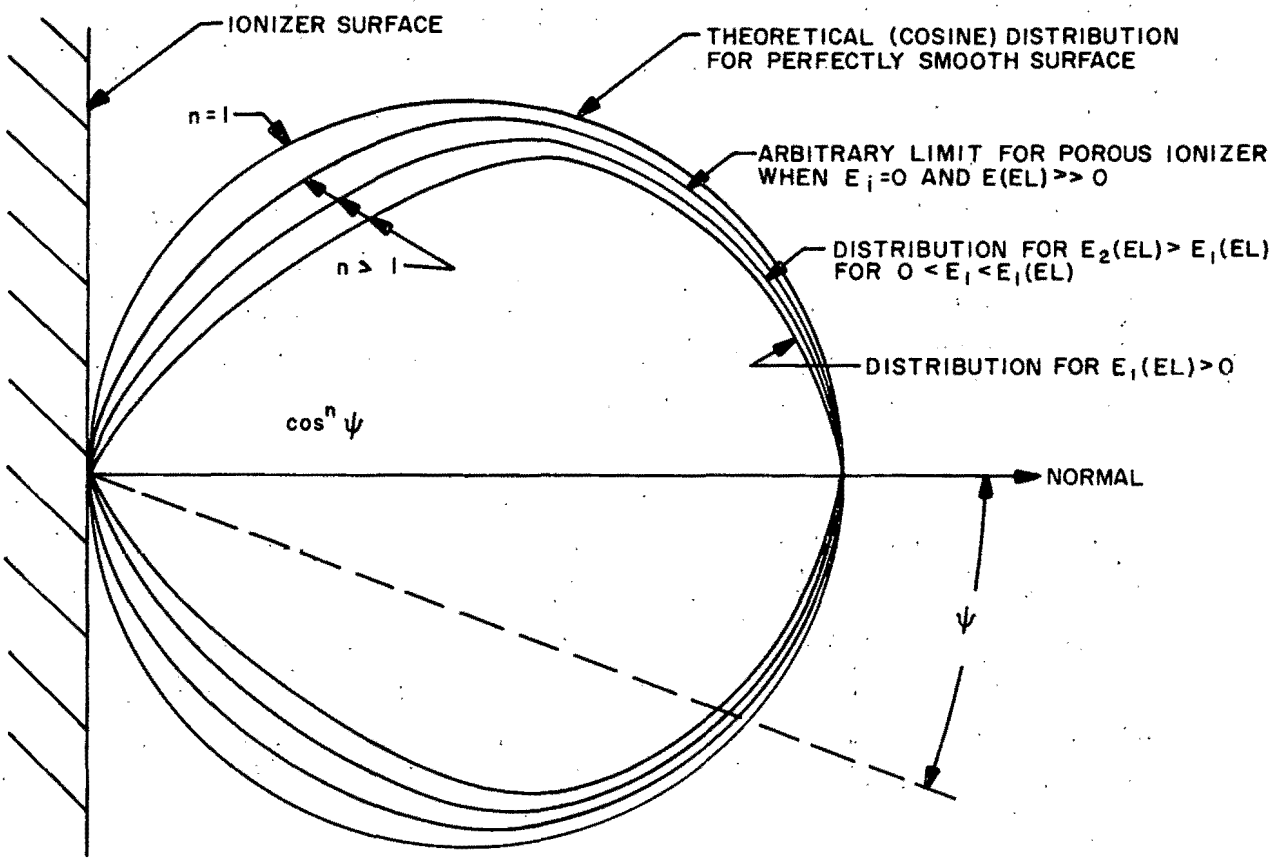

E_i = electric field for the i^{th} set of ionizer conditions

$E(EL)$ = value of the electric field when the ion current becomes emission limited

Figure 6 . . Angular Distribution of Neutral Atom Emission From a Porous Ionizer

as large as 2, the fraction of neutral atoms would be two-thirds as large and β would be 98 percent instead of a previously calculated 97 percent, or 99-1/3 instead of 99 percent.

During the preparation of this paper, some preliminary experimental results were reported (Ref. 11), which were performed with a different type of ionizer (wire bundle) for which a large degree of forward peaking in the neutral emission distribution might be expected because of the difference in pore structure. However, the statement is made that the experimentally measured neutral distribution, in the absence of ion emission, is consistent with a cosine distribution. Preliminary data are also presented which indicate that the distribution for one emission-limited condition is strongly forward peaked with a resulting poor ionization efficiency. A poor ionization efficiency and a rather large deviation from the cosine are consistent and indicate that a large fraction of the cesium is passing through the pore openings with trajectories at small angles (ψ) to the normal, having left the pore walls fairly deep within the pore where few if any electric field lines terminate and, hence, few if any ions can be extracted. (Ions are returned to the surface under the influence of their image changes; only neutral atoms are emitted). Comparing the structure of the wire bundle (Ref. 11) to the sintered porous powder ionizers of this work, it appears that the average pore size and interpore spacing of the former are about 6 to 13 microns, respectively, which compare roughly to the same parameters for the 8-micron specimens of this work.

4.14 COMPARISONS OF WIRE BUNDLE AND SINTERED POWDER POROUS IONIZERS

Thus, the basic difference between the wire bundle and the sintered powder structures may be that in the former, the pores are fairly straight, deep channels of rather uniform radius and small angle from the normal, from which neutral particles can escape with an overcosine distribution and, consequently, with a larger neutral fraction. For

the sintered powder structures, the very crooked, relatively shallow, pore exits of nonuniform radius and larger angles from the normal tend to cause the adatoms to be emitted much more randomly with respect to the normal, and to be in contact with the ionizer much nearer the surface, i.e., where the electric field can better allow ion emission to compete with neutral emission, thus enhancing the ionization efficiency.

4.15 SURFACE CONTAMINATION AND CLEANING

For the case of nonporous or filament ionizers, the surface can be largely cleaned of adsorbed foreign atoms by flashing to high temperatures for short periods of time in a high vacuum. This technique evaporates the atoms adsorbed on the surface to the point of equilibrium, with the incident flux of atoms of the background gas corresponding to the vacuum pressure. If the temperature is then decreased, the background gas atoms can condense back onto the surface, but other foreign atoms have been removed. If, however, the cesium vapor were introduced during the flashing time, thus changing the composition of the background gas, little contamination by atoms other than the desired adatoms could occur. Even then, as discussed in detail in Ref. 8, for the cesium-tungsten system, because oxygen is chemisorbed on the tungsten surface with strong adsorption energies and deep penetration, it cannot be completely removed from the surface by other than destructive processes, e.g., field evaporation. In addition, because oxygen cannot be completely removed from the cesium, oxygen is always contacting the surface at high temperature and can continually contaminate the tungsten surface.

For sintered porous ionizers, flashing cannot be safely employed because of the sensitivity of the porous surface structure to high temperatures. Additional sintering (if not rupturing) can quickly occur at temperatures of the order of the original sintering temperature which is sometimes

slightly above 2000 C but in other cases, lower. For example, the 0.9-micron ionizer used in this investigation was sintered and operated up to 1300 C. Undesirable thermal stresses would be applied to the ionizer during flashing and rupturing could occur.

For porous ionizers, another technique can be employed to reduce the effect of adsorbed contamination, particularly oxygen, although, as explained in Ref. 8 , operation with a tungsten surface completely free from oxygen will be impossible for two reasons, even in deep space. After the experimental system vacuum tank is evacuated, and before cesium flow is started (by opening the feed system valve), the background gas is a combination of air and diffusion pump oil (or other pumping fluid specie), i.e., nitrogen, oxygen, hydrocarbons, etc. These gases are impinging upon the ionizer and other surface contaminants are present which were there when the system was placed in the vacuum tank. If the ionizer is then heated to the high side of the operating range, 1200 to 1300 C, some of the adsorbates are driven off but many remain and, certainly, oxygen, nitrogen, and hydrocarbon molecules from the vacuum gas are condensing and evaporating continually on the ionizer surface at rates related to the background pressure. One source of ionizer deterioration which could lead to long-term deterioration of the ionizer permeability may be evident here which would not be true for operation in deep space or in the laboratory if a mercury diffusion pump vacuum system were used. The diffusion pump oil molecules suffer thermal decomposition when striking the 1200 C ionizer, resulting in the deposit of carbon atoms, which will not readily be evaporated, and in much more volatile products which will quickly leave. The resulting slow deposit of carbon which, like oxygen, is chemisorbed on tungsten, could eventually clog the surface pores of the ionizer.

With the ionizer now hot, if cesium is allowed to flow through the ionizer in the presence of an ion-extracting field, the cesium encounters a somewhat conaminated surface. Cesium has a gettering action, however, and as the ion current is drawn, it has a tendency to clean the surface of foreign adsorbates.

If the vacuum tank is of relatively small volume, another beneficial effect will occur. The composition of the background gas in the vicinity of the ionizer will gradually change from air plus diffusion pump oil to largely cesium. Although minute air leaks at the chamber walls will replenish the air component, the ionizer is a much larger cesium leak and, in its vicinity, cesium is leaving, is condensing on the collector and detector, and is being pumped out through the vacuum system. In time, the local background gas will become predominantly cesium as the gettering action cleans the surface and the foreign adsorbates are lost to the system. The impurity atoms in the cesium itself are still a source of contamination, of course. Commercial cesium can be obtained at a purity of only about 0.998.

Because most pressure gages are calibrated for air, inaccurate pressure readings probably result. In the experiments described herein, the initial air pressure reading (before cesium flow was started) was generally in the high 10^{-7} torr range. However, the pressure would gradually rise with operating time after cesium flow was started. Also, the pressure would rise and fall with the total emitted cesium flux. For fluxes less than about 10^{15} particles/sq cm-sec, the pressure would hold at about 10^{-6} torr, but for increasingly higher densities, the pressure would rise to a maximum of about 10^{-5} torr at about 3×10^{16} particle/sq cm-sec. Whether this increase of an order of magnitude in the pressure was caused entirely by a corresponding increase in actual particle density in the vacuum chamber or partially by a change in composition of the gas from air to cesium itself is not known.

4.16 DECREASING ACCELERATING FIELD TECHNIQUE

In all of the experiments described herein, a characteristic phenomenon, believed to be the effect of cesium gettering, was consistently observed and led to the establishment of an experimental technique which was employed to obtain all of the data reported. Whenever any ionizer was in

a space-charge-limited ion emitting condition (above the critical temperature threshold and below the saturation electric field), and the ion-extracting electric field was either initially applied or was increased in magnitude, regardless of the initial magnitude, the resulting increase in ion current from the initial value to the final equilibrium value occurred over a time interval of many minutes. When the system was initially started (cesium flow begun), several hours were required for the steady-state current to be attained; after longer periods of operation and a cesium atmosphere had had a chance to develop, about 30 minutes were required. Larger changes in electric field required longer times. Consequently, if it were desired to plot the ion current as a function of the electric field (current vs voltage) by increasing the electric field in steps, prohibitively long times would have been required to obtain enough points to show the details of the curve because a wait of many minutes would be required after each increase of accelerating potential (extracting electric field) to attain the steady equilibrium current. Whenever the magnitude of the electric field was reduced, however, the ion current fell immediately (within the reaction time of a Brown recorder) to the equilibrium value corresponding to the new electric field value regardless of the initial value of E. For this reason, all data reported herein were consistently obtained by the following standard operating procedure.

The ionizer temperature and the equilibrium conditions of cesium vapor pressure at the rear of the ionizer were first established at zero electric field. Then the electric field was increased to a maximum defined by the breakdown threshold of the voltage applied between the ionizer and the accelerating electrode (usually 8 to 10 kilovolts, depending upon the chamber pressure conditions). A rest period then ensued during which the ion current rose to some steady maximum value (30 minutes to several hours). The ion and neutral currents were then measured at their equilibrium values, corresponding to a series of electric field values always reached by a decrease in applied voltage. Smaller intervals of electric field were used when more detail was desired in the

ion current dependence, for example, at the knee between the emission-limited and the space-charge-limited portions of the curve where an accurate value of the maximum ion current is desired. By acquiring data in this manner, only the long initial wait was required and much more detailed and accurate information regarding the dependence of the ion current on the applied electric field (voltage) could be obtained during a run time of such duration that variations in thermal equilibrium in the ionizer temperature and the cesium vapor pressure (temperature) could be held to a desirable minimum.

A word about the time dependence of the ion current on changes in the other two primary variables, the cesium vapor temperature (pressure) and the ionizer temperature, may be appropriate here. While the ion-extracting electric field can be changed quickly, any change in these other two variables requires the slower process of thermal equilibration. The ionizer is heated indirectly by a large tungsten filament in close proximity. The ionizer temperature is increased by increasing this current, which increases the flux of radiated energy. When such an increase is made while an ion current is being recorded, the ion current is observed to increase at approximately the same rate as the measured ionizer temperature, which is much more rapid than the time rate of change of ion current described for a change in the electric field. That is, the ion current reaches a new constant value when the ionizer reaches thermal equilibrium and no time delay occurs, such as follows an increase in E. A similar situation is observed when the cesium vapor pressure is increased by increasing the temperature of the cesium reservoir, the coolest portion of the cesium feed system. However, because of the large mass of metal comprising the reservoir which includes a flow valve and a feed tube, the rate of increase of the reservoir temperature following an increase in the current in the Nichrome heating element embedded in a Sauereisen sheath is even slower than that resulting from an increase in electric field. The ion current increased very slowly corresponding to the slow rise in the measured reservoir temperature. Periods of time between 1 and 2 hours (depending upon the

magnitude of the change in P_V) were required for a steady ion current to be reached following an increase in cesium vapor pressure (temperature).

It is believed that for porous ionizers, the cause of the observed slow rises in ion current which follow successive increases in ion-extracting electric field but which do not follow similar decreases, is caused by a gradual cleaning (by gettering) of successively larger emitting surface areas around the active pores. Once an equilibrium set of conditions of cesium vapor pressure, P_V, and ionizer temperature, T, are established, an emission-limited or saturation current, I_{max}, is defined. When E is zero, no ions can escape ($J_+ = 0$), and because of the pressure drop across the porous ionizer, flow occures, resulting in an equilibrium evaporation rate of neutral cesium from the surface, which has an associated distribution of θ over the surface (θ is large near the active pores and decreases radially outward for a given I_{max}). For a higher I_{max}, θ is larger at all points but still decreases radially outward. As an electric field is applied, the corresponding space-charge-limited current is drawn. This current is emitted from the regions of greatest local work function, ϕ_k, which corresponds to the lowest θ, i.e., from the areas farthest from the active pores. These areas, therefore, are cleaned of adsorbed cesium, and probably foreign adsorbates, and the regions become even more capable of ion emission because of the increased ϕ_k. As E is increased, the emitting areas expand about the active pores, cleaning larger and larger areas of the surface. The ions are emitted primarily from the peripheries of these clean areas because although ion emission will occur from any clean (high ϕ_k) area, the areas are fed by neutral cesium only from localized regions (the pores) in the case of porous ionizers. Of course, for filament ionizers, θ and ϕ_k are essentially uniform over the entire surface because cesium is condensing uniformly and ions are being emitted relatively uniformly from the surface. (Microscopic surface variations in ϕ_k cause ion emission to be nonuniform on the atomic scale.) As E reached a value corresponding to the emission-limited current ion emission occurs very

near the active pores because the cesium is being converted to ions and being extracted as fast as they migrate onto the surface. Further increase in E does not necessarily produce more ion current because the current is now limited by the rate of flow of cesium from the active pores.

For the converse case, when the magnitude of E is reduced after equilibrium has been established at the higher value of E, the space-charge-limited current decreases and the required peripheral emitting area decreases. This area has, however, been previously cleaned and, therefore, no gradual cleaning action takes place and no associated equilibration time interval is observed.

THIS PAGE

WAS INTENTIONALLY

LEFT BLANK

5. EXPERIMENTAL RESULTS

5.1 INTRODUCTION

The ionizing surfaces of the porous tungsten ionizers used in this work are very inhomogeneous because of the grain and pore structure in addition to being polycrystalline, and therefore, even more than filament ionizers, are subject to the laws of surface ionization for inhomogeneous or patchy surfaces.

In Ref. 8, the theory of surface ionization for patchy surfaces is reviewed in detail. The application of this theory to the case of porous ionizers is then developed for surface ionization systems in general. The cesium-tungsten (Cs-W) system is one special case of the general theory. The results of this theory as it applies to the Cs-W system are summarized here.

The ion current density emitted from a surface of area A, composed of patches and from which is omitted a total particle flux, n_T, is developed using the following:

$$\alpha = n_+/n_o = \frac{1}{C} e^{(\phi + \psi - V)/kT} \quad \text{and} \quad \alpha_k = \frac{1}{C} e^{(\phi_k + \psi - V)/kT} \tag{12}$$

$$\beta = \frac{1}{1 + 1/\alpha} = \sum_k f_k \beta_k = \sum_k \frac{f_k}{1 + 1/\alpha_k} \tag{13}$$

$$I_+ = en_T A \beta = en_T A \sum_k \frac{f_k}{1 + 1/\alpha_k} = en_T A \sum_k \frac{f_k}{1 + Ce^{(V-\phi_k-\psi)/kT}} \tag{14}$$

Where

e = electron charge

n_T = total particle flux leaving the ionizer surface

f_k = fraction of the total surface having the particular value of local work function ϕ_k

A = nominal ionizer surface area (the actual surface can be larger than A)

β_k = ionization efficiency of a surface patch with work function, ϕ_k (in eV)

C = a function of the system (and is related to the statistical weight ratio of ionic and atomic states of the adatoms and to the reflection coefficient for the particular adatom on the particular surface) and is essentially 2 for the Cs-W system

V = ionization potential (energy) in eV of the adatom

ψ = electric field correction for the heat of vaporization of the adatom

k(of kT) = Boltzmann's constant

T = ionizer temperature

For the Cs-W system

$$J_+ = e\, n_T \sum_k \frac{f_k}{1 + 2\, e^{(V - \phi_k - \psi)/kT}} \qquad (15)$$

For filament ionizers, n_T is a function of the vapor pressure only, and is independent of T and E. For porous ionizers, n_T can be a strong function of both T and E as well as the vapor pressure. For the region of the normal Schottky effect, $\psi = \sqrt{eE}$, and for the region of the anomalous Schottky effect, the effect of ψ is to smooth out the effect of the patchy surface and to make all of the ϕ_k values nearly the same, possibly the average electron work function, ϕ_e. The ϕ_k values are functions of θ, the surface coverage coverage; ϕ_k decreases with increasing θ. For filament ionizers,

θ is approximately the same everywhere on the surface and therefore, the ϕ_k values are all reduced by about the same amount. As long as θ is not very large, $2e^{(V-\phi_k-\psi)/kT}$ will be very much less than unity for the Cs-W system ($V = 3.87eV, \phi_k \doteq 4.5eV$, and $kT \doteq 0.12eV$).

Therefore,

$$J_+ \doteq e\, n_T \cdot 1 \tag{16}$$

which states that β, the over-all ionization efficiency, is essentially 100 percent. Thus, the patchy theory causes no change in the theory of surface ionization for the particular Cs-W system as long as filament ionizers are employed until θ becomes large enough to cause the ϕ_k values to be reduced to the point where the above inequality does not hold.

For porous ionizers, however, θ is not uniform over the ionizing surface; it is very large at the pore walls and decreases over the pore lips and onto the ionizer surface. θ will, in general, vary from unity (although larger values are possible) to zero or some lower limit corresponding to the flow-rate, and therefore the ϕ_k values will vary from 0 to $\phi_{k_{max}}$ (4.68 eV for a clean Cs-W system or up to as much as 9.2 eV for a partially oxygenated tungsten surface). The general patchy surface equation is written as

$$J_+ = e\, n_T\, (P_V, T, E)$$

$$\left[\sum_k \frac{f_k}{1 + 2\, e^{(V - \phi_k - \psi)/kT}} + \frac{1}{2} \sum_{k'} f_{k'}\, e^{(\phi_k + \psi - V)/kT}\right] \tag{17}$$

where k' represents the patches for which $2e^{(V-\phi_k-\psi)/kT}$ is very much greater than unity (i. e., ϕ_k is large). This is the equation that applies

to the cesium-porous tungsten system where $\phi_{k_{mim}}(\theta) + \psi < V < \phi_{k_{max}}(\theta) + \psi$ ($\phi_{k_{min}}(\theta) \approx 0$ and $\phi_{k_{max}}(\theta = 0) \approx 4.68$ eV and V = 3.87 eV, 4.68 eV $< \phi_{k_{max}} <$ 9.2 eV if $\theta > 0$ and oxygen is the adatom specie).

Because some terms in the sums increase with T while other decrease, J_- may be an increasing or decreasing function of T. In addition, because n_T is a function of T and E as well as of P_V, J_+ may be a complex function of all three variables and only experiment can determine the relative influences of them.

5.2 INFLUENCE OF THE ELECTRIC FIELD

It is shown in Ref. 8 that the expressions for the laws of surface ionization on polycrystalline filament ionizers vary with the range of the magnitude of the ion-extracting electric field. In the strong field region (see Fig. 7 for the ranges of the magnitudes of the electric field for the three regions), such that $\sqrt{eE} \geq e/4x_0$, ψ corresponds to $Ex_0 + e/4x_0 + E^2(a_0 + a_+)/2e$, where x_0 is the distance at which electron, atom-ion charge-exchange vanishes and a_+ and a_0 are the ion and atom polarizabilities, respectively. No experimental results have been reported for the high field region.

For moderate fields, the theory states that $\psi = \sqrt{eE}$ (the normal Schottky effect) because the other terms in ψ can be neglected compared to $\sqrt{eE}$. The ion current increases with E because of a reduction of $e\sqrt{eE}$ in the heat of evaporation of the adsorbed ions, λ_+, and the resulting increased relative probability that absorbed atoms will evaporate as ions. This relationship, $\left[T \log I_+ = f(\sqrt{E})\right]$, and the dependence of the critical temperature, T_C, upon E (T_C decreases linearly as $\sqrt{E}$ increases) (Ref. 12), have been demonstrated experimentally for potassium and several light alkali halides (Ref. 13 and 14) and for lithium (Ref. 15) on polycrystalline tungsten.

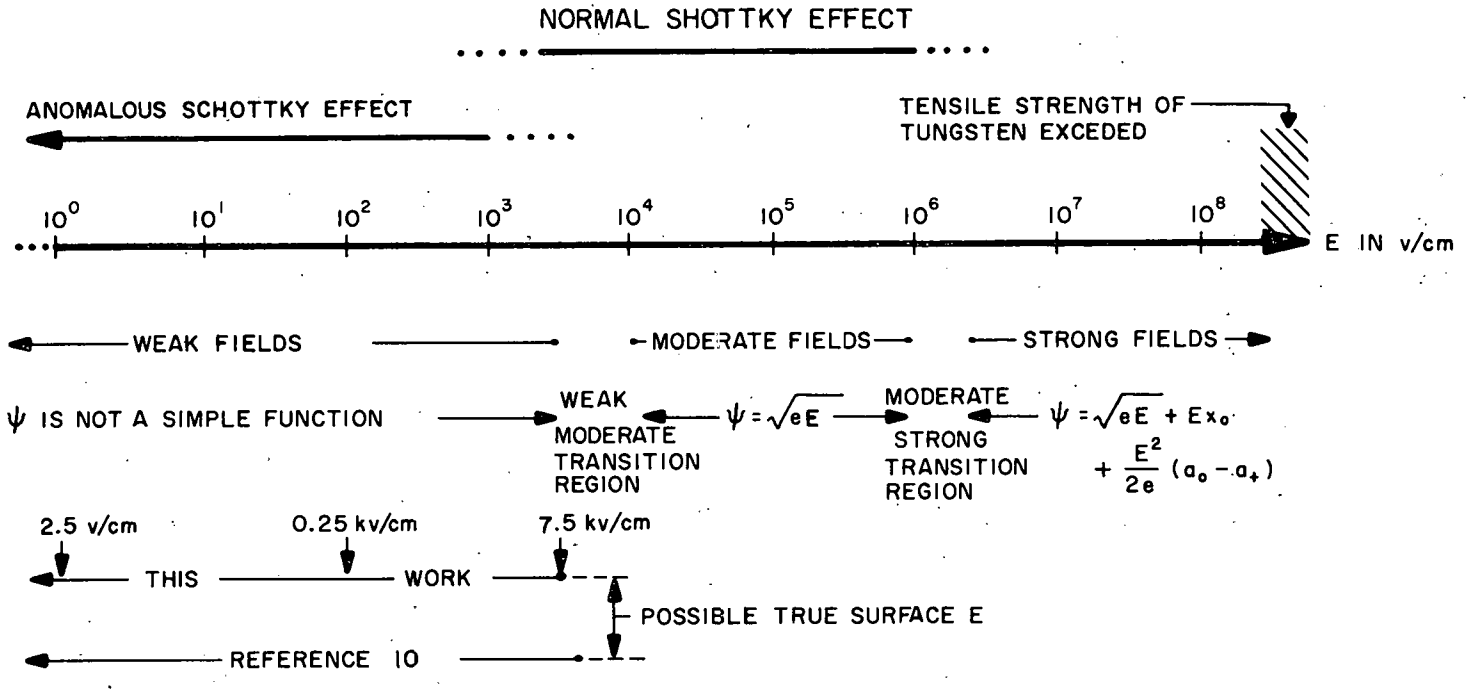

Figure 7. Electric Field Spectrum

In weak fields, the anomalous Schottky effect dominates. The heat of evaporation of ions is increased in the regions of a surface (patches) which have the largest value of ϕ_k by the contact field (potential). Thus, the anomalous Schottky effect tends to smooth out the effect of the inhomogeneous patchy surface by making all of the ϕ_k values more nearly identical. In this region, the ion current and $\alpha(n_+/n_o)$ do not necessarily follow the relationship for moderate fields. For fields in the weak and transition region between the weak and moderate field ranges, the increase of the ion current with the electric field has been observed in many publications for surface ionization on polycrystalline tungsten filaments. For example, it has been observed that the ion current increases exponentially with E $\left[\log I_+ \text{ (or } \alpha) = f(E) \text{ is linear}\right]$ for the ionization of sodium (Ref. 16) and of potassium (Ref. 17) in fields up to 1.5×10^4 v/cm. This effect has been attributed (Ref. 18 and 12) to a reduction of $e\sqrt{eE}$ in the heat of evaporation of ions, λ_+, in the moderate field region (the normal Schottky effect).

For porous tungsten ionizers, data have been obtained only in the range of E comprising the weak field region and the transition region between the weak and moderate fields (Fig. 7). The data obtained in this work indicate that the ion current may increase, decrease, or do either, followed by whichever did not first occur, as the ion-extracting electric field is increased. The mode in which a decrease is followed by an increase was most commonly observed. Examples of these dependences and the conditions under which they were obtained may be seen in Fig. 8, 9,23 to 25, and 30 to 34.

Because the ion current was observed to increase with increasing electric field above some value below the breakdown voltage for the experimental apparatus, which was nominally 3 to 4 x 10^3 v/cm for the majority of the cases in this work, the conclusion is drawn that the influence of the normal Schottky effect is being observed at high values of applied accelerating voltage, although not necessarily in its pure form. The same experimental data also show for the large majority of sets of conditions, that

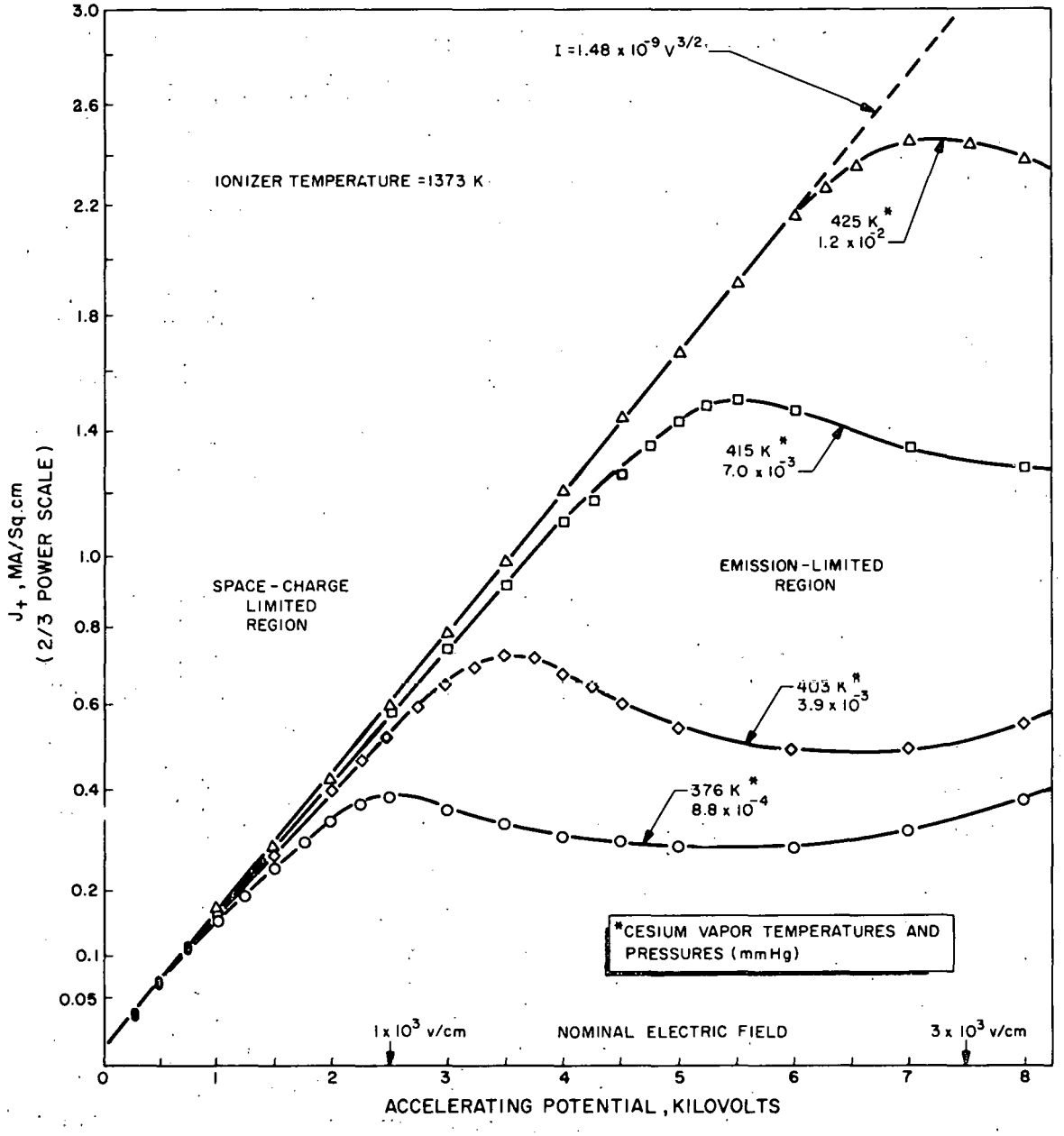

Figure 8. Current vs Voltage Characteristic Curves as a Function of Cesium Vapor Pressure for the 12- to 18-Micron Powder Size Porous Tungsten Ionizer

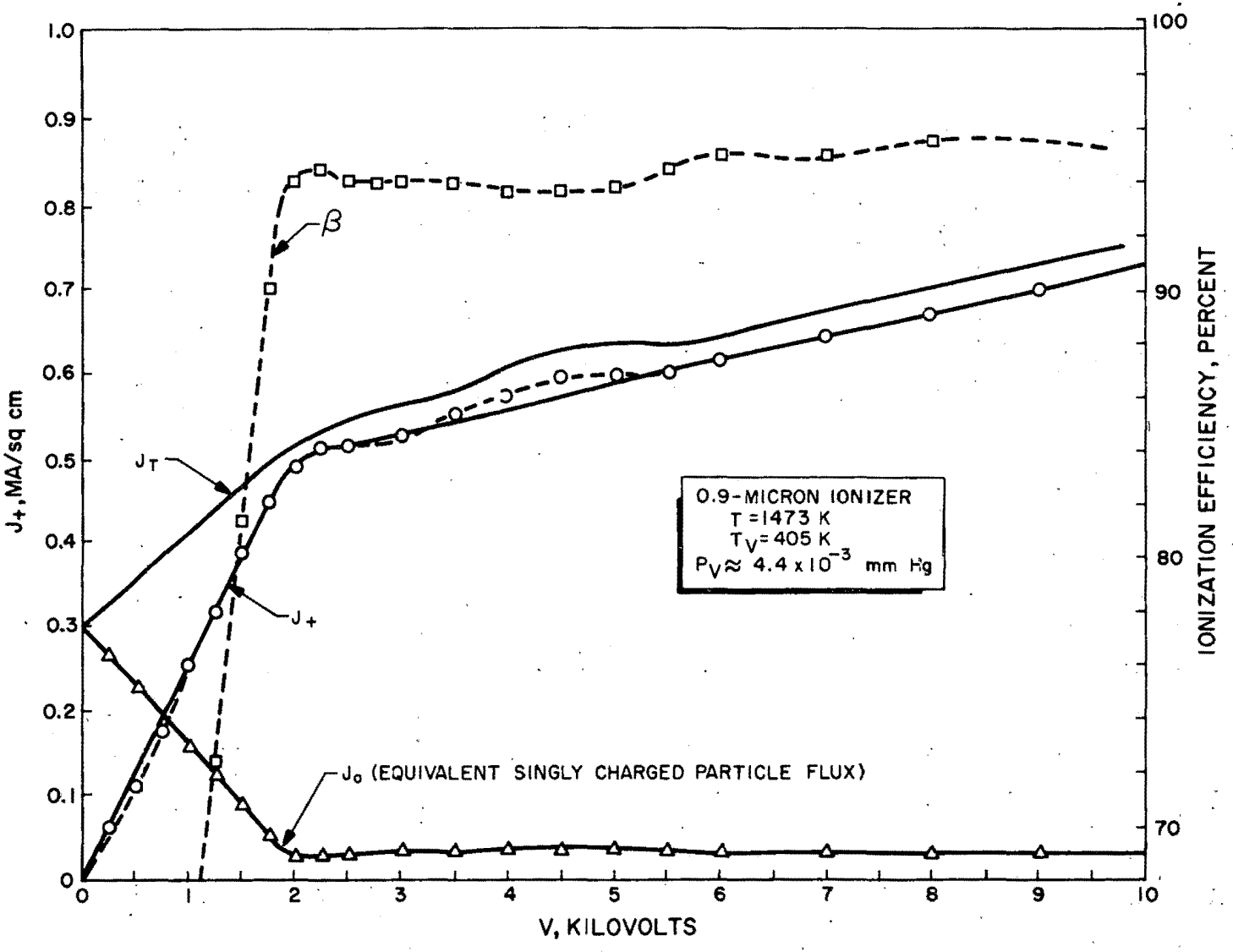

Figure 9. Current vs Voltage Characteristics for 0.9-Micron Ionizer

the emission-limited ion current decreases with increasing electric field in the region which is certainly the weak electric field, and that it reaches a minimum in the transition region or sooner. It is believed that this observed decrease is caused by the anomalous Schottky effect. Because the actual electric fields at the ion-emitting surfaces cannot be known because of the irregular surface structure of a porous ionizer, only a qualitative argument can be given, but they are probably substantially greater than the nominal value defined by the ratio of the voltage applied between the electrodes to the electrode spacing.

Figure 8 illustrates the general observation that the minimum in the ion current density occurs at successively higher values of the electric field as the magnitude of the emission-limited current is increased (by an increase in either the cesium vapor pressure or the ionizer temperature).

5.3 INFLUENCE OF EMISSION-LIMITED CURRENT DENSITY, CESIUM VAPOR PRESSURE, AND IONIZER TEMPERATURE ON THE PERVEANCE

The space-charge-limited current density that can be extracted from a smooth, homogeneous surface (one having a surface over which the extracting electric field and work function are uniform and everywhere identical, and from the entire surface of which, ions are extracted nonpreferentially) is obtained by substituting the conservation-of-energy equation into Poisson's equation, yielding

$$j_+ = \frac{4\epsilon_o}{9} \sqrt{\frac{2q}{m}} \frac{V_a^{3/2}}{\alpha^2} \quad \text{(MKS)} \tag{18}$$

where $\alpha^2 = L^2$ (L is the electrode separation) for the case of plane parallel electrodes, and where α^2 is more complex for the spherical (Ref. 19), cylindrical (Ref. 20), toroidal (Ref. 21), and arbitrary (Ref. 21) cases.

Equation 18 can be written as

$$I_+ = PV_a^{3/2} \tag{19}$$

where P is defined by this equation and is called the perveance of the ion gun.

It is assumed in this derivation for the homogeneous plane parallel case, that in the absence of space charge, the electric field at the ionizer surface is $E_a = V_a/L$ and in the presence of space charge, $E = 0$. For the geometries other than plane parallel, α^2 departs from L^2 because the geometry causes $E_a \neq V_a/L$ (for $\rho = 0$).

For porous ionizers, even in the plane parallel electrode case, a new geometrical parameter, ξ^2, must be substituted for α^2 which varies over the surface even for a given electrode geometry, and which varies with the emission-limited current density. ξ^2 must vary over the surface because the radius of curvature varies over the surface in both magnitude and in sign corresponding to convex and concave regions, which in turn, causes the current-producing electric field intensity to vary over the surface (Fig. 10). Some average ξ^2 can be defined correspondong to a measured perveance (relationship between current and voltage).

The parameter, ξ^2, must vary with the magnitude of the emission-limited current density because of the preferential ion emission. ξ^2 and hence the perveance will vary with both adatom vapor pressure and surface temperature because both influence the adatom flux. The emission-limited current density determines the location of the ion-emitting regions (Fig. 10). For small emission-limited current densities, the ions are extracted from a correspondingly small peripheral region of the advancing front of adatoms which will be located on the pore walls just inside the pore lips

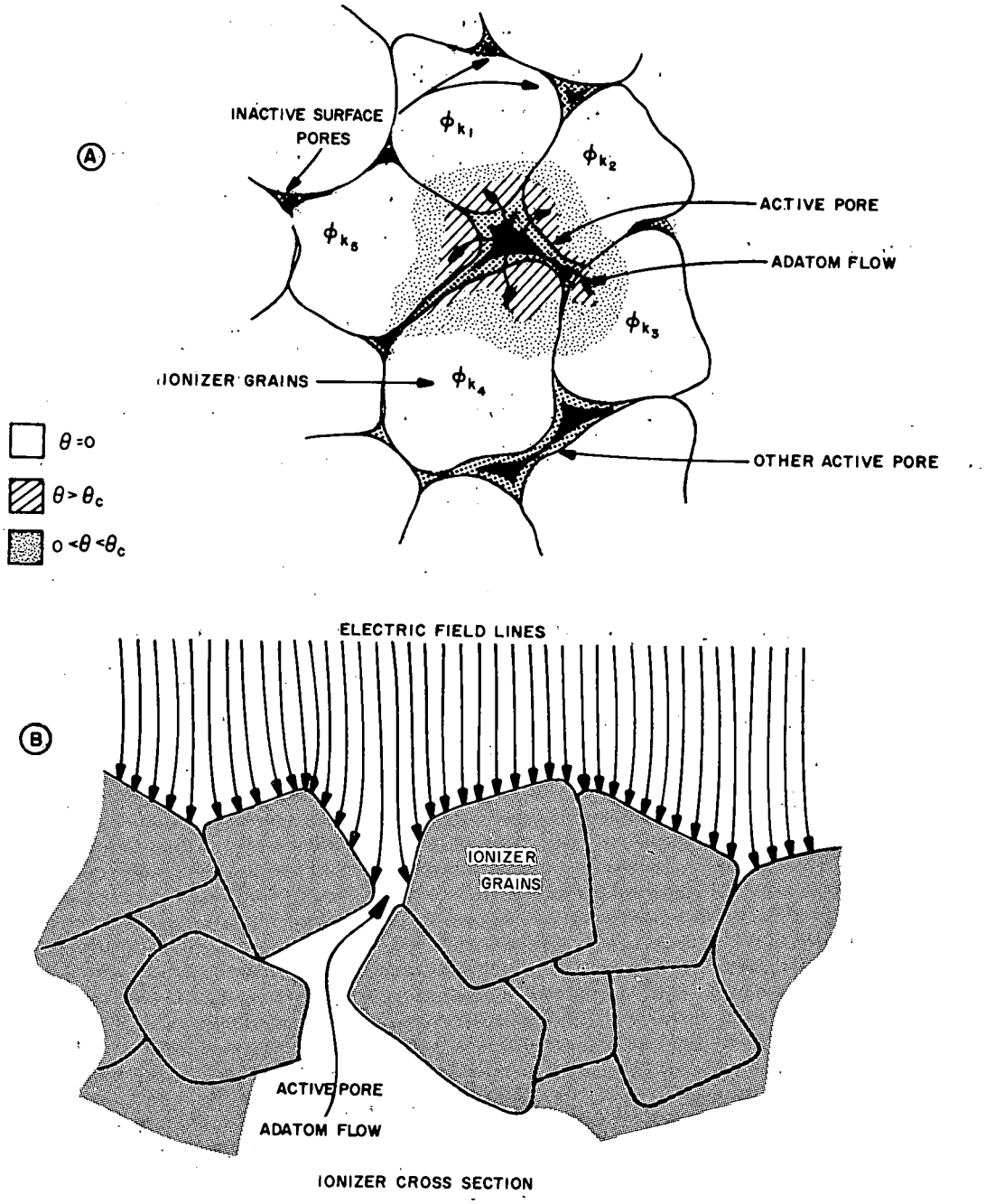

Figure 10. Variation of Electric Field and Surface Coverage, θ, About an Active Ionizer Pore. For Low Flow-rates, the Regions of $\theta > 0$ Can Occur Entirely on the Pore Walls

where the electric field intensity is low, i.e., where only a few electric lines terminate per unit area, resulting in a low perveance. For larger flowrates the peripheral front region of ion extraction will move farther out on the pore wall toward the pore lips, thus moving into regions of higher electric field intensity. Eventually, some ion emission will be occurring from the flatter regions beyond the pore lips where the electric field intensity will remain constant (over regions of area of a few grains or more). Therefore, the magnitude of ξ^2 corresponding to the regions of primary ion emission will at first decrease from the point where emission starts to occur from within the pore openings, until the ion emission is occurring largely from the pore lips when ξ^2 is a minimum and the perveance, a maximum, and beyond which ξ^2 will either decrease much less rapidly or remain constant. Only a qualitative theoretical description of this process can be given because of the irregular shapes of the pore openings, the variations of ϕ_k on the surface, and the fact that as the flux increases, the peripheral region from which ion emission occurs becomes less well defined because the radial spread of adsorbed atoms produces a radial decrease in θ, i.e., the width of the emitting region probably increases. Ions cannot be extracted from regions of the surface except near the periphery of the advancing front because everywhere else, either θ is larger than θ_c, defined as the value of θ corresponding to a ϕ_k less than V_i, or $\theta = 0$.

The qualitative variations of ξ^2 and P with emission-limited current density are illustrated in Fig. 11. The emission-limited current density itself, of course, determines the maximum current or macroscopic or system current density. The macroscopic current density, J_+, is defined as the total ion current obtained from a porous ionizer divided by the total ionizer area. It will be less than j_+, the current density of only the emitting areas, because of the fraction of the ionizer surface composed of local regions incapable of ion emission because $\theta_k > \theta_c$ or $\theta_k = 0$ (for low flowrates). The pores themselves are also relatively non-emitting.

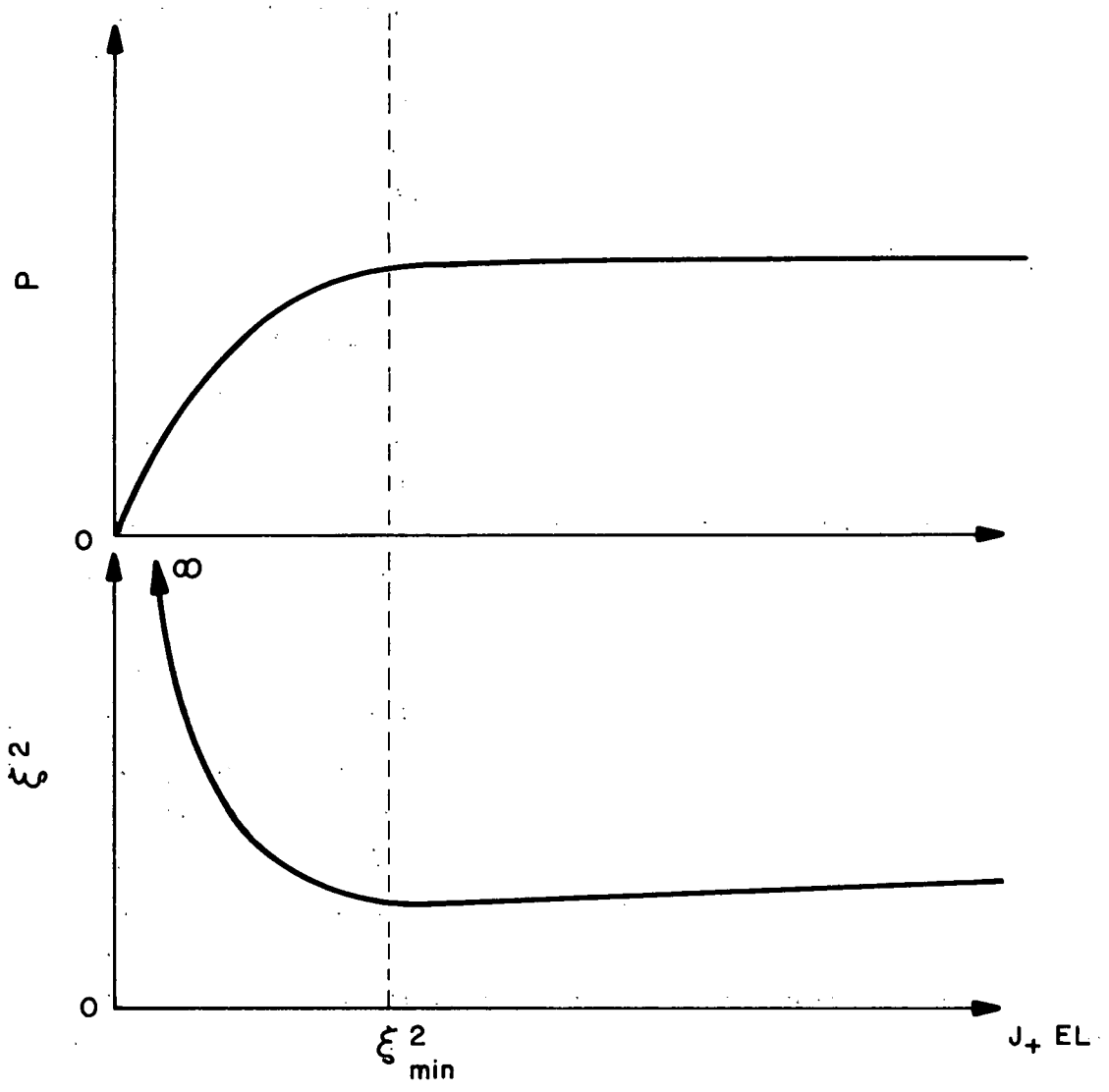

Figure 11. Qualitative Variation of ξ^2 and P With Emission-Limited Current Density

Experimental data for all of the ionizers, given in Fig. 12, illustrate the variation of experimental perveance with the emission-limited ion current density.

These data are consistent with the preceding qualitative theoretical discussion and with Fig. 11. They show quantitatively that the rise in perveance for low J_+ occurs within the first 1/4 ma/sq cm and that the leveling occurs substantially by 0.6 to 0.8 ma/sq cm. The perveance exhibits a slow rise with higher magnitudes of J_+. A few additional data for values of J_+ greater than 6 ma/sq cm for the 5-micron ionizer show the attainment of perveances between 3 and 4 x 10^{-9} amps/volt$^{3/2}$.

The curves of Fig. 12 (with two exceptions which will be discussed) are similar in shape and magnitude and are consistent with the specific periphery theory (defined in section 5.4) which in general indicates an increase in perveance with a decrease in basic powder size (at similar porosities) to the limit where the porous structure tends to disappear. Two exceptions are the data for the 0.9-micron ionizer at 1200 C and the majority of the data for the 44- to 74-micron ionizer. In the first case, as discussed in section 5.5, after the first data were obtained at 1100 C with the 0.9-micron ionizer, the permeability steadily decreased with operating time. Associated increases in densification and number of clogged pores resulted in the sharp decrease in perveance shown in Fig. 12. The data for the 44- to 74-micron ionizer form two curves, one which coincides with those for the other ionizers and one (with many data points) which is much lower. The explanation lies in consideration of the ionization efficiency and in the fact that the emission-limited ion flux, rather than the total flux, is the ordinate. The "normal" curve was obtained for a low value of vapor pressure and the ionization efficiencies were comparable to those of the other ionizers. The variation of emission-limited ion flux was accomplished by varying the ionizer temperature, T. However, the other curve is composed of data obtained at higher values of vapor pressure where both ionizer temperature and vapor

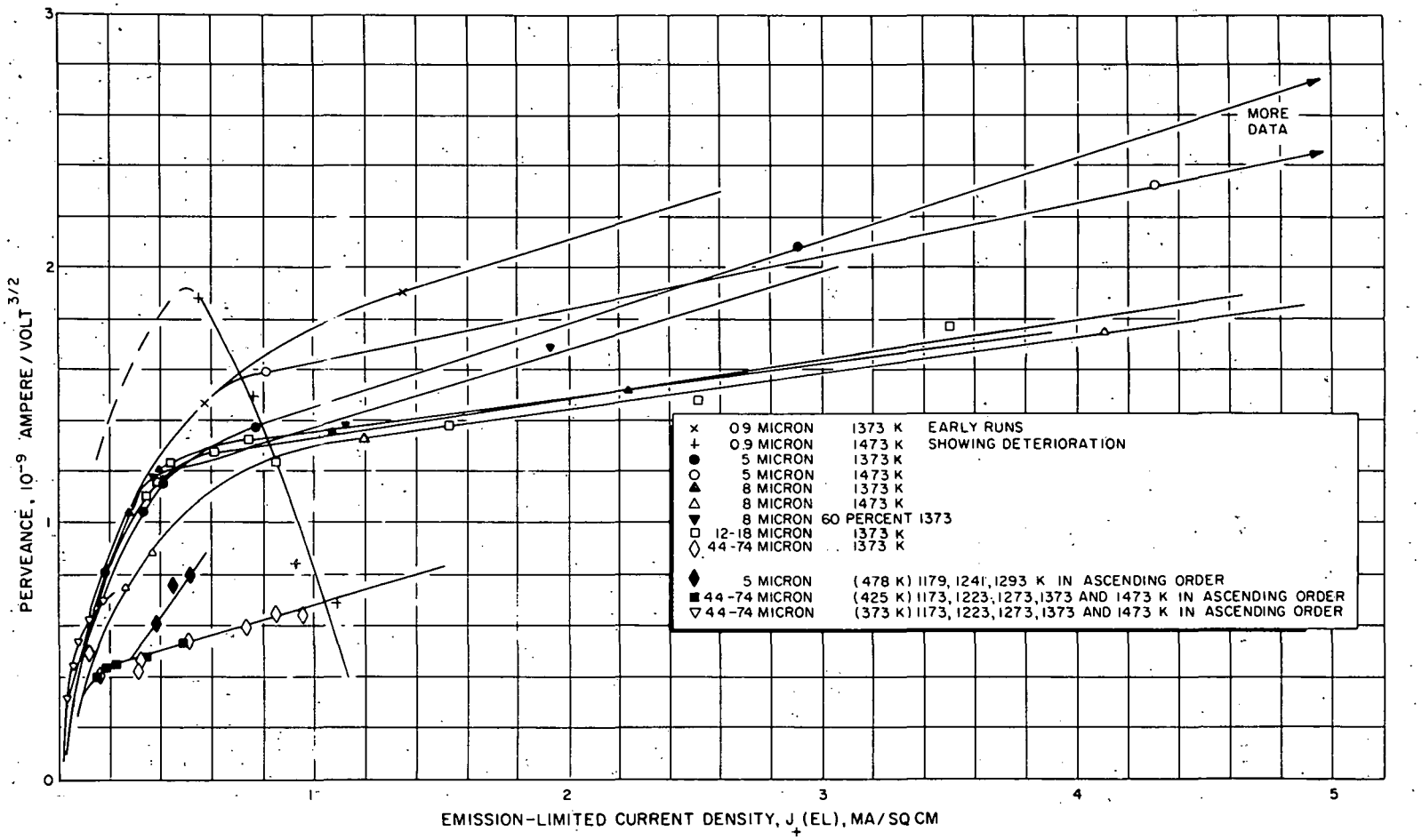

Figure 12. Perveance of all Porous Ionizers as a Function of Ion Current Density

pressures were varied. For the "anamolous" data points, the ionization efficiencies were substantially lower than for the other data points, a situation unique to the 44- to 74-micron ionizer.

In the preceding paragraph, the influence of the ionizer temperature on the perveance is mentioned. The ionizer temperature affects the perveance through its influence on the emission-limited ion flux. The two curves for the 44-to 74-micron ionizer serve to illustrate its quantitative effect. In the region of very low ion flux, the perveance rises rapidly with ionizer temperature because of the intermediate relationship of the ion flux; at higher values of ion flux, the effect of ionizer temperature is far less significant.

5.4 INFLUENCE OF POWDER AND PORE SIZE ON PERVEANCE THROUGH THE SPECIFIC PERIPHERY

For porous ionizers, the pore statistics will have an influence upon the current-producing capabilities of the ionizer, i.e., upon the perveance of the system. Because ions can be extracted from only a fraction of the total ionizer surface for a given set of conditions of vapor pressure and surface temperature, corresponding to that fraction of the surface for which $0 < \theta < \theta_c$ the size and surface density of the pores will affect the ion current density. For low flowrates, $\theta = 0$ over a large fraction of the surface; for high flowrates, $\theta > \theta_c$ over a large fraction. A term can be defined which will serve as a relative measure of the current-producing capabilities of various ionizers under identical conditions of P_v and T. This term will be called the specific periphery, P_s, defined as the total pore periphery per unit area of ionizer surface, measured in reciprocal centimeters, in analogy to the specific surface of a porous ionizer, the total internal pore surface area per unit volume. An exact measure of P_s cannot easily be made because the details of the shapes of the individual pore openings and their surface distributions would need to be known. However, a significant relative value can be obtained by assuming that all of

the pores are circles with a diameter equal to the mean pore diameter obtained from metallographic and gas-flow measurements and that they are spaced uniformly in some geometrical array for which the mean interpore spacing can serve as a measure. For example, if a square array is assumed,

$$P_S = \pi \frac{d}{S^2} \tag{20}$$

and if a hexagonal close-packed array is assumed,

$$P_S = \frac{2\pi d}{\sqrt{3}\, S^2} = 3.6 \frac{d}{S^2} \tag{21}$$

Arbitrarily choosing the hexagonal close-packed values 3.6 d/S^2, the relative values of P_s have been calculated for the ionizers studied and are presented in Table 2. The left-hand values of d and S are from the gas-flow measurements, the right-hand values are from the metallographic studies, and the center values are these felt to be the most accurate or are an average and have been used to calculate the quoted values of P_s. It is seen that the 5-, 8-, and 12- to 18-micron ionizers all give nearly the same value, while the 44- to 74-micron ionizer yields a value much lower, ~ 0.4 of the former, and the 0.9-micron ionizer shows a much higher value, ~ 3 times the first. Experimentally measured values of the perveance for these five ionizers obtained at T = 1373 K and P_v = 0.06 mm Hg are also displayed in Table 2 for comparison to the values of the specific periphery.

Experimental perveances for the 8-, 12- to 18- and 44- to 74-micron ionizers follow quite well the pattern of the specific pheripheries, as the normalized values show (Table 2). The values for the 5- and 0.9-micron ionizers are 40 and 50 percent low, respectively. It is noted, however, that the densities to which these ionizers were sintered are different. Those of the 8-, 12- to 18-, and 44- to 74-micron ionizers are very similar, while those of the 5- and 0.9-micron ionizers are considerably higher. Because of the higher densities of the latter two, more of the pores which are exposed on the surface may be inactive as a result of internal blocking.

TABLE 2

COMPARISON OF CALCULATED SPECIFIC PERIPHERIES AND EXPERIMENTAL PERVEANCES FOR THE POROUS TUNGSTEN IONIZERS

Basic Grain Diameter, microns	0.9			5			8			12-18			44-74		
Sintered Density, Percent of Theoretical Maximum	76			80			68			68			63		
Mean Pore Diameter, d, microns	1.1	1.1	1.3	---	2.8	2.8	5.9	6.0	6.0	16	13	9.7	35	37	40
Mean Interpore Spacing, S, microns	5.4	5.4	4.2	---	12	12	---	17	17	27	27	27	61	70	77
Specific Periphery $P_S = 3.6\ d/S^2$ microns-1	0.13			0.070			0.062			0.064			0.027		
Experimental Perveance, P, amp/volt 3/2 x 10^9 (P_V = 0.06 mm Hg, T=1100C)	1.59 to 0.60			1.06			1.53			1.60			0.63		
P_S, Normalized to P_S for 12-18 ionizer	.3.3			1.75			1.55			1.60			.67		

Thus the measured perveance could be expected to be lower than the calculated one. Also, the measured perveance of the 0.9-micron ionizer decreased with operating time (particularly at high temperatures) as discussed in section 5.5. This deterioration was attributed to additional sintering implying that pores gradually become closed or clogged internally.

5.5 EFFECT OF OPERATION ON CHARACTERISTICS OF 0.9-MICRON IONIZER

In the case of the 0.9-micron ionizer, the possibility of changes in the operating characteristics with time at high temperatures existed because the sintering conditions used to obtain the 76-percent density were only 15 minutes at 1300 C, and because of the severe changes in porous structure described in 3.2 which occurred for the 0.1-micron ionizer at normal ionizer operating temperatures. It was expected that operation at 1300 C would cause additional sintering, resulting in further densification, pore closing, and greater resistance to flow, and that prolonged operation at 1200 C might also produce observable changes. That this did occur, is clearly demonstrated by the data presented in Table 3 and Fig. 13. In Table 3, the ionizer temperature and cesium vapor pressure are presented for a few representative runs, together with an operating history which gives the cumulative hours of operation at 1100, 1200, and 1300 C for each of these selected runs, and the measured values of three important operating characteristics: J_o, the neutral cesium flux for no electric field (no ion current); P, the experimental perveance; and β_{max} the maximum ionization efficiency (at emission-limited current conditions).

Because the significance of the J_o data is difficult to see readily in the form presented in Table 3, the neutral flux is plotted as a function of the cesium vapor pressure in Fig. 13. The curve formed by data points 1 and 2 (for T = 1100 C) is what would be expected from work with other ionizers. These data were obtained before the ionizer had ever been operated at temperatures above 1100 C. Then point 3 was the first one obtained at 1200 C and a dashed curve is shown, corresponding to what would be expected for a T = 1200 C curve. However, points 4 and 5 show that after several hours of

TABLE 3

HISTORY FOR 0.9-MICRON IONIZER

Run Number	T, C	T_V, C	P_V mm Hg	History, hours			$J_o \times 10^{-15}$ $\frac{\text{atoms}}{\text{sq cm-sec}}$	$P \times 10^9$, $\frac{\text{amperes}}{\text{volt}^{3/2}}$	β_{max}, percent
				at 1100 C	at 1200 C	at 1300 C			
1	1100	196	0.073	3	0	0	2.0	1.8	94 1/2
2	1100	230	0.25	4	0	0	4.0	1.5	94 1/2
3	1200	131	0.0039	4	3	0	1.9	1.9	94 3/4
4	1200	190	0.057	4	5	0	2.6	1.5	95
5	1200	272	0.97	6	13	0	4.5	0.78	96 1/2
6	1200	270	0.88	9	18	1	2.1	0.69	97 1/2
7	1200	310	2.6	13	19	12	1.6	0.42	98 3/4

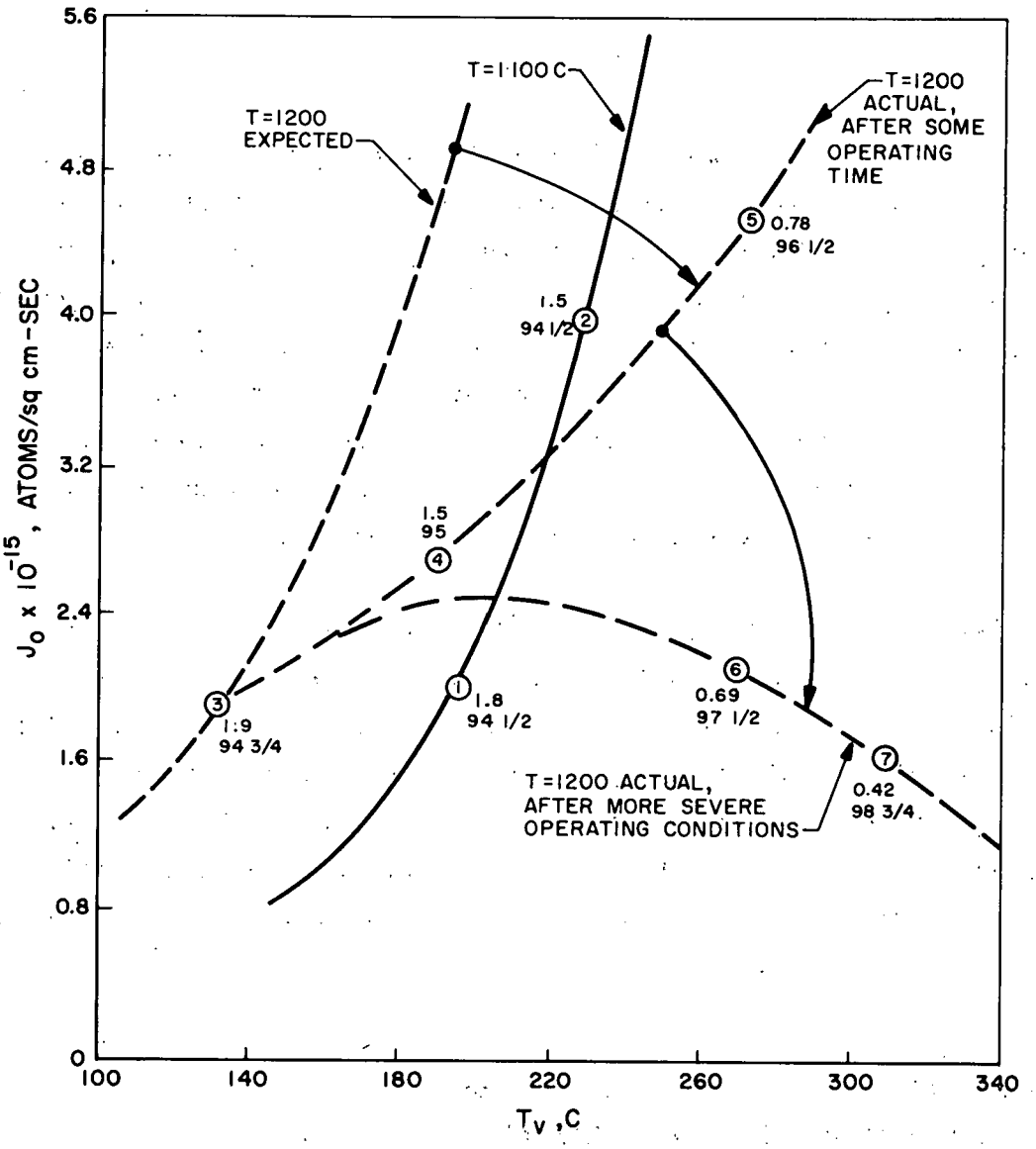

Figure 13. Effect of Operating Time at High Temperature on Flowrate of Neutral Cesium Through 0.9-Micron Ionizer. Data Point Numbers Represent the Run Number of Table 3 in Which the Operating History is Given. The First Number by the Data Point is the Perveance ($\times 10^9$) and the Second Number is the Ionization Efficiency

operation at 1200 C, a much larger cesium vapor pressure was required to produce a corresponding neutral flux. Point 6 was obtained at the same vapor pressure and ionizer temperature as point 5, but the ionizer had been subjected to a temperature of 1300 C for one hour, four times the sintering time at the sintering temperature. The neutral flux is seen to have decreased to less than 50 percent of the former value. Point 7 was obtained after long operation at 1300 C, such that nearly all further sintering effects should have occurred. The neutral flux is down still further even at a 40-degree-higher vapor temperature.

The corresponding effects on P and β can easily be seen in Table 3 . The perveance changed less rapidly at first, but after longer times at 1200 and 1300 C, it dropped sharply to finally less than 25 percent of the original value, implying that many of the formerly active pores had closed or become blocked. The emission-limited ionization efficiency increased only slowly at first, but by the final selected run (No. 7), had increased to a value corresponding to a reduction in the neutral fraction of more than 75 percent.

5.6 FACTORS INFLUENCING THE FLOW OF CESIUM THROUGH POROUS TUNGSTEN IONIZERS (ANALYTICAL)

In Ref. 8, the various modes for the passage of gases through porous media are considered in detail. The validity of the basic assumptions underlying their application to the case of alkali metals and refractory metal porous ionizers for surface ionization systems is examined. Comparable equations governing the flow through the porous ionizer are developed. Consideration of the basic assumptions for the equations and the dependence on pressure, temperature, and porous structure, compared with the experimental results, indicates that the transport occurs

primarily as simple (equal to or less than monolayer) surface diffusion or migration, with free molecular flow contributing an increasing fraction of the total flow as the flowrate increases and that viscous flow, turbulent flow, multilayer adsorptive flow, and flow by capillary condensation are at most secondary modes of transport.

In the treatment of the transport modes and their relative importance, the degree of sorbability of the particular transport a material on the particular porous medium is of importance. The pure gas flow modes, viscous and free molecule, will predominate for substances with low sorbability (at a given pressure), while the sorptive modes, monolayer surface diffusion, multilayer surface diffusion, and the existence of capillary condensation will become relatively more important for more sorbable substances. For the particular cases of porous tungsten (and possibly the refractory metals in general), gases generally used for porous material permeability measurements (H_2, N_2, dry air, He, Ne, A, and Kr--H_2, dry air (N_2), and A in this work) are nonabsorbed (Ref. 22) and the pure gas flow modes are applicable as shown in section 2 where the free-molecule flow mode predominates up to about 100 mm Hg pressure when the effects of viscous flow begin (Fig. 1). The particular transition pressure increases with the mean pore diameter. Contrarily, the alkali metals are very sorbable on tungsten; the cesium-tungsten system possibly represents the most sorbable combination of all elemental species because the surface tension of liquid cesium is the lowest, while that of tungsten is the highest of all (51) metals (Ref. 23). The wetting conditions between cesium and tungsten are probably the best of all combinations of materials. The flow of cesium on tungsten by wetting (surface tension effects) increases with temperature above the melting point so that at the temperatures of cesium feed systems, some flow of cesium may actually occur by surface diffusion with little pressure drop. For these reasons it is expected that for the transport of cesium through porous tungsten, the sorptive modes will be significant.

The comparable equations developed for four flow modes applied to this system are:

For viscous flow,

$$n_o = \frac{\pi N_a}{256} \left\{\frac{Hd^4}{L}\right\} \left\{P_V^2\right\} \left\{\frac{1}{T\eta_v(T)}\right\} \tag{22}$$

For free molecule flow,

$$n_o = \frac{1}{3M} \left(\frac{\pi N_a}{2k}\right)^{1/2} \left\{\frac{Hd^3}{L}\right\} \left\{P_V\right\} \left\{T^{-1/2}\right\} \tag{23}$$

For surface diffusion (monolayer or less),

$$n_o = \frac{\alpha}{4} \left(\frac{N_a}{kM}\right)^{1/2} \left\{\frac{H\delta}{L} \left(\frac{L}{L_c}\right)^2\right\} \left\{P_V\right\} \left\{T^{-1/2}\ e^{-V_m/kT}\right\} \tag{24}$$

For capillary condensation

$$n_o = \frac{\pi k N_a^2}{4M^2} \left\{\frac{Hd^2k_p}{L}\right\} \left\{\ell n \frac{P_V}{P_o}\right\} \left\{\frac{T\rho_c^2(T)}{\eta_c(T)}\right\} \tag{25}$$

In each case, the constant terms precede the first bracketed term, the first bracketed term contains the dependence on the porous structure, the second is the pressure dependence, and the third shows the temperature dependence. The terms are defined below:

N_a = Avagadro's constant

k = Boltzmann's constant

M = molecular weight

α = adsorption coefficient

H = number of pores per unit ionizer area

d = mean pore diameter

L = thickness of porous medium (ionizer)

L_c = mean length of pore in porous medium ($L_c > L$)

δ = average distance between adsorption sites

k_p = permeability of porous medium (ionizer)

P_V = vapor pressure of the transport substance (on upstream side of ionizer)

P_o = pressure of space or vacuum tank (on downstream side of porous medium)

T = temperature of porous medium

$\eta_v(T)$ = viscosity of vapor phase of transport substance

$\eta_c(T)$ = viscosity of condensed phase of transport substance

$\rho_c(T)$ = density of condensed phase of transport substance

V_m = activation energy for migration (diffusion) of transport material adsorbed on porous medium material (0.59 eV/atom for Cs-W)

n_o = the neutral flux from the downstream (ionizing) surface of the porous medium

Viscous flow is ruled out relative to free molecular flow because the magnitude of $K \equiv \lambda/D$, the ratio of the mean free path of the transport molecule to the pore diameter, which is 10^3 to 10^6. The three remaining modes must be considered for the case of cesium flow through porous tungsten and compared to the experimental results. The details of the derivations of Eq. 22 through 25 and a discussion of the assumptions

regarding their applicabilities are given in Ref. 8. An outline of the derivations and assumptions in included in the following sections.

It is interesting to note that the derivation of the free molecule mode requires the assumption of the existence of adsorption of the transport molecules for a certain length of time following collisions with the porous medium channel walls.

Provided that the volume of the adsorbed surface diffusion film comprises a negligible part of the total pore volume, it should exert no influence on the steady-state flow of the gaseous phase, whether viscous or free molecule, (Ref. 22). Therefore, simultaneous transport by both free molecular flow and surface diffusion will occur.

In regard to the sorbability of substances on tungsten, two other elements should be mentioned. N_2, H_2, and the inert gases have been described as nonsorbable, and the alkali metals as very sorbable. Oxygen and carbon are two elements which react in a third way, by chemisorption. They are bound to the tungsten surface by much higher energies (heats of adsorption) and hence are much more difficult to remove. They migrate according to different laws and, in time, can penetrate deeply into the tungsten structure. As described elsewhere, these two elements cannot be completely removed by gettering or by high-temperature flashing of tungsten surfaces, though they can be removed by field emission etching. Any oxygen or carbon impurities in the diffusing cesium will become chemisorbed in the tungsten ionizer over the period of operation. As discussed elsewhere, oxygen may have a favorable effect because it increases the work function of the ionizing surface, but carbon probably has an opposite effect, and over a long operation time might tend to clog narrow flow channels where it is gradually chemisorbed.

5.6.1 Surface Diffusion

Basic Assumptions:

1. Steady-state flow (no transient effects)
2. Accompanied by some amount of flow in the gas phase, either viscous or free molecule modes or both, each (gas flow and surface diffusion) along its own concentration gradient.
3. To each value of pressure corresponds a value of volume concentration, c, so that a value of the adsorption coefficient, α, can be defined which is relatively independent of c.
4. Assumption of a model porous structure: a bundle of parallel channels (not necessarily straight) of average length, L_c.
5. No capillary condensation.
6. An irregular, energetically unsmooth, adsorption surface with equal site adsorption energies but with an energy barrier to surface migration, V_m, plus others covered in the derivation (Fig. 14).

Derivation: (This derivation is given in more detail here because of the conclusion that this mode is predominant in the case under consideration.) Fick's first law of diffusion can be stated: the number of atoms diffusing per unit area per unit time (flux), n_o, equals the diffusion coefficient, D, times the volume concentration gradient of atoms, c, in moles per unit volume, in the direction opposite the flow

$$n_o = - N_a D \frac{\partial c}{\partial x} \quad \frac{\text{atom}}{\text{sq cm-sec}} \tag{26}$$

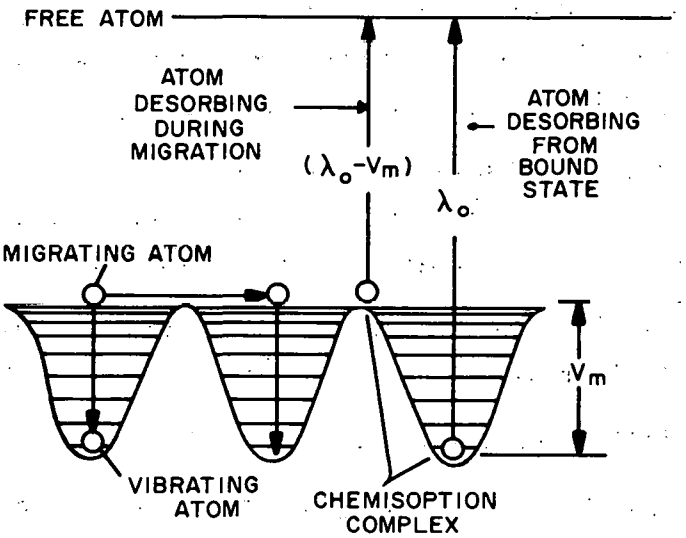

V_m = potential barrier to surface migration of an adsorbed atom

λ_o = heat of desorption (evaporation) of an adsorbed atom

For cesium on tungsten:

V_m = 0.59 eV ad λ_o = 2.7 eV

Figure 14. Potential Diagram for Surface Migration

This equation applied to two-dimensional surface diffusion or migration through a porous medium (Ref. 22) can be stated: the number of adatoms diffusing per unit perimeter per unit time equals the diffusion coefficient times the surface concentration gradient of adatoms, or the adsorbed atoms per unit area of the porous medium per unit thickness. The perimeter is ALS_V/L_c and the surface concentration gradient is $\Delta c_s/S_V L_c$, where A is a unit area and L is the thickness of the porous medium, L_c is the average porous medium channel length ($L_c > L$), S_V is the specific surface of the porous medium (internal surface area per unit volume), and c_s is the volume concentration of adsorbed atoms ($\partial c_s/\partial x \longrightarrow \Delta c_s/L$). Substituting:

$$n_o = -N_a D_s \left(\frac{L}{L_c}\right)^2 \frac{\Delta c_s}{L} \tag{27}$$

$(L/L_c)^2$ represents a tortuosity (Ref. 22) or pore structure factor; c_s is related to the gaseous concentration, C, by the adsorption coefficient, α. Thus,

$$\Delta c_s = \alpha \Delta C \tag{28}$$

i.e., $\partial c_s/\partial x = \alpha \partial C/\partial x$. Now ΔC is related to the pressure drop across the porous medium and the medium temperature by

$$\Delta C = -\frac{\Delta P}{RT} \tag{29}$$

Therefore,

$$n_o = N_a D_s \alpha \left(\frac{L}{L_c}\right)^2 \frac{\Delta P}{RTL} \tag{30}$$

If the porous medium surfaces were smooth with no definite adsorption sites, there would be no barrier to surface migration of adsorbed atoms. If, in addition, the degree of surface coverage, θ, is small, the kinetic theory of a two-dimensional gas could be applied, which would yield

$$D_s = 1/2\ \bar{v}_{th}\ \lambda_s \tag{31}$$

where $\bar{v}_{th}$ is the mean thermal velocity and λ_s is the surface mean free path. However, for a polycrystalline sintered powder metallic medium, (e.g., sintered tungsten), the surface consists of many irregularly spaced adsorption sites which are the crystal face steps (Ref. 24). For example, cesium slides to a crystal face step when adsorbing onto a tungsten surface. Migration of a cesium atom then consists of jumps among adsorption sites, probably as a jump to a surface followed by a slide to a crystal face step where it remains for a characteristic time, τ. The adsorption energy is similar for all sites, with possible small variations depending upon which crystal faces comprise the steps, but there is an energy barrier between sites and a characteristic activation energy for migration, V_m (in ergs or eV per atom), for every system (V_m = 0.59 eV/atom for Cs on W) required before surface migration can occur to another site. A larger energy is required for desorption, λ_o (atom) or λ_+ (ion). Therefore surface migration is more probable than desorption (evaporation) from any site. For this situation, a method has been developed (Ref. 25) for calculating the associated diffusion coefficient, $D_s = \delta^2/2N\tau$, where N is the number of dimensions. Thus, for two-dimensional surface diffusion,

$$D_s = \delta^2/4\tau \tag{32}$$

where

δ = average distance between adsorption sites

τ = average characteristic time a site is occupied

The time, τ, is related to the period of site vibration (Fig. 14), τ_o, by

$$\tau = \tau_o \, e^{\frac{V_m}{kT}} \tag{33}$$

where

V_m = surface migration activation energy

T = surface temperature

τ_o can be related roughly (Ref. 22) to the time needed to cover one δ at the thermal velocity, $\bar{v}_{th}$, or

$$\tau_o = \delta / \bar{v}_{th} \tag{34}$$

Combining Eq. 32, 33, and 34:

$$D_s \doteq 1/4 \; \delta \; \bar{v}_{th} \, e^{-\frac{V_m}{kT}} \tag{35}$$

For a two-dimensional gas, $\bar{v}_{th} = (N_a kT/M)^{1/2}$, and substituting Eq. into Eq. 30 yields

$$n_o \doteq \frac{\alpha}{4} \left(\frac{L}{L_c}\right)^2 \left(\frac{N_a}{kTM}\right)^{1/2} \frac{\delta \Delta P}{L} \; e^{-\frac{V_m}{kT}} \tag{36}$$

If the pressure at the downstream side is very much less than that at the upstream side, $\Delta P = P_u - P_d = P_u$. In the case of pressurized flow

through a porous ionizer, $P_u \rightarrow P_V$, which is 10^3 to 10^6 times larger than the downstream vacuum tank pressure, and $>10^{12}$, the pressure of space. Substituting P_V for ΔP, grouping dependence terms, and accounting for the area of the porous medium surface which is composed of pores:

$$n_o = \left[\frac{\alpha}{4}\left(\frac{N_a}{kM}\right)^{1/2}\right]\left[H\left(\frac{L}{L_c}\right)^2 \frac{\delta}{L}\right]\left[P_V\right]\left[\frac{e^{-\frac{V_m}{kT}}}{\sqrt{T}}\right] \quad (37)$$

where the first bracketed term is a constant, the second gives the dependence on the porous medium structure, the third is the pressure dependence, and the fourth is the temperature dependence.

Arguments for the applicability of surface diffusion to the case in question are as follows:

1. The pressure dependence agrees with the experimental observations of this work.
2. The temperature dependence is consistent with the observation of this work, particularly at low flowrates.
3. The value of n_o calculated from this equation for a particular ionizer is of the same order of magnitude as the measured value of n_o for the same ionizer. The calculated value could vary somewhat with the assumption of the values for α and L/L_c (each of which, however, could be wrong by no more than a factor of two), but the order of magnitude is correct. The largest pore ionizer was chosen for the calculation because of the probability that fewer of the pores are blind (dead end) than those of smaller powder size.

5.6.2 Free Molecular Flow

Basic assumptions:

1. Gas flow limited by collisions between molecules and channel walls, not by intermolecular collisions.
2. Adsorption on the channel walls occurs for a time sufficient for diffuse reflexion (the velocity and direction of emission become independent of the velocity and direction of collision) to occur. For nonsorbable gases such as H_2, N_2, and the inert gases, this occurs but is negligible and unmeasurable. For a very sorbable element like cesium, it occurs to a large extent, to the point of allowing the surface diffusion transport mode to be significant.
3. $L_c \geq 100\ d$, where L_c is the channel length and d is the pore diameter. In the case under consideration, $L_c > 10^{-1}$ cm and $d \approx 10^{-3}$ cm. In addition, the crookedness and variation of diameter of the pores will aid in the validity of application.
4. $\lambda/d \gg 1$ where λ is the mean free path of the gas and d is the pore diameter. In this case $\lambda/d \approx 10^3$ to 10^6 depending upon P_V.

Derivation:

$$n_o = HN_a\nu = \frac{HN_aFP}{MkN_aT} \tag{38}$$

where

ν = flowrate in molecules/sec per orifice

F = orifice conductance

all other terms are as before

Substituting (Ref. 26),

$$F = 1/W \sqrt{\rho/P} \tag{39}$$

and

$$W = \frac{\sqrt{2\pi}\, v_a}{4F} = 3\sqrt{\frac{2}{\pi}}\, \frac{L}{d^3} \tag{40}$$

Using

$$F = \frac{4}{3} \frac{v_a}{\int_0^L \frac{P}{A^2}\, d\ell} = \frac{v_a \pi d^3}{12L} \tag{41}$$

yields

$$n_o = \frac{Hd^3P}{3LM} \left(\frac{\pi N_a}{2\ kT}\right)^{1/2} \tag{42}$$

Arguments for the applicability of free molecular flow are as follows:

1. This mode has been shown to be valid for this application when the nonsorbable gases are used, and therefore should apply to the unadsorbed mode for cesium.
2. The pressure dependence agrees with that measured in this work.
3. The temperature dependence for this mode alone does not agree with that measured in this work but combined with the equation for surface diffusion, it accounts for the observed temperature dependence at higher flowrates. [The free molecule flowrate decreases with $T(T^{-1/2})$, and the experimentally observed flowrate increases with $T(\geq T^1)$].

5.6.3 Capillary Condensation

Basic assumptions:

1. Action of capillary surface tension forces and not surface diffusion.
2. The pressures on the opposite sides of the porous medium, P_V and P_o, are different and both are less than P_s, the normal saturation vapor pressure, yet greater than the vapor pressure required to saturate the largest pores.
3. Both P_V and P_o are greater than P_e, the pressure at which evaporation occurs (otherwise evaporation will destroy the condensed phase).

Derivation: The volume flowrate of the condensed phase is

$$\frac{\pi d^2}{4} u_c \tag{43}$$

where

u_c = linear flowrate of the condensed phase

d = mean channel or pore diameter

The mass flowrate is

$$\frac{\pi d^2}{4} u_c \rho_c \tag{44}$$

where

ρ_c = density of the condensed phase

Therefore,

$$n_o = \frac{N_a H \pi d^2 \, u_c \rho_c}{4M} \text{ atoms/sq cm-sec} \tag{45}$$

where

H = number of active pores or channels per unit surface area

N_a = Avagadro's number

M = molecular weight of the transport substance

Now

$$u_c = \frac{k_p}{\eta_c L_c} \Delta P_c \tag{46}$$

where

k_p = permeability of the porous medium

η_c = viscosity of the condensed phase

L_c = length of the flow channel ($L_c > L$, the thickness of the porous medium)

and

$$\Delta P_c = \frac{\rho_c k N_a T}{M} \ell n \left(\frac{P_V}{P_o} \right) \tag{47}$$

from Ref. 22, where

k = Boltzmann's constant

P_V = upstream vapor pressure of the uncondensed phase

P_o = downstream pressure (the pressure of space or a laboratory vacuum tank)

Putting Eq. 46 and 47 into Eq. 45 yields

$$n_o = \frac{\pi k N_a^2}{4M^2} \cdot \frac{Hd^2 k_p}{L_c} \cdot \frac{\rho_c^2 T}{\eta_c} \cdot \ell n \left(\frac{P_v}{P_o} \right) \qquad (48)$$

In general, ρ_c and η_c are functions of temperature. For the case of cesium in the temperature range used in ion engine applications, 1000 to 1500 K, both of these quantities are relatively independent of temperature; ρ_c varies only 7 percent and η_c, approximately 1 percent over this range, with the average values being, ρ_c = 1.61 gm/cu cm and η_c = 276 gm/cm-sec (Ref. 27). Therefore, it is assumed that the temperature dependence for capillary flow would be simply as T.

Arguments against the applicability of capillary condensation to the case in question:

1. It seems doubtful that basic assumptions 2 and 3 will apply.
2. The pressure dependence definitely does not agree with the experimental observations of this work, regardless of the value assumed for P_o at the ionizer surface.
3. The value of n_o calculated with this equation is at least three orders of magnitude larger than a corresponding value of n_o measured in this work for a particular ionizer and set of pressure and temperature conditions.

5.7 EXPERIMENTAL FACTORS INVLUENCING FLOW OF CESIUM

Four primary factors influence the cesium flow through the ionizer and, hence, the rate of delivery of the cesium to the front ionizer surface. These factors are (1) the cesium vapor pressure at the rear ionizer

surface, (2) the ionizer (porous plug) permeability, (3) the ionizer temperature, and (4) the electric field at the front surface and the resulting rate of ion formation and extraction. The way in which these parameters influence the flow of the transport specie through a porous medium are discussed in more detail in Ref. 8. For filament ionizers, only the vapor pressure (or beam flux) determines the total particle flux (ions plus neutrals) which can leave the ionizer surface; this quantity is independent of the ionizer temperature and the surface electric field, and no permeability concept exists.

5.8 INFLUENCE OF CESIUM VAPOR PRESSURE AND IONIZER PERMEABILITY

The influence of the vapor pressure at the rear of a porous ionizer is two-fold. It determines the flux of incident adatoms onto the rear surface and it produces the pressure drop across the porous plug. The porous ionizer structure determines its permeability. At constant ionizer temperature and in the absence of any electric field and subsequent ion emission, these two quantities should determine the flowrate through the ionizer.

The data which illustrate this relationship are presented in Fig. 15 for all of the ionizers studies, and Fig. 16 is one representative case showing the way in which the actual data points occur. In every case, data for an ionizer temperature of 1373 K are presented, and in some cases, data are also shown for 1473 K. The curves of n_o (the neutral particle flux) are for no electric field and consequently no ion emission. These curves then show the effect of P_V and permeability alone. In all cases, a linear relationship is exhibited between n_o and P_V, when P_V is the only variable influencing flow. This is consistent with either the free molecular (Knudsen) flow regime or surface diffusion in

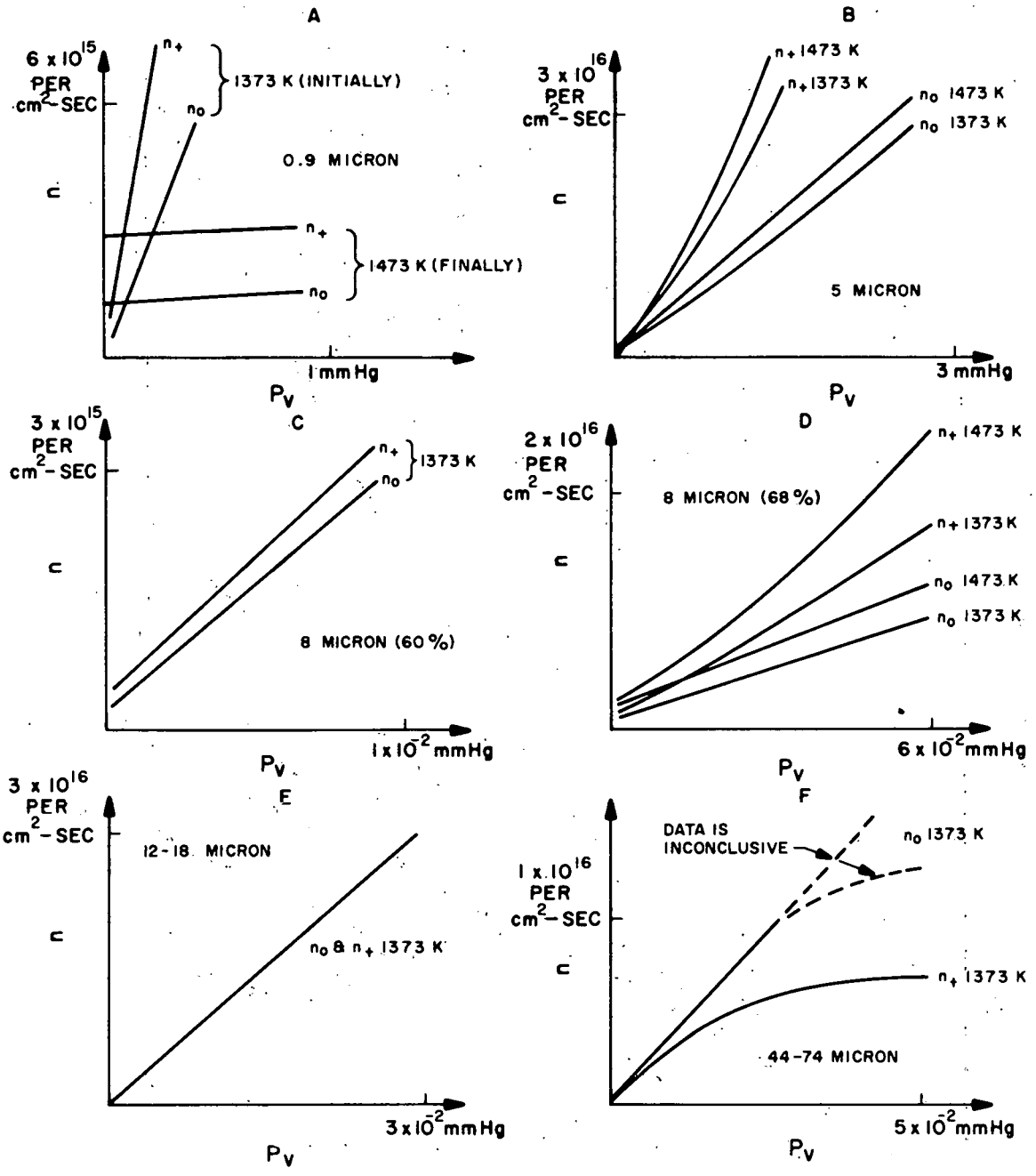

Figure 15. Particle Fluxes vs Cesium Vapor Pressure Relationships. The values of n_0 are for no electric field and hence no ion emission

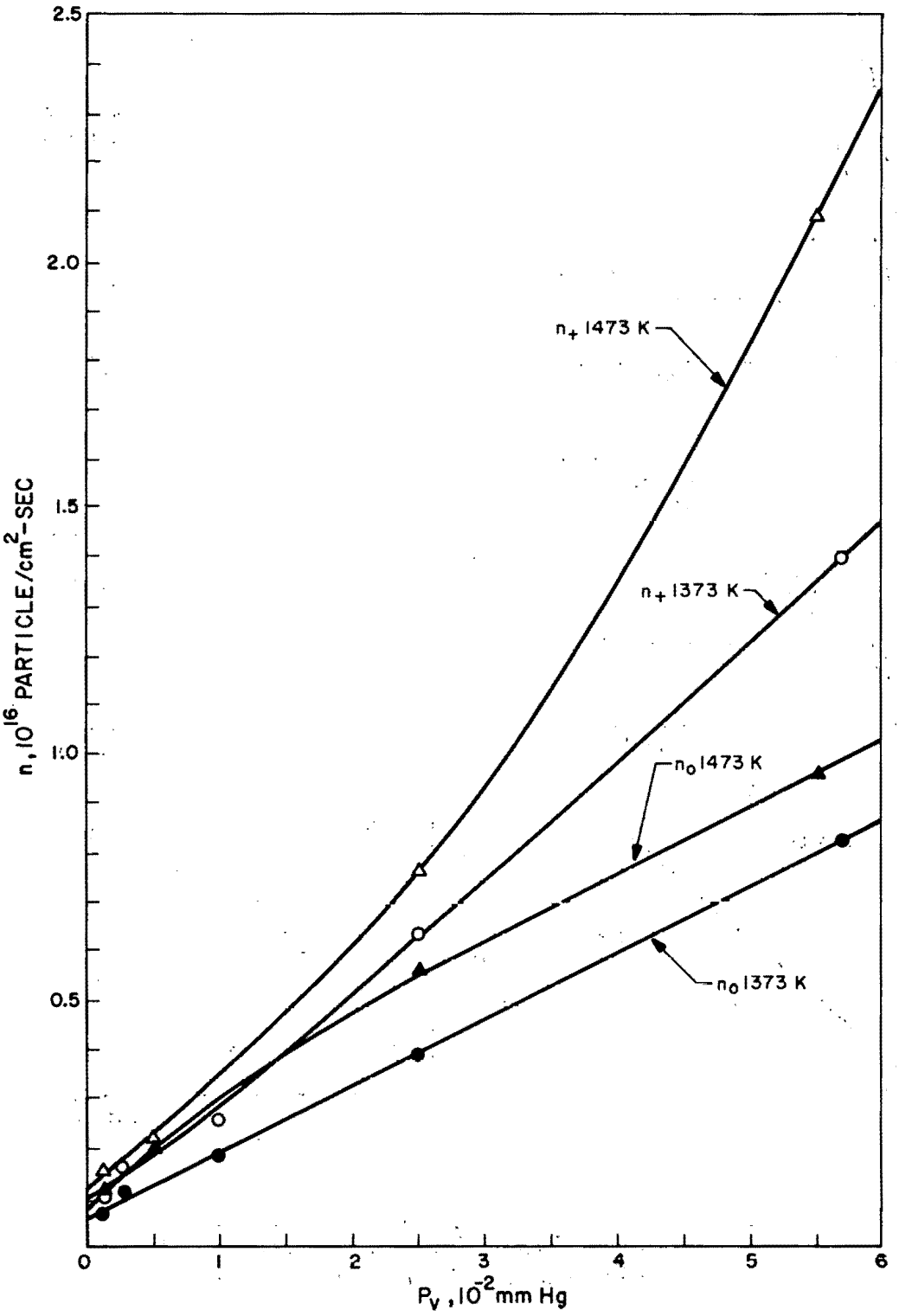

Figure 16. Particle Fluxes vs Cesium Vapor Pressure for 8-Micron (68-percent Dense) Ionizer

each of which the flowrate is proportional to the pressure drop. It is not consistent with flow by capillary condensation. The slopes of the curves of n_o vs P_V (E = 0) for the various ionizers are displayed in Table 4 together with the ionizer permeabilities from the gas flow measurements. The slopes are $\Delta n_o/\Delta P_V$ in atoms/sq cm-sec-mm Hg. A favorable comparison is observed in all cases except for the largest powder size.

The data for the 0.9-micron ionizer show the effect of operating time discussed in more detail in section 5.5. The steep curves (at 1373 K) were taken early in the ionizer's history, and can be used to compare with the other ionizers for powder size effects. The nearly flat curves (at 1473 K) were obtained at approximately the time that the permeability measurement reported in Table 1 was made, and should therefore be used in comparison with the measured permeability.

5.9 INFLUENCE OF ELECTRIC FIELD AND ION EMISSION

Also shown in Fig. 15 are similar plots of n_+ (J_+ in ma/sq cm = 1.60 x 10^{-16} n_+) vs P_V at 1373 and 1473 K. The values of n_+ are the emission-limited (knee) ion fluxes measured on curves of J_+ vs E at the given constant values of P_V and T. In all cases except for the 44-to 74-micron ionizer, the ionization efficiency is high and n_T is only slightly greater than n_+. In the case of the 44-to 74-micron ionizer β was somewhat lower, and when n_+ is corrected by β ($n_T = n_+/\beta$), n_T is somewhat larger but still below n_o (E = 0). An interesting relationship between the ratio of the total particle flux for emission-limited ion production to total particle flux for E = 0 and the ionizer powder size, and hence the influence of E on the cesium flowrate, is observed. This ratio decreases consistently with increasing powder size, having the value of unity at about 15 microns and being less than unity for larger

TABLE 4

COMPARISON OF IONIZER PERMEABILITY AND SLOPE OF PARTICLE FLUX VS P_V AT 1373 K IONIZER TEMPERATURE

Powder Size, Microns	Density, Percent	Permeability, sq cm	Slope, $\frac{\text{Particles}}{\text{sq cm - sec - mm Hg}}$
0.9	76	$? \rightarrow 9 \times 10^{-12}$	$4 \times 10^{15} \rightarrow 2 \times 10^{14}$
5	80	$\sim 3 \times 10^{-10}$	1.2×10^{16}
8	68	$\sim 2 \times 10^{-9}$	1.4×10^{17}
8	60	7×10^{-9}	2.6×10^{17}
12 to 18	68	2×10^{-8}	8×10^{17}
44 to 74	63	9×10^{-8}	5×10^{17}

powder sizes. There are only five data points to confirm this conclusion, but they are all consistent. For the 0.9-micron ionizer, the ratio of n_+ (EL)/n_o (E = 0) is about 2 at low flux and probably increases for higher flux, although insufficient data exist at higher n_+ to determine a quantative value. For the 5-micron ionizer, the ratio is 1 to 1.1 at 5×10^{-2} torr at 1373 and 1473 K and increases steadily with n_+ until it is 1.8 and 2.3 at 1 torr for 1373 and 1473 K respectively. For the 8-micron (68 percent) ionizer, it is 1.3 at 7×10^{-3} torr and 1.9 and 2.1 at 5×10^{-2} torr for 1373 and 1473 K respectively. For the 8-micron (60 percent) ionizer it is 1.3 at 7×10^{-3} torr., the same as for the 8-micron (68 percent) ionier, but the ratio this time remains the same or decreases slightly at higher flux. The ratio for the 12- to 18-micron ionizer is approximately unity for all fluxes (at least to $J_+ = 5$ ma/sq cm). For the 44- to 74-micron ionizer, n_+ is less than n_o for all measured fluxes, the ratio being about 3/4 at low pressures (to 1×10^{-2} torr) and about 1/2 at higher pressures. The reason why the total particle flux variesin the presence of an emission-limited, current-producing electric field and the corresponding ion emission is postulated in Ref. 8 on the basis of the concept of cesium presentation to the ionizer surface and the resulting surface phenomena. The effect is dependent upon where the ion formation occurs on the ionizing surface, and the effect of E on the heat of vaporization of the adsorbed ions and atoms. Examples of the effect can be seen in Fig. 9 for the 0.9-micron ionizer, where J_+(EL) is seen to be greater than n_o (E = 0), and in Fig. 32 where J_+(EL) is seen to be less than n_o (E = 0). In all cases, the electric field and ion emission influence the total particle flux through the ionizer. In some cases n_T rises steadily with E, in some it decreases steadily (e.g., Fig. 31), and in still others n_T is relatively constant (e.g., Fig. 9), or is constant followed by a sharp decrease (e.g., Fig. 33).

5.10 INFLUENCE OF IONIZER TEMPERATURE

For all of the porous tungsten ionizers and conditions studied in this work, the flow of cesium through the ionizers increased significantly with ionizer temperature when all other variables were held constant (a few examples are Fig. 27, 36, 39, and 41). Because of the influence of the electric field and ion emission on the flowrate, only the neutral emission for E = 0 and the emission-limited ion current at near-maximum ionization efficiencies will be discussed. Equation 17 of section 5.1 then reduces (for β near unity) to

$$J_+ = en_T(T)$$

because the term in square brackets (Eq. 17) is just the ionization efficiency. Therefore, in this case, as well as for the flow of neutral cesium at E = 0 (no ion emission , and β = 0) the observed temperature dependence should be simply that for cesium flow through the ionizer.

As discussed in section 5.6, the cesium flow is expected to be a combination of free molecule and surface diffusion. The total flowrate (or particle flux) would be the sum of a term (free molecule) proportional to $T^{-1/2}$, which (at large T and over a relatively small range of T, as in this case, 1000 to 1500 K) would appear to decrease rather linearly with T, plus a term (surface diffusion) proportional to $T^{-1/2}\ e^{-V_m/kT}$ which is a modified (reduced) exponential and which, at larger T and over a small range of T, could appear nearly linear with T, though toward an exponential. This latter dependence would have an extrapolated positive temperature intercept if the exponential term predominated. The relative magnitude of V_m compared to kT determines the relative strength

of the exponential; if V_m/kT is large, the exponential will predominate. All of the experimental curves of both n_o (T) and $J_+(T)$ are consistent with this exponential dependence, and all have extrapolated positive temperature intercepts. Under no conditions was either n_o (E = 0) or $J_+(EL)$ observed to decrease with T. The free molecule dependence, $T^{-1/2}$, may influence the total temperature dependence at higher flow-rates, but for ion current densities up to at least 5 ma/sq cm, the exponential (surface diffusion) dependence predominates. The curves of $n_o(T)$ exhibit a stronger exponential dependence at low values of flow-rate and all of the curves of emission-limited $J_+(T)$ fit the expected exponential form

$$J_+ = J_{+_o} e^{-V_{m+}/kT} \tag{50}$$

where

V_{m+} = energy barrier for surface migration (diffusion) for ions

The value of V_{m+} is expected to be close to the value of V_m for adsorbed atoms, though higher if an additional barrier exists as a result of the interaction of the ion with the ionizer lattice through its bound electron. Table 5 is a tabulation of the values of V_{m+} and J_{+_o} (together with the average ionization efficiencies) obtained from plots of $\ell n\, J_+$ vs 1/T for the cases which gave the best straight lines with a minimum of 5 data points. Two examples are presented in Fig. 17. It is interesting to note that the two lowest values of V_{m+} are just the value of V_m, the activation energy for surface migration, which is 0.59 eV/atom. The average of the experimentally measured values of V_{m+}, 0.68 eV/atom (Table 5), is just 0.09 eV/atom greater than V_m.

TABLE 5

EXPERIMENTAL VALUES OF CONSTANTS IN EQUATION 50

Powder Size, Microns	T_V, K	J_{+o}, ma/sqcm	V_{m+}, eV/atom	β, Percent
0.9	423	348	0.76	95 1/2
0.9	463	180	0.59	95 1/2
8	443	150	0.77	95
12 to 18	388	273	0.72	95
44 to 74	425	43	0.58	90
Averages		200	0.68	

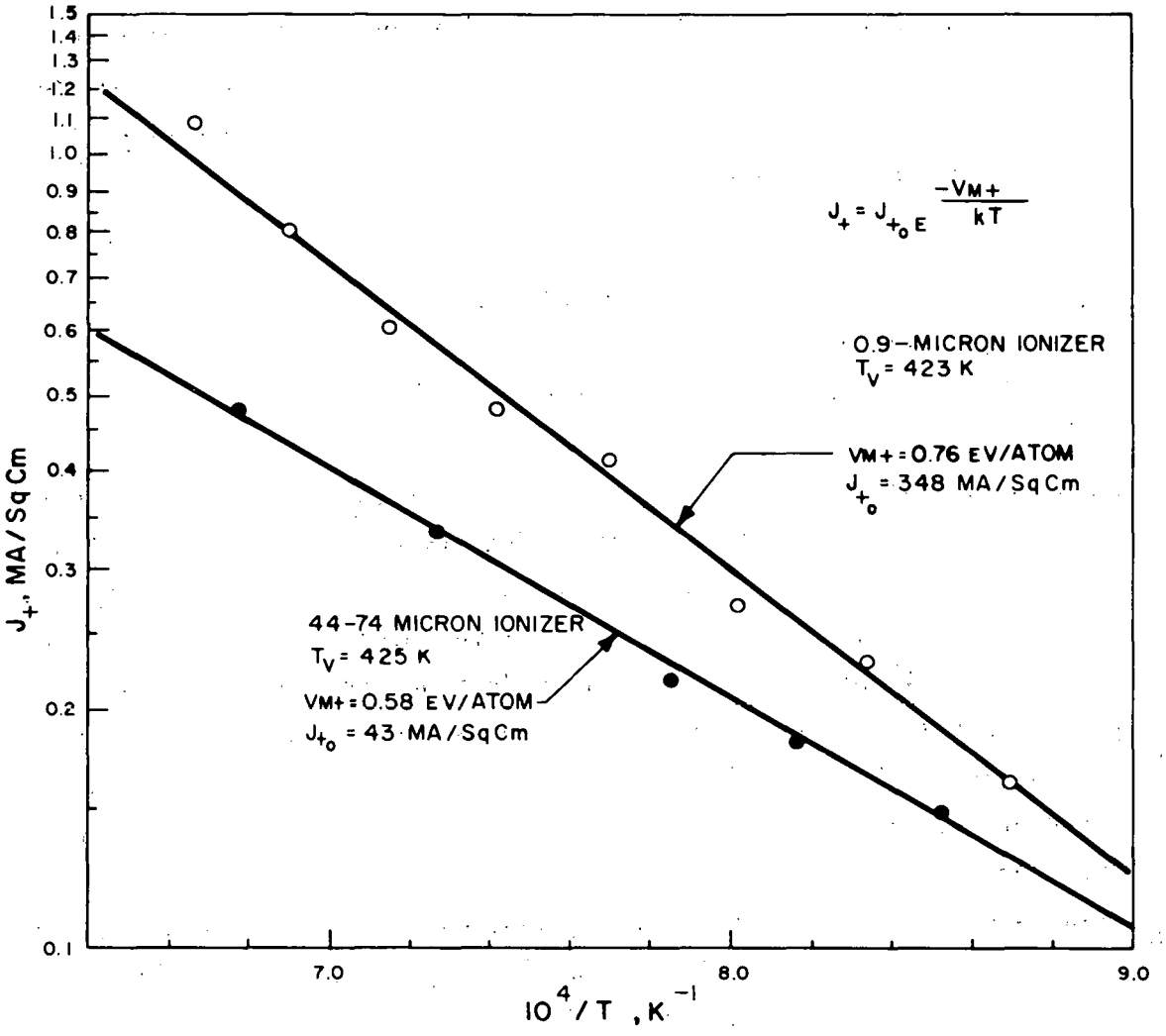

Figure 17. Data Illustrating Relationship of Eq. 50

It is interesting to note that the experimentally measured value of kT_{CL} in this work ($T_{CL} \approx 1120$ K) is just 0.096 eV/atom. The significance of kT_{CL} is that in the presence of an electric field at the ionizing surface, no ion current is observed until the temperature of the ionizing surface is raised to T_{CL}.

5.11 RELATIONSHIP BETWEEN IONIZATION EFFICIENCY AND ION CURRENT DENSITY

Data showing the dependence of the ionization efficiency, β, upon the extracted cesium ion flux or current density produced by the variation of both the cesium vapor pressure and the ionizer temperature for the porous tungsten ionizers of various initial powder sizes are presented in Fig. 18, 19, and 20. The detailed data points are displayed in Fig. 18 for the 44- to 74- and the 12- to 18-micron ionizers, and in Fig. 19 for the 8- and 5-micron ionizers. The results for the 0.9-micron ionizer are discussed in detail in section 5.5. Figure 20 is a combination of just the smooth curves from Fig. 18 and 19 together with the reported results of two other experimental investigations employing cesium and porous tungsten ionizers (Fig. 7 of Ref. 9, and Fig. 5 of Ref. 10 converted to β). In one case (Ref. 10), data are quoted for an 8-micron ionizer, and in the other (Ref. 9), the mean pore diameters and interpore spacings correspond to the same parameters for the 5-micron ionizer of this work. Both of these studies by other workers, in which it is stated or assumed that the increases in ion current density were produced primarily by increases in the cesium vapor pressure, rather than by significant changes in the ionizer temperature, indicate a decrease in β with J_+ (at constant T). Insufficient data have been

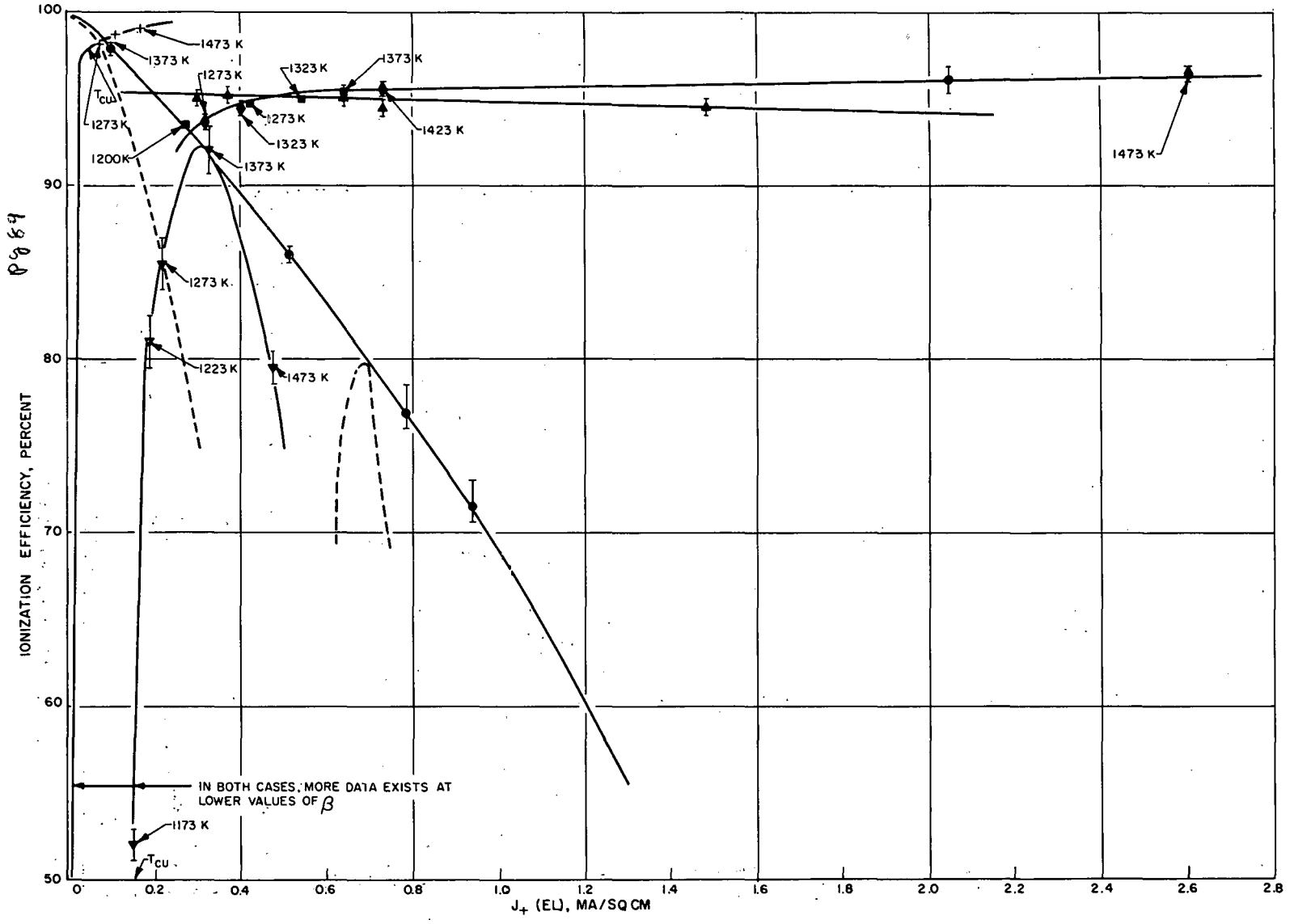

Figure 18. Ionization Efficiency vs Ion Current Density Data

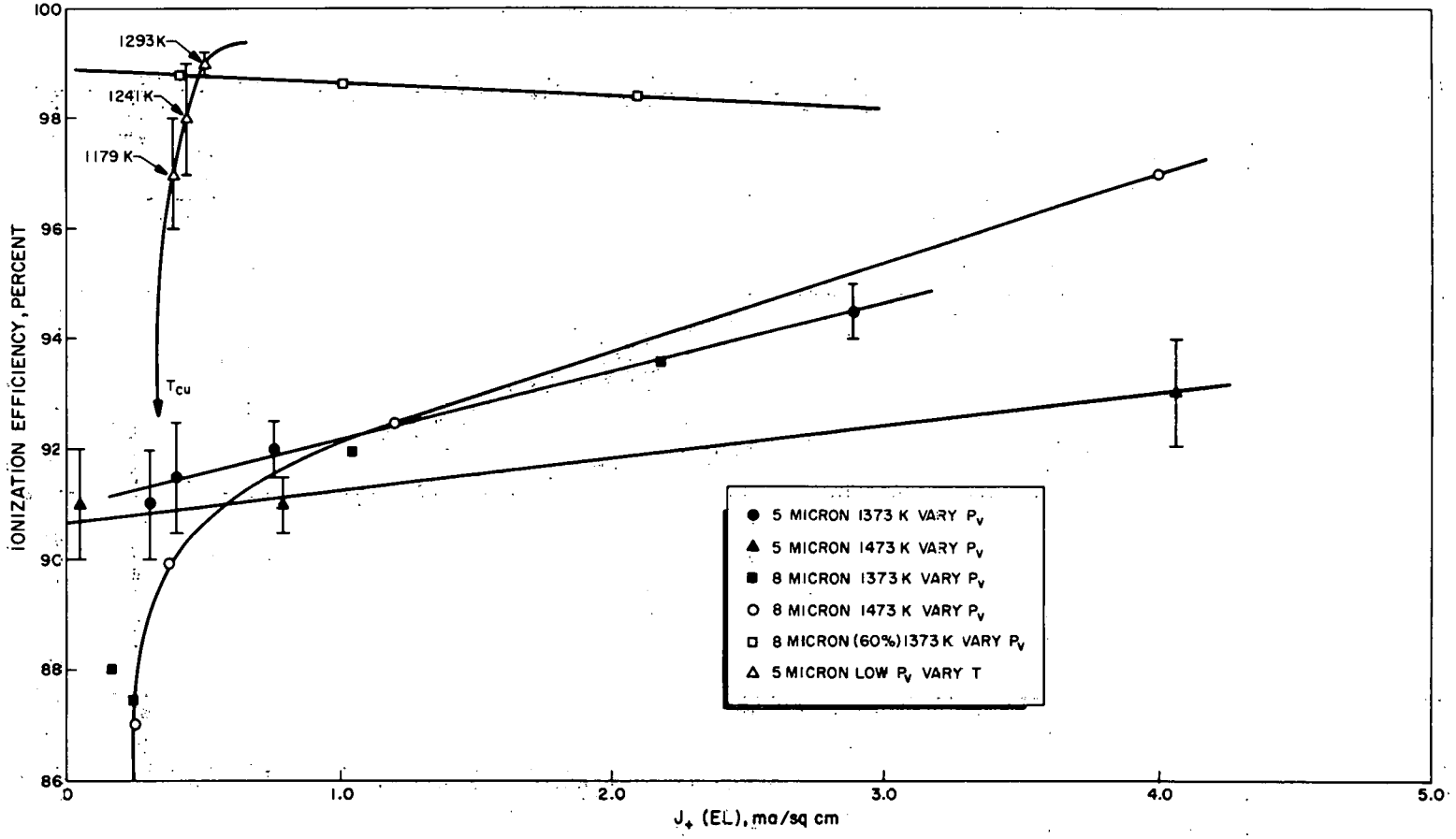

Figure 19. Ionization Efficiency vs Ion Current Density Data

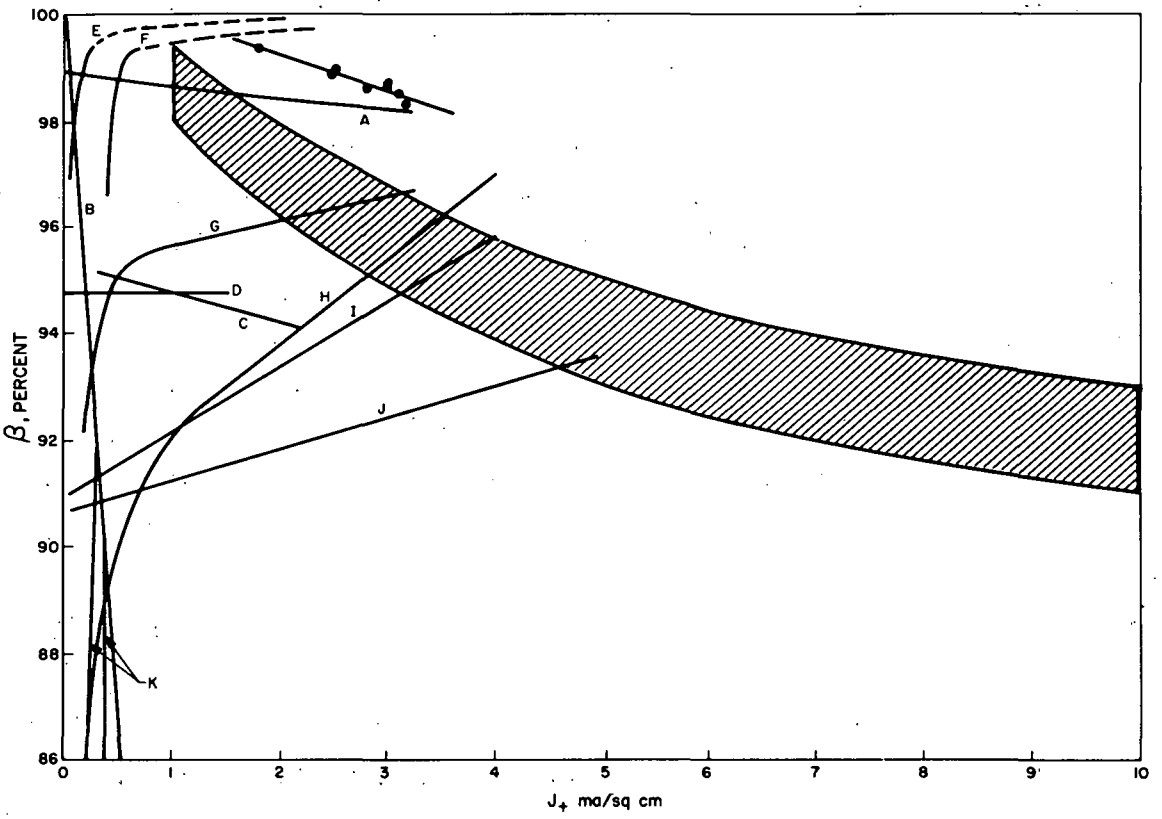

• Ref. 10 8-micron

▨ Ref. 9 mean pore diameter and interpore spacings correspond to the 5-micron ionizer of this work

A. 8-micron (60 percent), varying P_V at 1373 K; very first operation of ionizer
B. 44-to 74-micron, varying P_V at 1373 K
C. 12-to 18-micron, varying P_V at 1373 K
D. 0.9-micron, very early data; see section 5.5 for later data
E. 44-to 74-micron varying T at very low P_V
F. 5-micron, varying T low P_V
G. 12-to 18-micron, varying T at moderate P_V
H. 8-micron, varying P_V at 1473 K } after considerable operating time
I. 5-micron, varying P_V at 1373 K } after considerable operating time
J. 5-micron, varying P_V at 1473 K } after considerable operating time
K. 44-to 74-micron, varying T at moderate P_V

Figure 20. Ionization Efficiency vs Current Density (From the point-by-point plots of Fig. 18 and 19)

obtained to determine any dependence between ionization efficiency and tungsten powder size, and no information has been reported for surface temperature affects.

The results of this work tend to support the conclusion that β decreases with increasing J_+ at constant T (curves A, B, C, and D of Fig. 20) with, however, exceptions noted for certain cases (curves H, I, and J of Fig. 20) which lead to some inconsistency. A possible explanation for the exceptions is that the surface conditions of the two involved ionizers have changed because of their use as ionizers for longer times than the others, for example, by chemisorbed deposits (carbon and/or oxygen). The data of Fig. 20 are entirely consistent in leading to two new conclusions, however. In every case where J_+ was increased by increasing T at constant P_V, β is observed to increase with increasing J_+ (curves E, F, G, and K), with large slope at low J_+ and with small slope at higher values of J_+. In one case (curve K), a maximum in β was reached and a strong decrease in β occurred with further increase of J_+. This is believed to be caused by and unique to the very large pore diameter ($\sim$38 microns) of the particular ionizer. The reproducibility of these experiments is proved by the data plotted in Fig. 18. For the three cases where curves of β vs J_+ (obtained at different conditions and on six different days) intersect, the data points on the varying T curves corresponding to the constant value of T for the varying P_V curves, fall on or very near the varying P_V curves. Also of interest are the data for the 44- to 74-micron ionizer. The ionization efficiency is observed to drop sharply with increasing J_+, produced by increasing P_V, after starting near unity, probably because of the large pore diameters that may serve as sources of more neutrals at higher flowrates. A maximum is exhibited for β at about 1375 K when T was varied at moderate P_V.

The details of this phenomenon are discussed in section 5.16. A postulated curve for higher P_V is shown in Fig. 18. This hints of the possibility that all β vs J_+ curves at constant P_V and varying T may exhibit maxima, but at higher values of J_+ than were attained in this work.

Curves A, B, C, and D of Fig. 20 display a consistent and interesting correlation of the relationship between β and J_+ at constant T and the basic ionizer powder size. The negative slope of β vs J_+ increases with increasing powder size roughly as either the pore size or the specific periphery. The ionization efficiency is nearly constant with J_+ for the smallest powder size for which data could be obtained (0.9 micron, $d = 1.2\,\mu$, $P_s = 0.13\,\mu^{-1}$) β decreases slightly with increasing J_+ for the 8-micron ionizer ($d = 6\,\mu$, $P_s = 0.062\,\mu^{-1}$) and slightly more for the 12- to 18-micron ionizer ($d = 13\,\mu$, $P_s = 0.064\,\mu^{-1}$), and decreases so rapidly with J_+ for the large-pored, 44- to 74-micron ionizer ($d = 37\,\mu$, $P_s = 0.027\,\mu^{-1}$) that it is less than 70 percent at 1 ma/sq cm (Fig. 18), whereas it extrapolates to 100 percent at $J_+ = 0$.

If high β and high J_+ are simultaneously desirable, and if J_+ is to be increased by increasing P_V at constant T, then these data lead to the conclusion that as small a powder size as possible, within the lower limit imposed by sintering changes (0.9 micron was too small in this work), and as high an ionizer temperature as possible, within the limits imposed by power efficiency (higher T results in higher radiated power losses), are required. The observation that T_C increases with J_+ (discussed elsewhere) is consistent with this desirability of a high T, because T must exceed T_C, but a strong contradiction occurs when the relationship between J_+ and powder size is examined. In that case, the permeability to cesium flow decreases significantly with decreasing

ionizer powder size at constant porosity, and hence high J_+ and smaller powder size are incompatible. One method for partially correcting for the inhibition of J_+ by small powder size is pointed out in section 3.7, in which it is shown that k increases with decreasing ionizer density (increasing porosity) at constant powder size. Thus, a benefit is gained for J_+ by combining small powder size and high ionizer porosity.

The optimum relationship among powder size (probably between 2 or 3 and 20 microns), porosity, ionizer temperature, and propellant vapor pressure must be found for each specific application of porous ionizers depending upon the system limitations on the ion current density, the ionizer temperature (from power efficiency considerations), and the ionization efficiency (from charge-exchange electrode sputtering considerations). That is, any β can be had at some T, though a sacrifice in J_+ may be required; or any J_+ (subject to other system limitations) can be had at some T, if a sacrifice in β can be tolerated. In any case, high porosity ($\geq 1/3$) seems to be valuable in increasing ion current density with no sacrifice in ionization efficiency, according to the results of this work.

5.12 EXPLANATION OF VARIATION OF IONIZATION EFFICIENCY WITH VAPOR PRESSURE AND IONIZER TEMPERATURE

It is known that for the nonsorbable gases (H_2, N_2, air, and the inert gases, He, Ne, A, Kr, and Xe), flow through sintered porous tungsten ionizers occurs via the free molecular mode for mean pressures across the porous plug of up to about 100 mm Hg, depending upon the mean pore diameter (Fig. 1). At higher pressures, the influence of viscous or

laminar flow is observed (when the particle mean free path becomes comparable to the channel diameter). If either of these modes were to account for the transport of cesium through these same ionizers, large numbers of unadsorbed atoms would be expected to issue from the active ionizer pores as neutrals, resulting in a low ionization efficiency.

Cesium and the other alkali metals, fortunately, are very sorbable on tungsten; other transport modes, the adsorptive modes, can compete with free molecular flow. As the flowrate, and hence J_+, is increased, the influence of free molecular flow becomes stronger and the ionization efficiency decreases because of the increased probability of neutral atom escape from the pores without being in contact with the ionizing surface, and hence, not being ionized. That is, the surface diffusion mode accounts for the high ionization efficiency at low J_+, and free molecular flow accounts for the decrease of the ionization efficiency as J_+ is increased and the flowrate increases.

When T is increased, the surface diffusion flowrate is increased by $T^{-1/2}\ e^{-V_m/kT}$ while the free molecular flowrate is decreased by $T^{-1/2}$, resulting in a net increase in J_+ because of the predominance of the exponential term. However, the ionization efficiency is also increased if the initial T is just greater than T_C. The ionization efficiency will continue to increase with T until the value of T is reached where β is maximum or nearly constant, and will then decrease or increase slowly with increasing T depending upon the relative magnitudes of $\phi_k\left[\theta(J_+)\right]$ and V_i (β will increase if ϕ_k drops below V_i, and will decrease with T if ϕ_k remains greater than V_i). For cesium and tungsten, the decreasing β mode is expected to predominate up to fairly large values of J_+ when θ becomes large enough over the entire surface to cause $\phi_{k_{max}}(\theta)$ to approach V_i.

If P_v is increased (at constant T), both the surface diffusion and the free molecular flowrates are increased linearly, so J_+ increases linearly. Because T is constant, θ_{min} increases and $\phi_{k_{max}}$ decreases toward V_i, causing the ionization efficiency at the particular T to decrease.

5.13 CRITICAL TEMPERATURES AND HYSTERESIS

In studies of surface ionization, the term critical temperature is defined in two different ways. These will be distinguished in this work as follows: T_C will refer to the general concept of critical temperature, T_{CL} will refer to the lower critical temperature, defined as the surface temperature at which ion formation first occurs, and T_{CU} will refer to the upper critical temperature, defined as the surface temperature at which the emission-limited current is first drawn (or the temperature at which the ion current begins its sharp drop as T is decreased). T_{CU} is the minimum ionizer temperature required to guarantee an emission-limited current density and a reasonably good ionization efficiency, but according to the data presented in this work, it is not the temperature at which the maximum ion current density can be drawn, nor is T_{CU} the ionizer temperature at which the maximum ionization efficiency occurs.

For filament ionizers, a given vapor pressure (P_V) defines the incident atomic flux (n_T) and the equivalent total emitted particle flux ($n_+ + n_o$), both of which are uniform over the ionizing surface. A given T then leads to specific ion and neutral atom residence times (τ_+ and τ_o), and together, P_V and T lead to particular surface concentration of ions and neutrals (σ_+ and σ_o) and hence to a given surface coverage (θ), all of which are uniform over the surface. Thus, as T is raised at constant n_T (P_V), τ (for evaporation of neutrals) decreases and the corresponding σ and θ decrease via evaporation of neutrals which is governed by the requirement that the total ion energy (thermal, etc.) exceed λ_o, the heat of evaporation of a neutral adatom. (λ_o is a function of such quantities as the applied electric field.) When θ

has decreased to θ_c, the value of θ for which $\phi_{k_{max}}(\theta)$, the highest local surface work function, just exceeds V_i, the ionization potential, adsorbed atoms can become adsorbed ions on the patches of maximum ϕ_k and patches of a geometry such that λ_+, the heat of evaporation of an adsorbed ion, may be reduced by such influences as the electric field strength, and an ion current can be drawn by an applied electric field. Thus, T_{CL} is defined as the value of T for which $\theta \leq \theta_c$ on the patches of $\phi_{k_{max}}$ and $\lambda_{+_{min}}$ at a given P_V (n_T).

As T is raised further, V_i is exceeded by ϕ_k (θ) on more and more patches of lower and lower ϕ_k, until finally θ becomes less than θ_c on the patches of lowest ϕ_k $(\phi_{k_{min}})$. At this time the emission-limited ion current is drawn provided that the applied electric field exceeds that value corresponding to the space-charge-limited, emission-limited voltage knee. In the space-charge-limited region, although nearly all adatoms are in the ionic state for $T > T_C$, the ion current density is limited and many ions are returned to the surface by their image charges. Because the probability of neutral emission is enhanced by the resulting higher θ and because the extracted ion current is low, the measured ionization efficiency is low. Thus T_{CU} occurs when $\theta \leq \theta_c$ on the patches of $\phi_{k_{min}}$ (the entire surface).

Now, if P_V is raised, n_T, σ, and θ are also increased for corresponding T's. As T is again increased, τ and θ decrease but θ_c (and λ_+) is first exceeded at a higher T, and T_{CL} is therefore higher. In the same manner, T_{CU} is increased. Therefore, for filament ionizers, T_C increases with increasing P_V (n_T).

In addition, because of the uniformity of θ for filament ionizers resulting from the process of presentation by condensation rather than by flow through pores for porous ionizers, a critical temperature

hysteresis effect can occur. (It has not been observed in all filament ionizer experiments reported in the literature for all conditions, including adatom and surface species.) The best explanation for this phenomenon is (following the above discussions) that as T is increased and θ decreases from values near unity to smaller values, the adsorbed neutrals experience two binding forces, that to the surface and that to the adjacent adatoms, resulting in a particular value of λ_o. On the contrary, as T is decreased and condensation onto the surface increases, the individual adsorbing atoms experience binding only to the surface and not to adjacent adatoms. Because θ is very low, and λ_o is thus lower, a lower T is required for evaporation. Therefore, T_C is lower for decreasing T (increasing θ) than for increasing T (decreasing θ) as has been reported in many instances for cesium on polycrystalline tungsten filaments.

5.14 CRITICAL TEMPERATURE VS ION CURRENT DENSITY

The most reliable data obtained in this work for the variation of T_C with J_+ are presented in Fig. 21, together with most of the other published data for the ionization of cesium on porous tungsten (Ref. 9, 10, 11, and 28), and one curve for cesium and filament tungsten for comparison (Ref. 7). The data are plotted in the standard form of $\ell n J_+$ vs $1/T_C$. Both T_{CL} and T_{CU}, as defined in section 5.13, are plotted for this investigation in which the range of J_+ is extended to lower values. The values of T_{CL} and T_{CU} reported here were obtained from curves of the maximum emission-limited ion current density vs ionizer temperature obtained in turn, from plots of J_+ vs E at many various T's, not from a single plot of J_+ vs T at one particular value of V (or E).

The former technique is believed to be superior to the latter for reasons discussed later in this section.

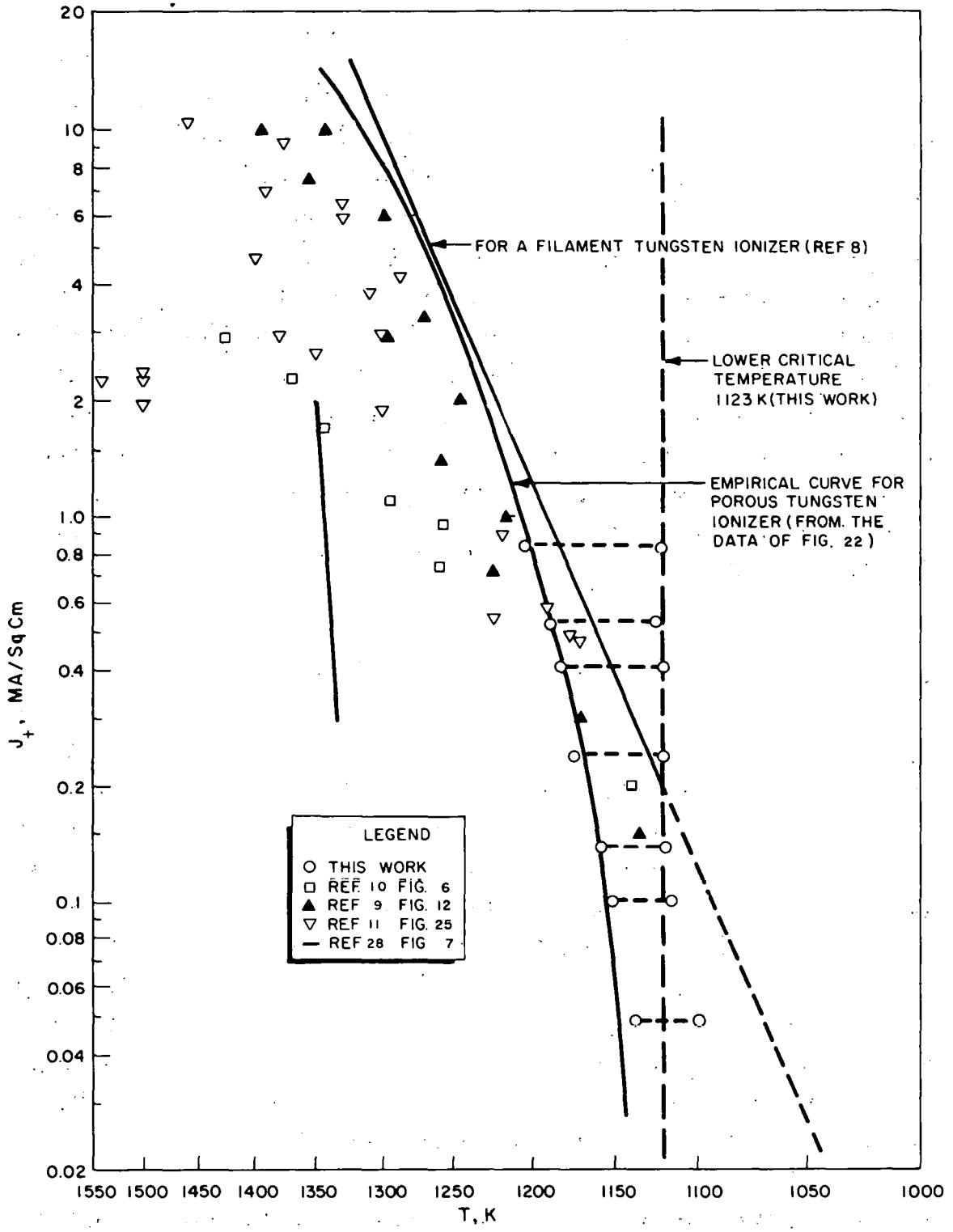

Figure 21. Upper and Lower Critical Temperatures as a Function of Current Density for Porous Tungsten Ionizers

The T_{CL} values of Fig. 21, and a number of others not shown, fall within the rather narrow range of 1123 ±5 K (with one exception). This is consistent with the theory of surface ionization with porous ionizers (Ref. 8) and it is expected that T_{CL} should remain close to 1120 K for still higher J_+ (up to the 10 ma/sq cm of the reported T_{CU} values in Fig. 21). Although the slope of J_+ vs T increases for increasing emission-limited J_+, an increase in T_{CU} still occurs with $J_+(EL)$. The values of T_{CU} for the higher J_+ fall among the data reported by other investigators. The rate of increase of the difference between T_{CU} and T_{CL} with J_+ was observed to fit best a straight line on a log-log plot as shown in Fig. 22. An extrapolation of these data into one-decade-higher values of J_+ then allowed the empirical curve of T_C vs J_+ to be extended to J_+ = 10 ma/sq cm as shown in Fig. 21. The increasing value of (T_{CU} minus T_{CL}) was always added to the assumed constant T_{CL} for porous tungsten ionizers. That is,

$$T_{CU}(J_+) = T_{CL} + B(J_+)J_+ \qquad (51)$$

where $B(J_+)$ is obtained from Fig. 22 and T_{CL} is a constant equal to 1123 K. This empirical curve falls very close to the empirical curve for filament tungsten above 1 ma/sq cm (Ref. 7).

It was observed in this work that if T_C was obtained from simple plots of J_+ vs T at some arbitrary value of V (E), the points for T_C vs J_+ fell with a great deal of scatter to the left of the empirical curve shown in Fig. 21, much as did the compilation of points reported by all investigators. It was then discovered that the points obtained in the manner described above fell more nearly on a smooth curve and fairly close to the filament ionizer curve (at higher J_+), although still toward higher values of T_C. This may be one explanation of the gross scatter of the experimental data which was found for porous ionizers.

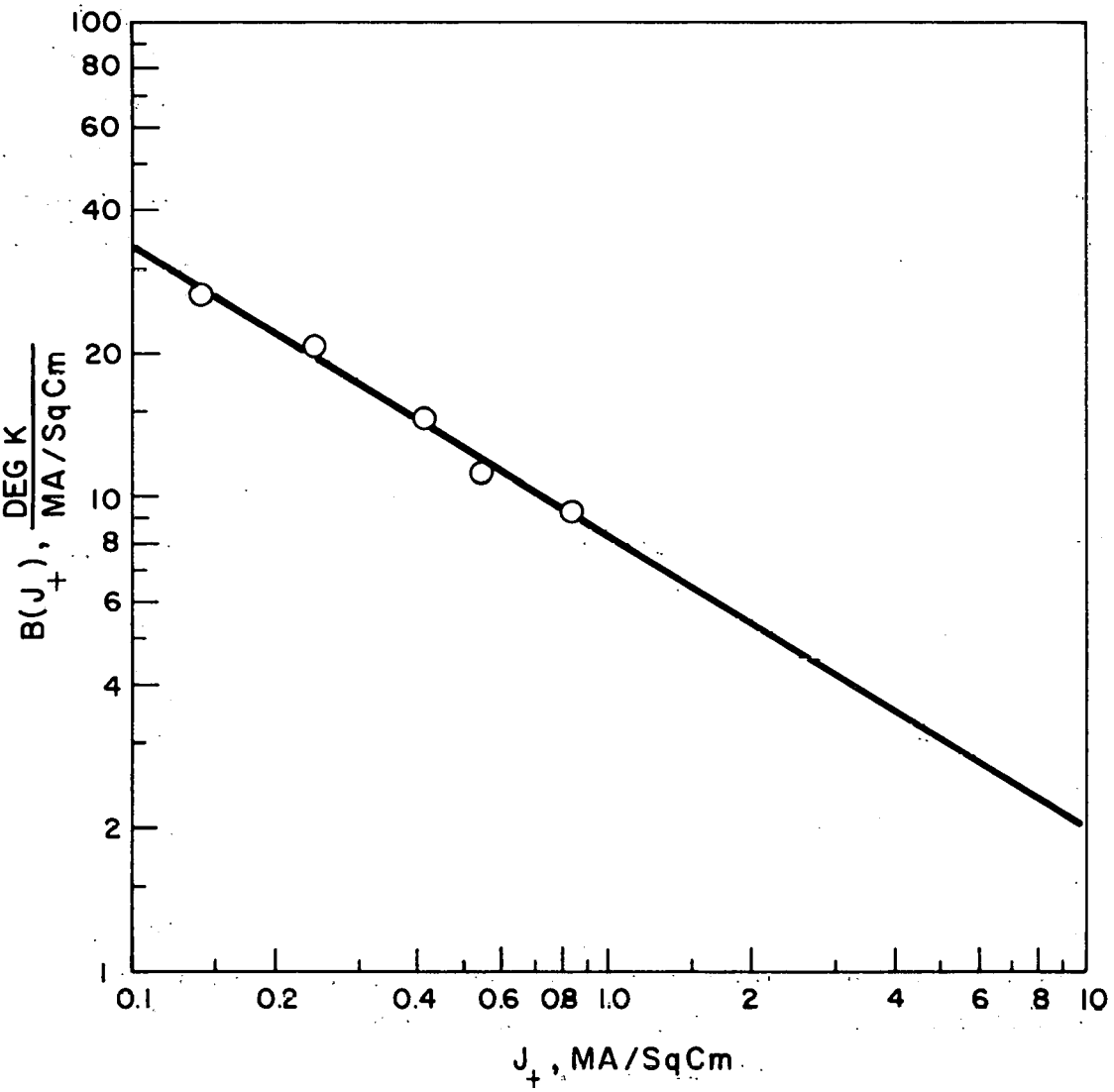

Figure 22. $B(J_+)$ vs J_+ for Empirical Curve of T_C vs J_+

(Possible reasons for this effect are described in Ref. 8 .) It is possible, then, that for porous ionizers the choice of the proper value of V can cause the reduction of T_C (for a given J_+) as implied by the scatter of the data in Fig. 21. The data points at the higher J_+ of Fig. 21 may define a possible lower limit on T_C which is much more attractive for ion engine applications.

If the critical temperature is defined as the ionizer temperature at which the ionization efficiency is a maximum or reaches a nearly constant value, then the plotted values of T_C will scatter toward higher values of T because of the several conditions which can influence the relationship between T and β_{max}, such as the magnitude of β_{max} itself. If T_C is defined as the temperature where the sharp rise in ion current (via the critical temperature) intersects the emission-limited ion current curve (at higher temperatures), a fairly smooth curve of T_C vs J_+ is obtained. The corresponding β will be high but not necessarily maximum.

If, on the other hand, T_C is defined as the temperature at which the ionization efficiency is a maximum, then T_C will occur at some value of T above the previously defined T_C because β may become a maximum or be nearly constant at larger values of T. Actually, for very large values of J_+, β may never become truly a maximum because it will approach unity asympotically with T. As J_+ increases, the minimum value of θ on the surface patches (those farthest from the active pores) increases and causes the corresponding maximum ϕ_k to decrease toward the value of V_i (for cesium on tungsten--for other systems, a different situation may exist). At low values of J_+, $\phi_{k_{max}}$ (θ_{min}) is enough larger than V_i to cause β to have a definite maximum at T close to T_C. As J_+ is increased, $\phi_{k_{max}}$ decreases and becomes more and more constant with T to some point near the condition $\phi_{k_{max}} = V_i$, beyond which β begins to

increase with T. For much larger values of J_+, a maximum in β may never be reached with increasing T. Thus, the decision of the individual investigator concerning where T_C is chosen could account for the variations in a plot of T_C vs J_+, particularly at increasingly larger values of J_+.

One other possible cause of the data scatter of Fig. 21 could be varying degrees of surface contamination. Foreign atoms chemisorbed on the surface could cause the effective critical temperature to be raised because the work functions of the surface patches would be lowered (in all cases except oxygen) by the foreign adsorbates (Ref. 8).

A possible explanation for the superiority of the method described herein for plotting points on the T_C vs J_+ curve is seen in the following discussion. T_C is actually a function of θ, not J_+, although no method is known for measuring the microscopic values of θ on the individual surface patches under the exact conditions of surface ionization. Because field emission techniques are performed at such high values of applied electric field that $\lambda_o(E)$, $\lambda_+(E)$, $\beta(E)$, and T_C are drastically changed, such experiments are quite irrelevant, if not incorrect, for application or comparison to the process of surface ionization which is performed at values of E 4 to 5 orders of magnitude lower. Therefore, T_C is plotted as a function of J_+. However, this leads to possible errors because, for example, if the ionization efficiency is less than unity, J_T is greater than J_+ and therefore θ is actually greater than that which corresponds to J_+. If then, T_C were plotted against $J_T = J_+ + J_o = J_+/\beta$, the values of T_C would be plotted higher on the scale of J_T and hence lie closer to the curve for filament ionizers (Fig. 21), for which β is essentially unity. This might also eliminate some of the scatter in the porous ionizer data. Other similar considerations exist, all of which lead to higher values of θ for a given T than implied by the measured value of J_+. All of this, of course, does not

change the fact that for the operation of porous ionizers, T_C will be somewhat higher for a given J_+ than the corresponding T_C for a filament ionizer. It does mean, however, that conditions can be established for porous ionizers so that lower values of T_C than implied by some of the data of Fig. 21 can be employed to ensure a given value of emission-limited J_+.

The explanation for the prediction of a possible constant T_{CL} or at least a less rapid change of T_{CL} with J_+ at low J_+ for porous ionizers is given in detail in Ref. 8. In brief, it is related to the fact that, for porous ionizers, σ and θ are not uniform over the surface, but are high at the pore lips or walls and decrease radially outward, being higher at the grain steps than on the flat surfaces. Therefore, for low and moderate flowrates (J_+), areas with θ from unity to zero exist in contrast to the filament ionizer on which θ is nearly constant and uniform, and dependent upon P_V (n_T) only.

In Ref. 10, it was observed that for a porous tungsten ionizer the maximum β occurred about 100 K above T_{CU}. In this work it is observed that β_{max} occurs at a T above T_C, but that the amount varies inversly with β_{max}. When the maximum emission-limited current is plotted as a function of T, as in Fig. 29, β_{max} occurs within about 20 K when β_{max} is 98 to 99 percent, within about 50 K when β_{max} is about 95 percent, within about 120 K when β_{max} is approximately 90 percent, and as much as 250 K higher when β_{max} is as low as 70 percent. If β is plotted as a function of T for various V (or E), as in Fig. 28, 37, and 39, then for certain V, β_{max} may occur for a T closer to T_C (Fig. 21).

5.15 EXPERIMENTAL HYSTERESIS FOR A POROUS IONIZER

Critical temperature hysteresis effects have been observed in many experimental investigations of surface ionization with filament ionizers of several elements and with a number of different atomic and molecular adatom species. The data from four such references (Ref. 29, 30, 11, and 31) which report information for cesium on tungsten will be tabulated for comparison with the results of this work for porous ionizers. This effect has not been observed for all adatom-surface specie combinations, but has always been observed for the Cs-W system. The magnitude of the upper critical temperature difference (called ΔT_C herein) for increasing T and decreasing T seems to increase with n_o or J_+ as does T_C itself. No similar experiments or results have been published for porous ionizers. The explanation for this phenomenon was discussed briefly in section 5.13. The theory for porous ionizers developed in Ref. 8 predicts that little or no critical temperature hysteresis effect should occur for porous ionizers and that the single critical temperature which does occur should be the critical temperature obtained for a decrease of ionizer temperature in the case of filament ionizers.

An experiment was performed with the 5-micron porous tungsten ionizer and cesium to measure experimentally the magnitude or upper limit of this effect for porous ionizers. The technique used was the standard one employed throughout this work to obtain emission-limited current densities as a function of ionizer temperature. The results of this experiment are presented in detail here because they will be used in other sections to illustrate relationships among variables and experimental techniques, and will serve for comparisons with experiments with other ionizers of different powder size.

Because this experiment required many hours of continuous ionizer operation, during which time maintaining a constant cesium vapor pressure was very critical if the results were to be meaningful, a long thermal equilibration time was allowed for the cesium reservoir and feed systems, and great care

was taken to maintain the cesium reservoir at as constant a temperature as possible throughout the experiment. The reservoir is the coolest part of the cesium feed system and therefore determines the cesium vapor pressure. The reservoir temperature was established at 480 K for this experiment, and it was possible to maintain this over the many hours required for the experiment within ±3 K according to the iron-constantan thermocouple.

Curves of J_+, J_o (n_o), and β vs E from 0 to 7 or 8 kilovolts were obtained at ionizer temperatures of 956, 1005, 1047, 1081, 1121, 1141, 1159, 1179, 1241, and 1293 K in increasing order followed immediately by curves at 1190, 1168, 1136, and 1094 K in decreasing order, having first reduced the temperature from 1293 K. Three of these curves are presented in Fig. 23, 24, and 25. One (1141 K) curve occurs on the sharp rise of T_C and therefore illustrates the data for low ionization efficiency; one (1179 K) occurs at the knee between the sharp rise and the subsequent emission-limited current region, i.e., at T_{CU}, where the ionization efficiency is high but not maximum; and one (1293 K) occurs at some distance on the emission-limited current curve where is optimal (99.0 percent in this case, from 3.5 to 6 kv). Plots of neutral flux, ion current density, and ionization efficiency vs ionizer temperature obtained from the 14 specific temperature plots like Fig. 23, 24 and 25, are displayed in Fig. 26, 27, and 28, respectively. Figure 26 shows the nearly linear dependence of cesium flow through the ionizer with ionizer temperature for no electric field and hence for no ion formation, which was consistently observed in this work. The slope between T_{CL} and T_{CU} is seen to increase with V resulting in the variation of T_{CU} with V discussed in section 5.13. The neutral flux at 4 kv is a minimum; it is increasingly higher for high voltages (5 to 8 kv). The ion current follows a similar pattern (Fig. 27) leading to a nearly constant β. Figure 27 shows a corresponding plot for the ion current density vs T. T_{CL} is seen to be approximately 1123 K, but again, T_{CU} varies slightly with V until the emission-limited condition is well established. An indication of a second critical point is observed at a lower temperature ($\sim$ 900K). A much better indication is seen in Fig. 28, where the dependence of ionization efficiency with temperature is shown. A second source of ions

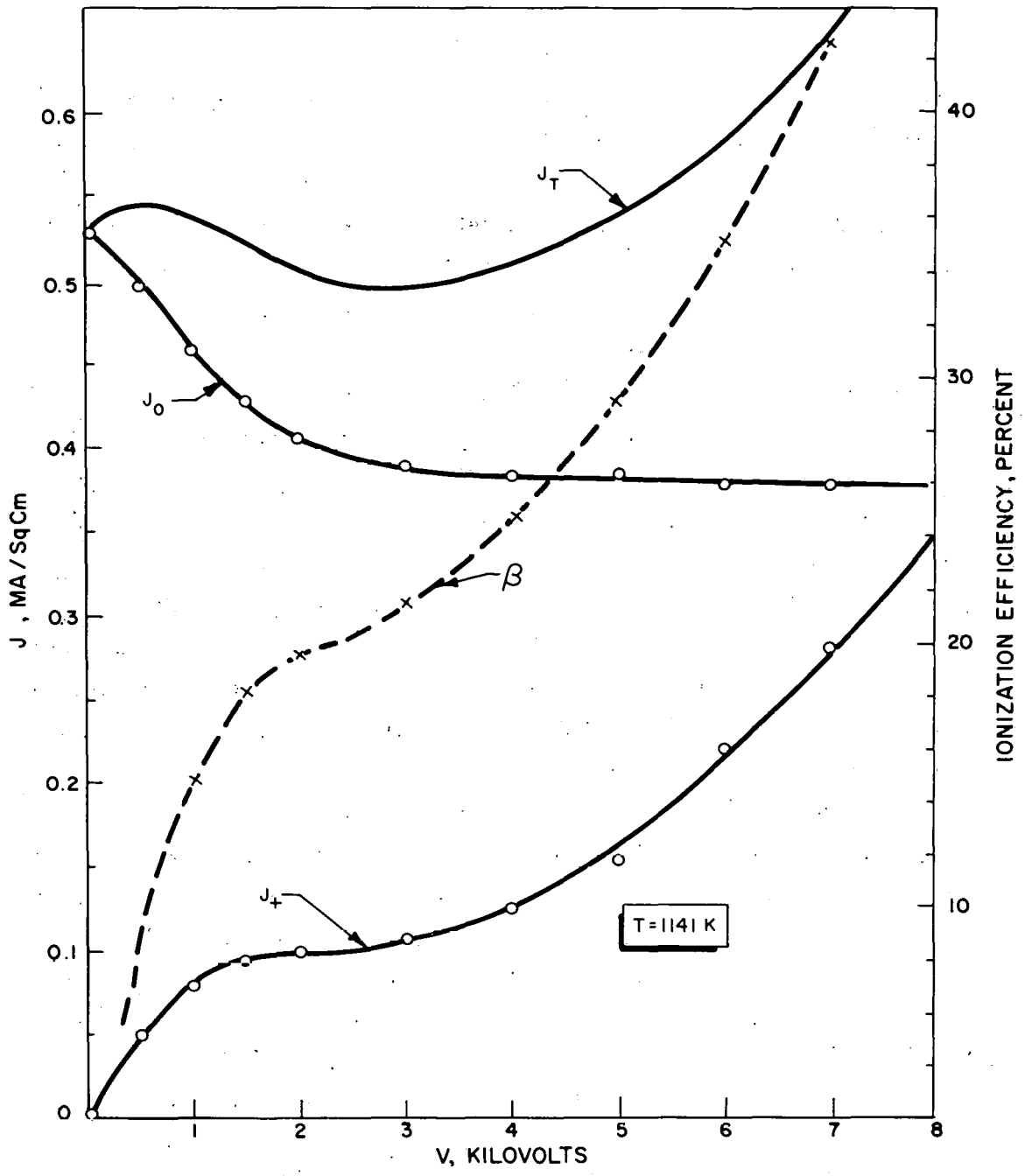

Figure 23. Particle Fluxes and Ionization Efficiency vs V for ΔT_C Experiment

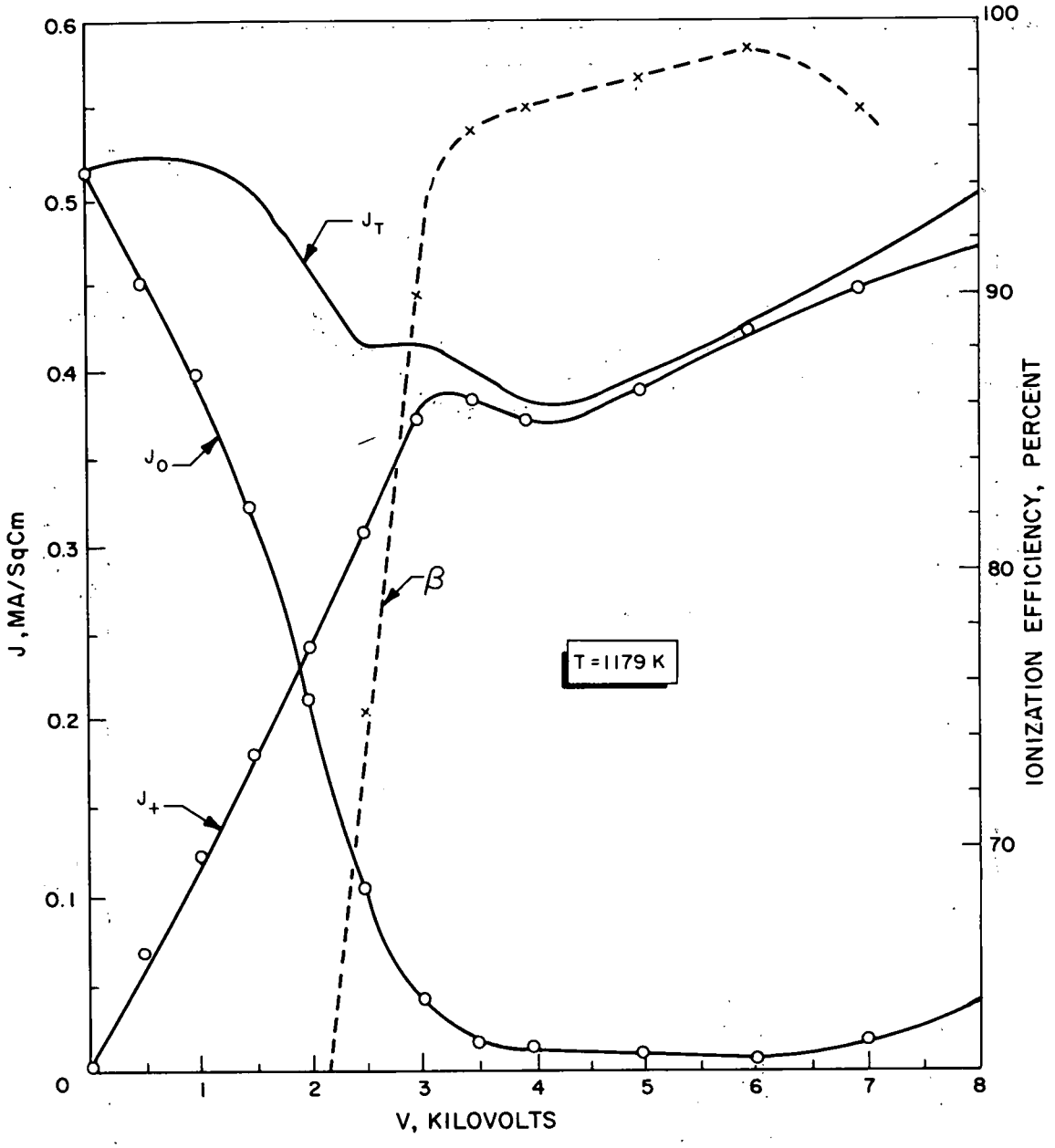

Figure 24. Particle Fluxes and Ionization Efficiency vs V for ΔT_C Experiment

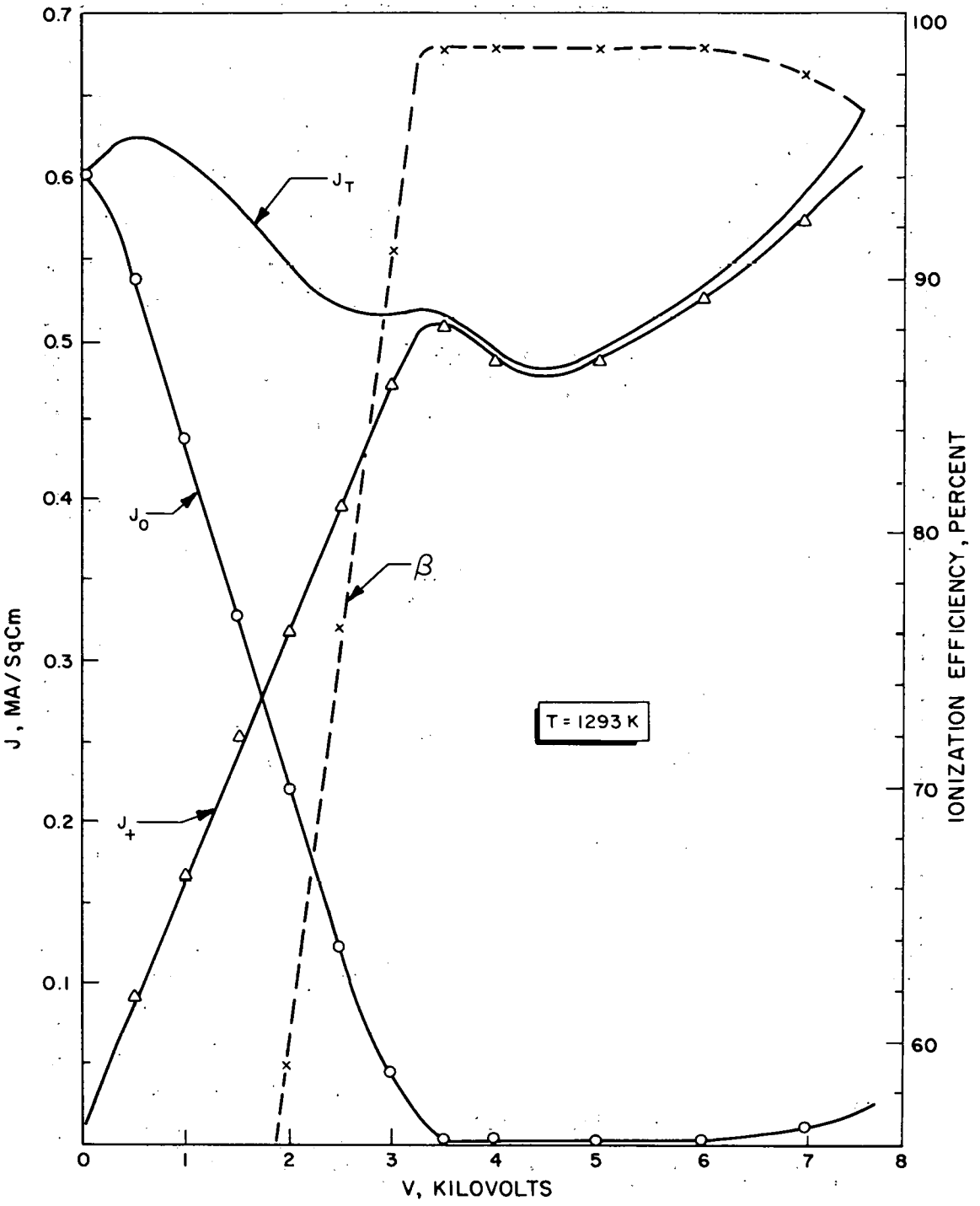

Figure 25. Particle Fluxes and Ionization Efficiency vs V for ΔT_C Experiment

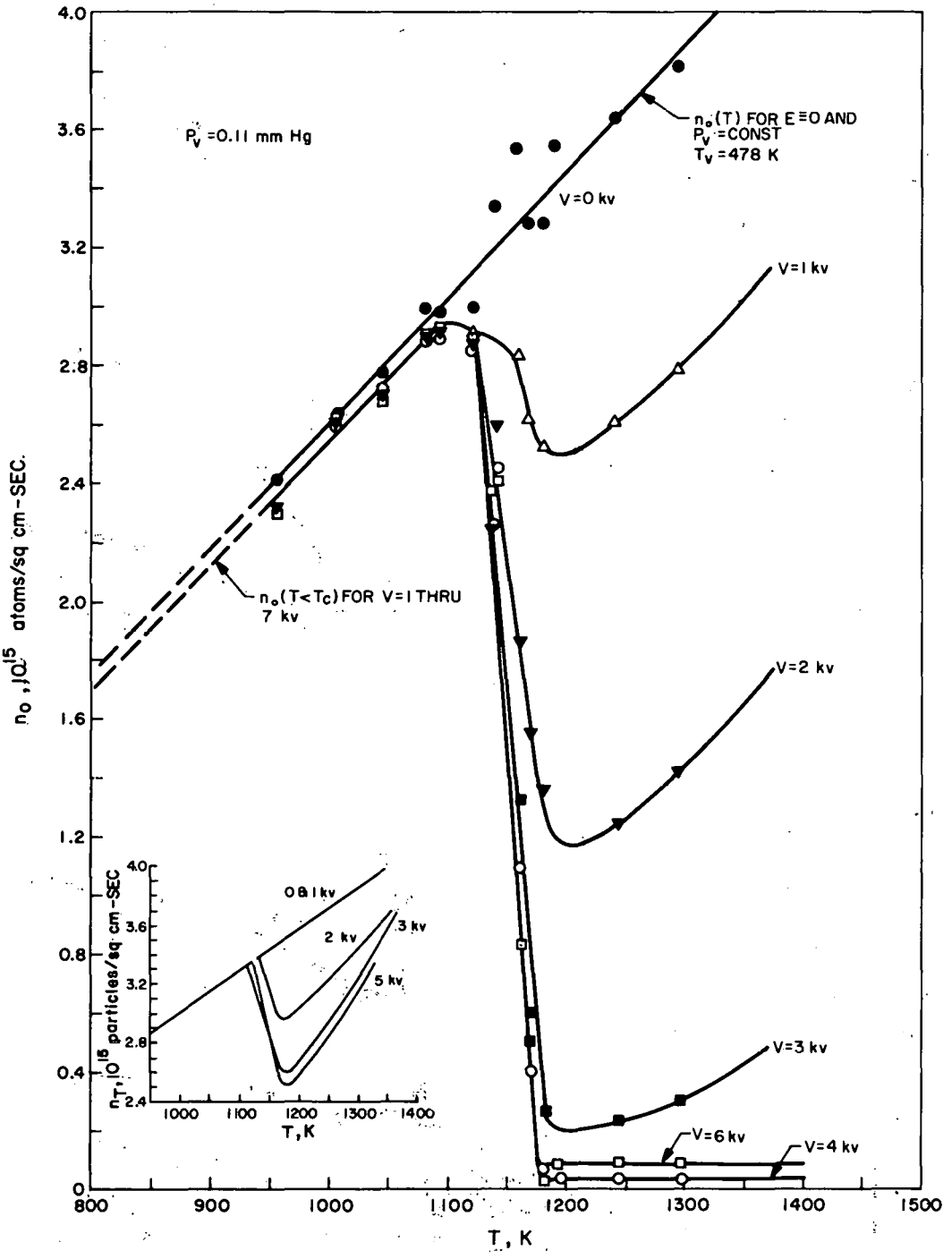

Figure 26 . Neutral Flux vs T at Constant P_V for the 5-Micron Ionizer ΔT_C Experiment

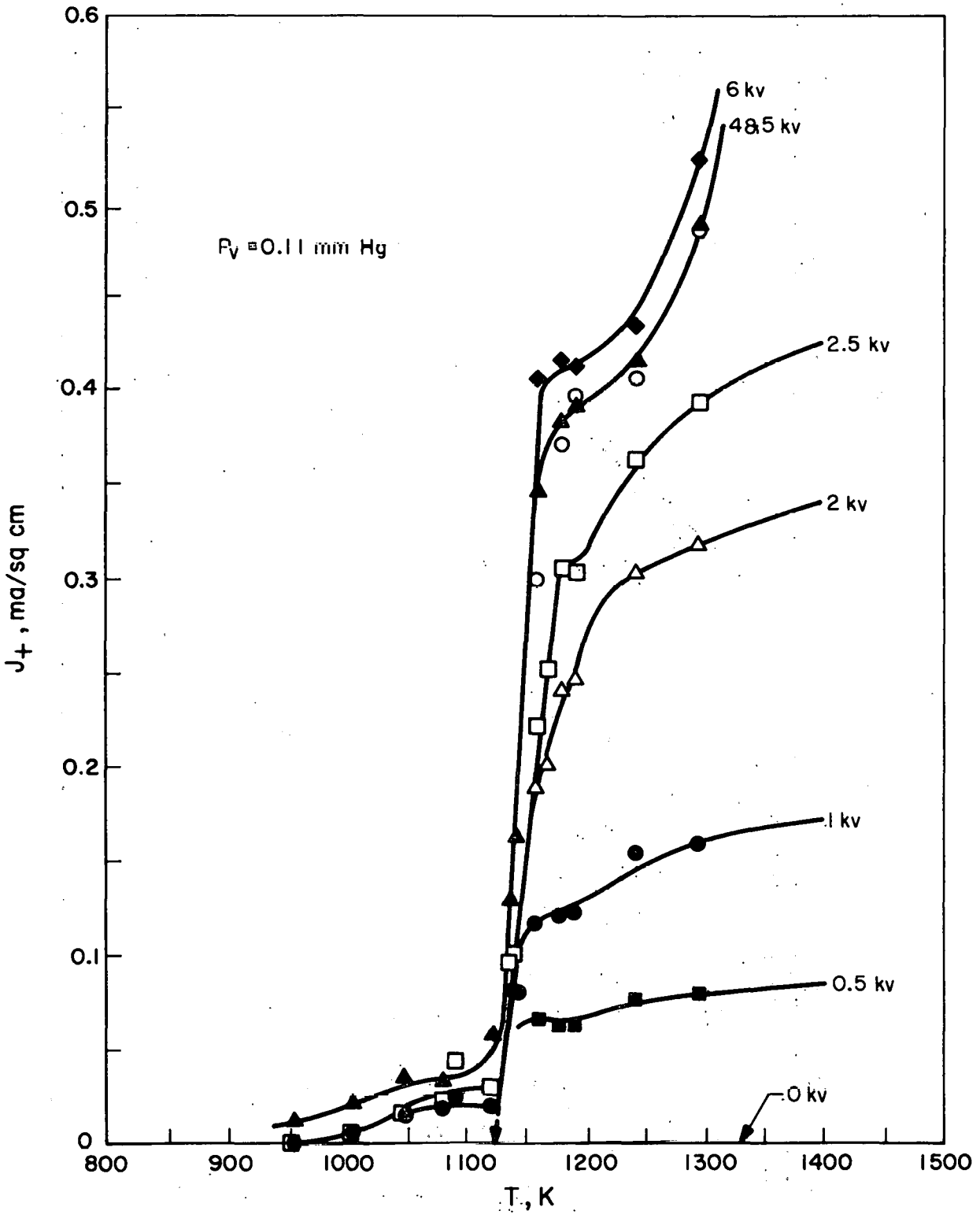

Figure 27. Ion Current Density vs T at Constant P_V for 5-Micron Ionizer ΔT_C Experiment

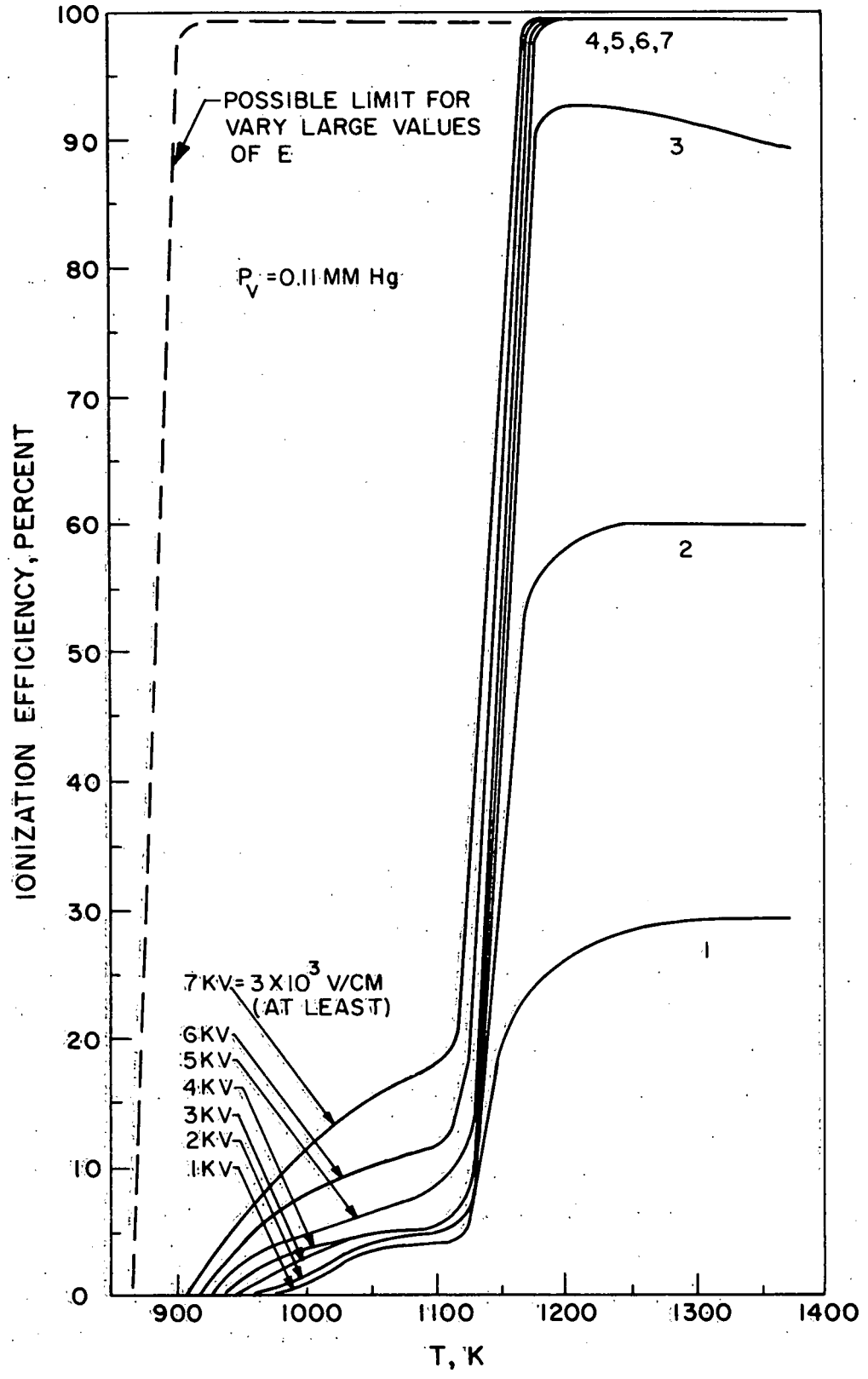

Figure 28. Ionization Efficiency vs T at Constant P_V for 5-Micron ΔT_C Experiment

seems to be appearing at lower temperatures, particularly at higher electric fields. It seems possible that for electric fields orders of magnitude larger, the curve of β vs T might approach the dotted curve in Fig. 28. No explanation for this observation is offered at this time. This figure also shows a tendency for a general shift of critical temperature to lower values for increasing electric field, very much like the data of Ref. 31 for considerably larger electric fields. The influence of T on the total flux is shown in the insert in Fig. 26 .

The data are then presented in a slightly different manner in Fig. 29 which is used to measure the effect of critical temperature hysteresis for this porous ionizer (5-micron tungsten). The values of the maximum ion current density at the space-charge-limited, emission-limited knee of each of the 14 plots of J_+ vs V at different constant T are plotted as a function of T. For example, in Fig. 24 , the value of J_+ (0.38 ma/sq cm) at 3.3 kv is plotted in Fig. 29 at 1179 K. The value of J_+ is not necessarily the maximum value of J_+ observed for any V because, as in Fig. 24 , slightly higher values of J_+ are attained for $V > 5$ kv. The percentages at each data point are the corresponding ionization efficiencies. Ascending and descending temperature curves are drawn through the data points of Fig. 29 and are distinguished by arrows. The descending points lie at slightly lower temperatures and the curves indicate about a 5 K difference between them. However, because only a few points exist on each curve (although they fall on fairly straight, parallel lines) and because the accuracy of the individual temperature measurements is only within the accuracy of the optical pyrometer, a definite statement that the descending curve lies 5 K below the ascending curve cannot be made. However, the statement can be made that little or no critical temperature hysteresis occurs for porous ionizers (at least for the Cs-W system) at this neutral flux.

Values of ΔT_c resulting from similar experiments with filament ionizers are presented in Table 6 for comparison. The same Cs-W system is included

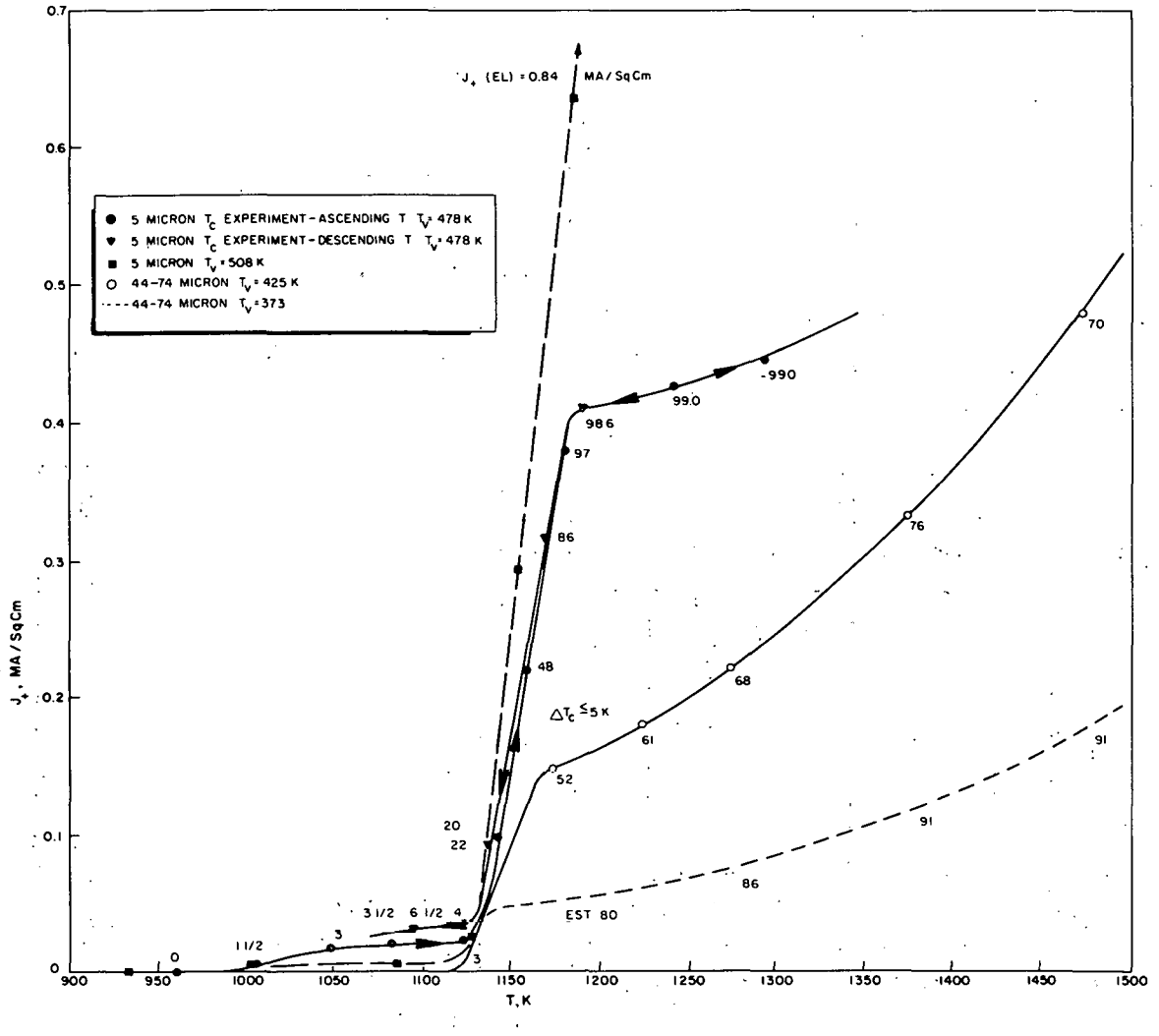

Figure 29. Critical Temperature Hysteresis Data and Other J_+ (EL) vs T Data (Percentages Adjacent to Data Points = Corresponding Ionization Efficiencies)

TABLE 6

TABULATION OF APPROXIMATE EXPERIMENTAL VALUES OF ΔT_C IN DEGREE K

System	Ref. 29 (Filament)	Ref. 30 (Filament)	Ref. 11 (Filament)	Ref. 31 (Filament)	This Work (Porous)
Cs-W	40 (780)	105 (1220) 120 (1120)	70 (1240)	-	≤ 5 (1180)
Cs-Re	-	90 (1110) 70 (1295)	130 (1235)	-	-
K-W	-	-	-	175 (715) 190 (910)	-

NOTE: (The number in parentheses is the T_{CU} for the descending filament ionizer curves which then compares with the T_{CU} of the porous ionizer.)

together with one additional surface specie (Re) with cesium and one additional adatom specie (K) with tungsten. The values of ΔT_C cover a rather large range, but they are all very significant compared to the results of this experiment.

5.16 SPECIAL PRESENTATION OF 44- to 74-MICRON IONIZER DATA

The largest-powder-size ionizer studied (44- to 74 microns) yielded some characteristics different from the smaller-size powders studied in this work and by other investigators. Some interesting results were obtained at the higher cesium vapor pressures used for this more permeable ionizer. To show some of these characteristics and to illustrate the way in which data were obtained for these ionizers, some of the data for the 44- to 74-micron ionizer are presented here. Plots of J_+, J_o, and hence J_T and β vs E were obtained at various ionizer temperatures and at two values of vapor pressure, one low enough to produce relatively good ionization efficiencies but low ion current densities, and one at a higher cesium vapor pressure which produced higher current densities and some other effects which include lower values of β.

Measurements were performed at a cesium vapor pressure of 7×10^{-4} mm Hg (373 K) for ionizer temperatures of 1019, 1123, 1173, 1273, 1373, and 1473 K, and at a pressure of 1.3×10^{-2} mm Hg (426 K) for temperatures of 973, 1073, 1123, 1173, 1223, 1273, 1373, and 1473 K. Some typical curves are shown in Fig. 30, 31, 32, and 33 for the second case, and in Fig. 34 for the low-pressure case. The ion flux, neutral flux, total flux, and ionization efficiency are shown. Some constant voltage cross sections of the plots at the higher pressure for neutral flux, ion flux, total flux, and ionization efficiency are shown in Fig. 35, 36, 37, and 38. Figure 39 is a constant voltage cross section of ionization efficiency for the lower vapor pressure, to be compared to Fig. 37.

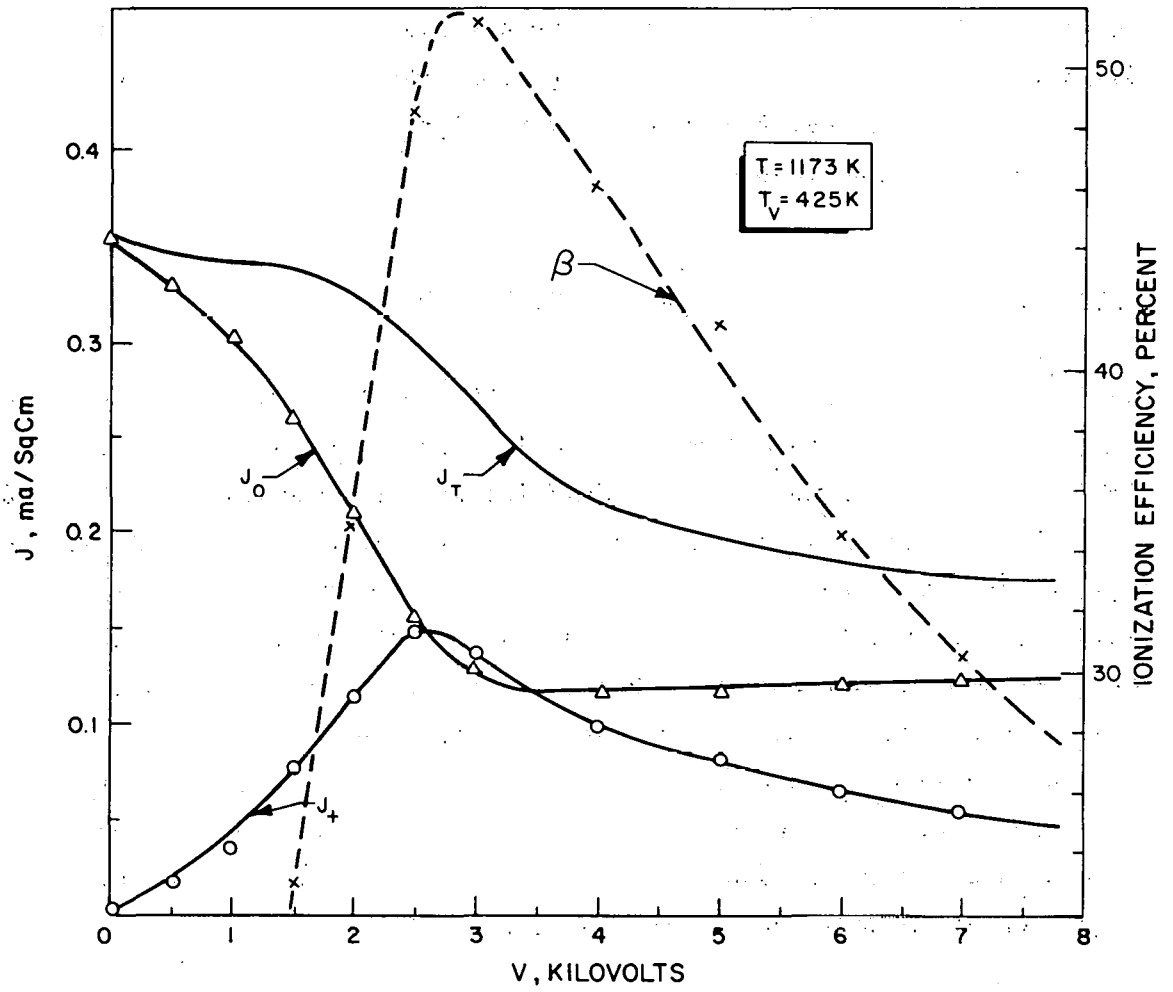

Figure 30. Particle Fluxes and Ionization Efficiency vs V for 44- to 74-Micron Ionizer

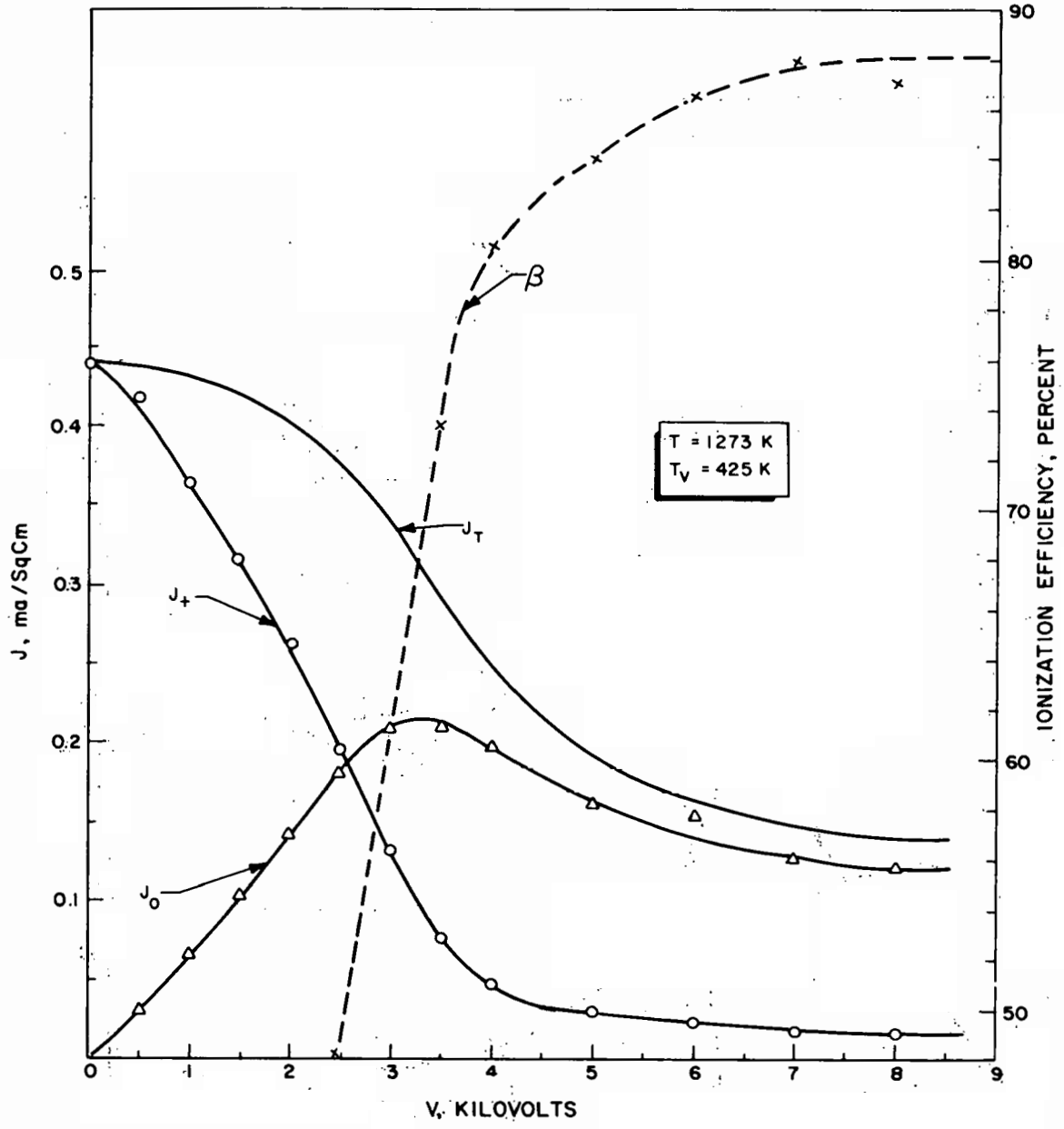

Figure 31. Particle Fluxes and Ionization Efficiency vs V for 44- to 74-Micron Ionizer

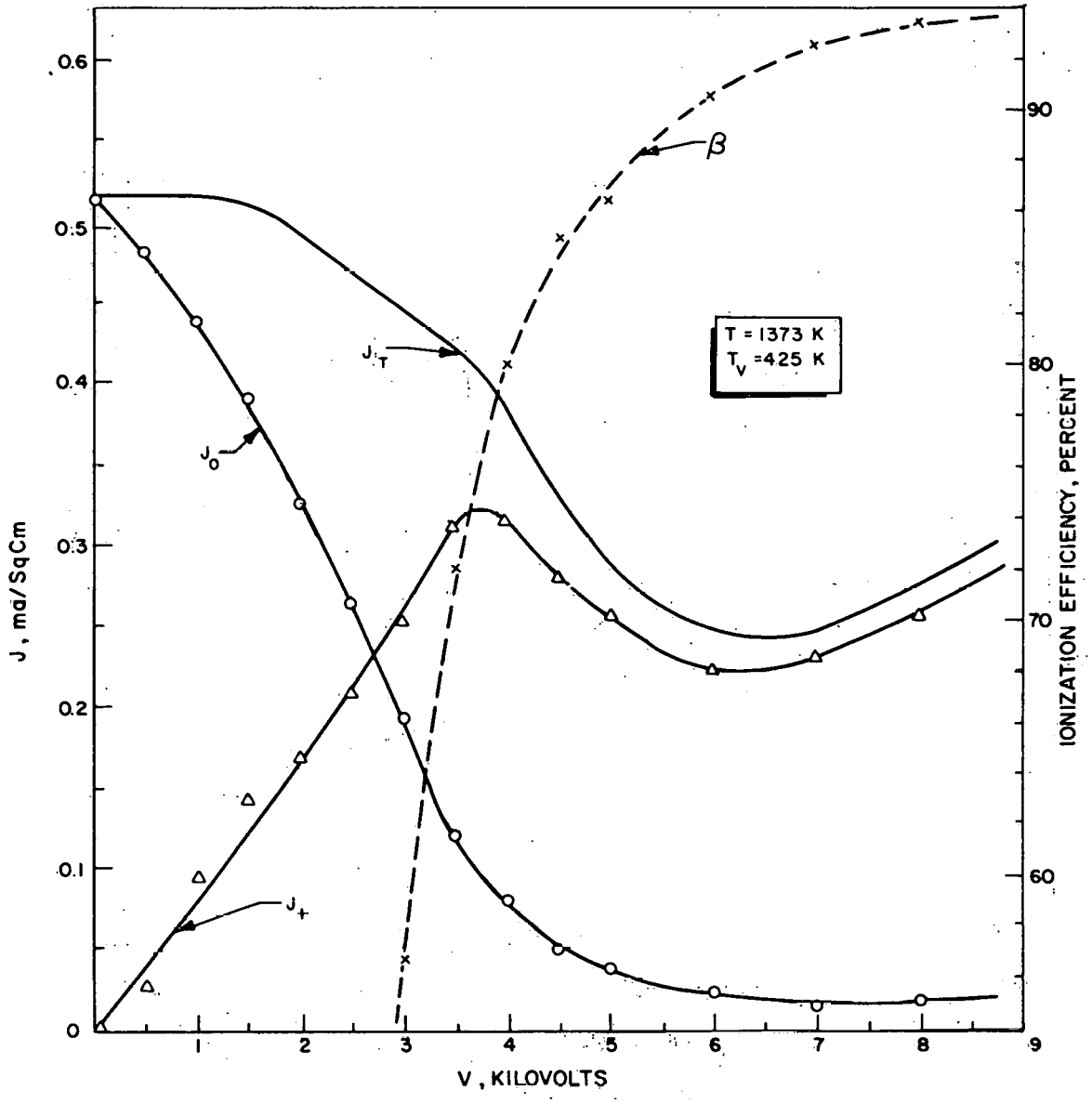

Figure 32. Particle Fluxes and Ionization Efficiency vs V for 44- to 74-Micron Ionizer

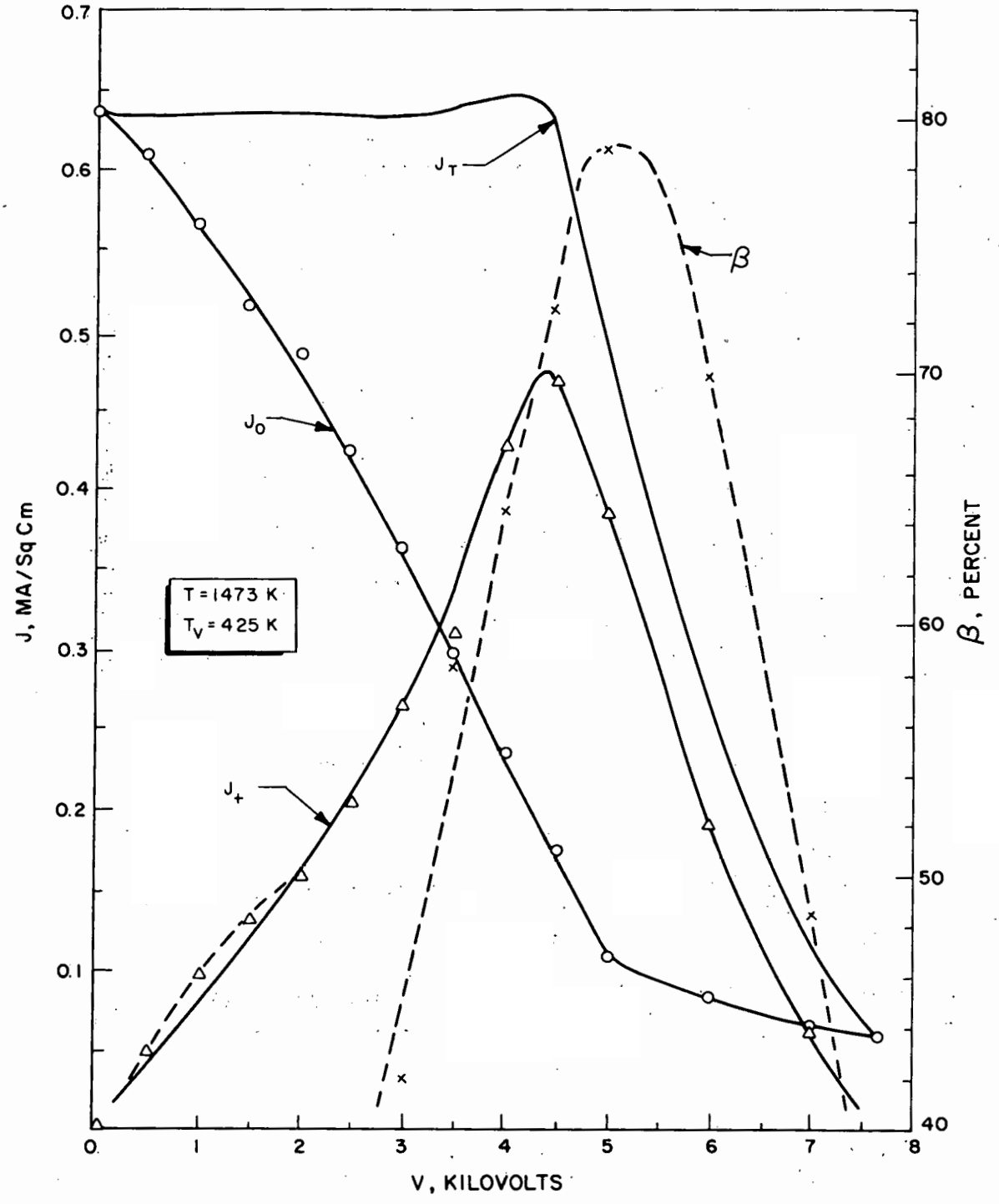

Figure 33. Particle Fluxes and Ionization Efficiency vs V for 44- to 74-Micron Ionizer

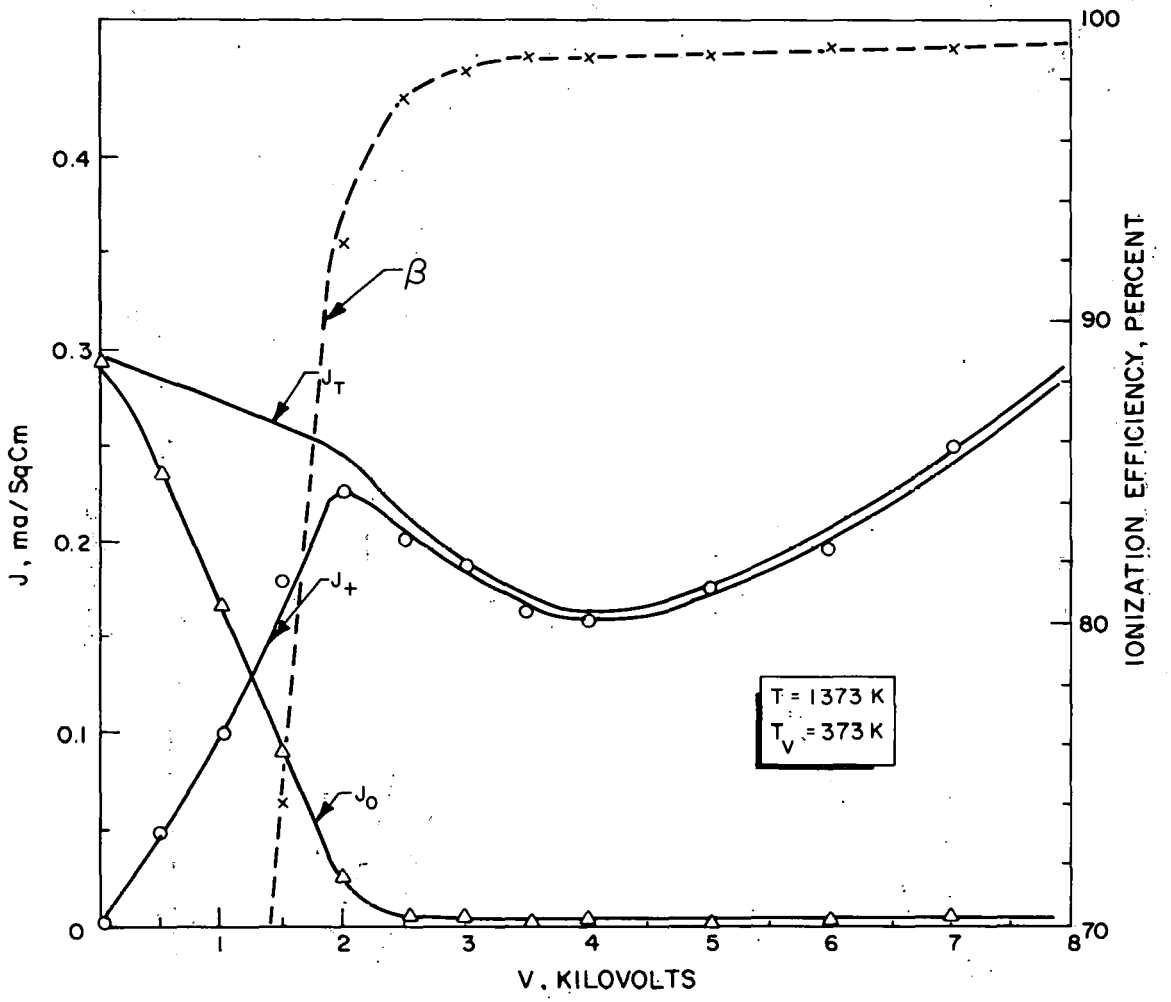

Figure 34. Particle Fluxes and Ionization Efficiency vs V for 44- to 74-Micron Ionizer

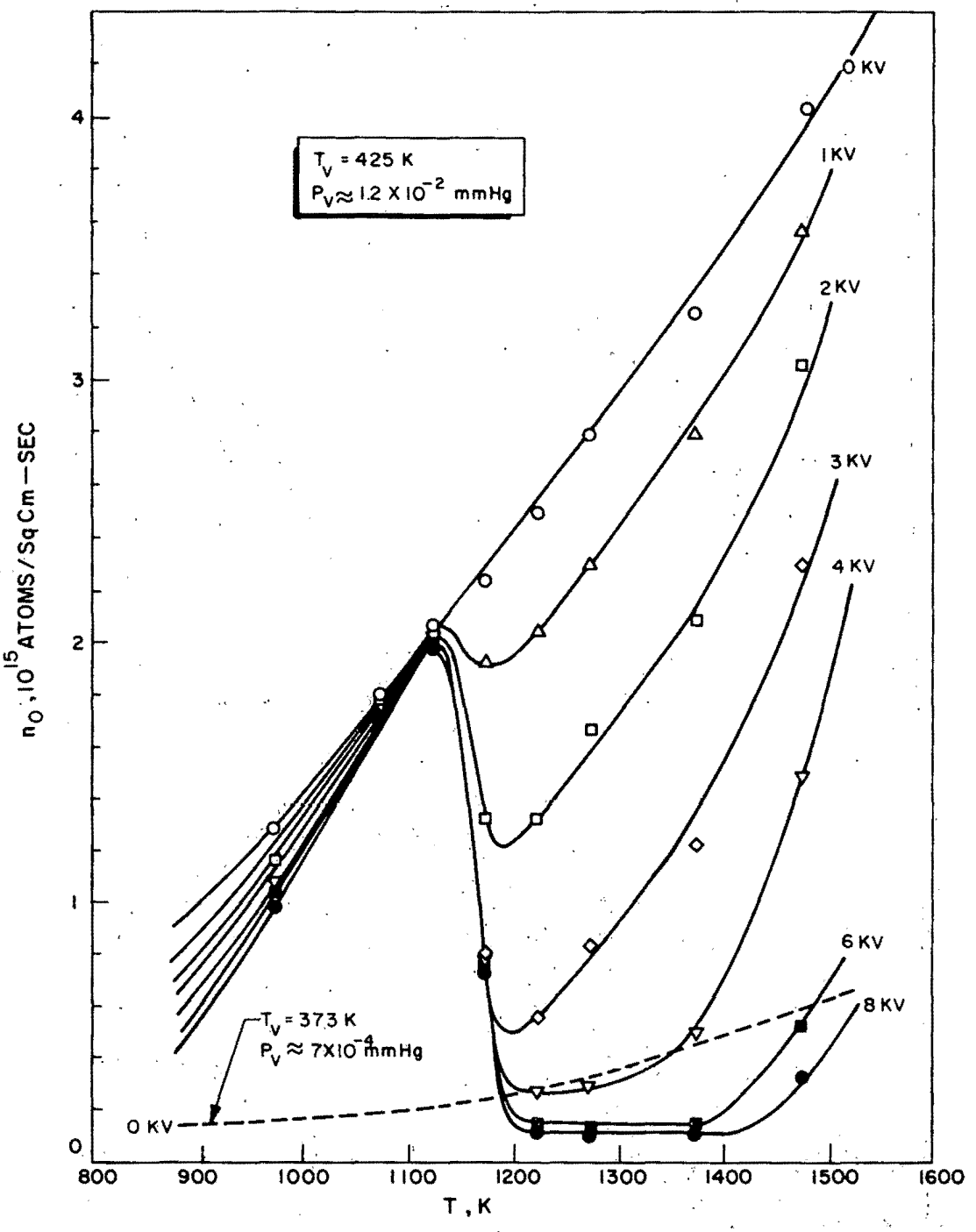

Figure 35. Neutral Flux vs Ionizer Temperature for Various Accelerating Voltages for 44- to 74-Micron Ionizer

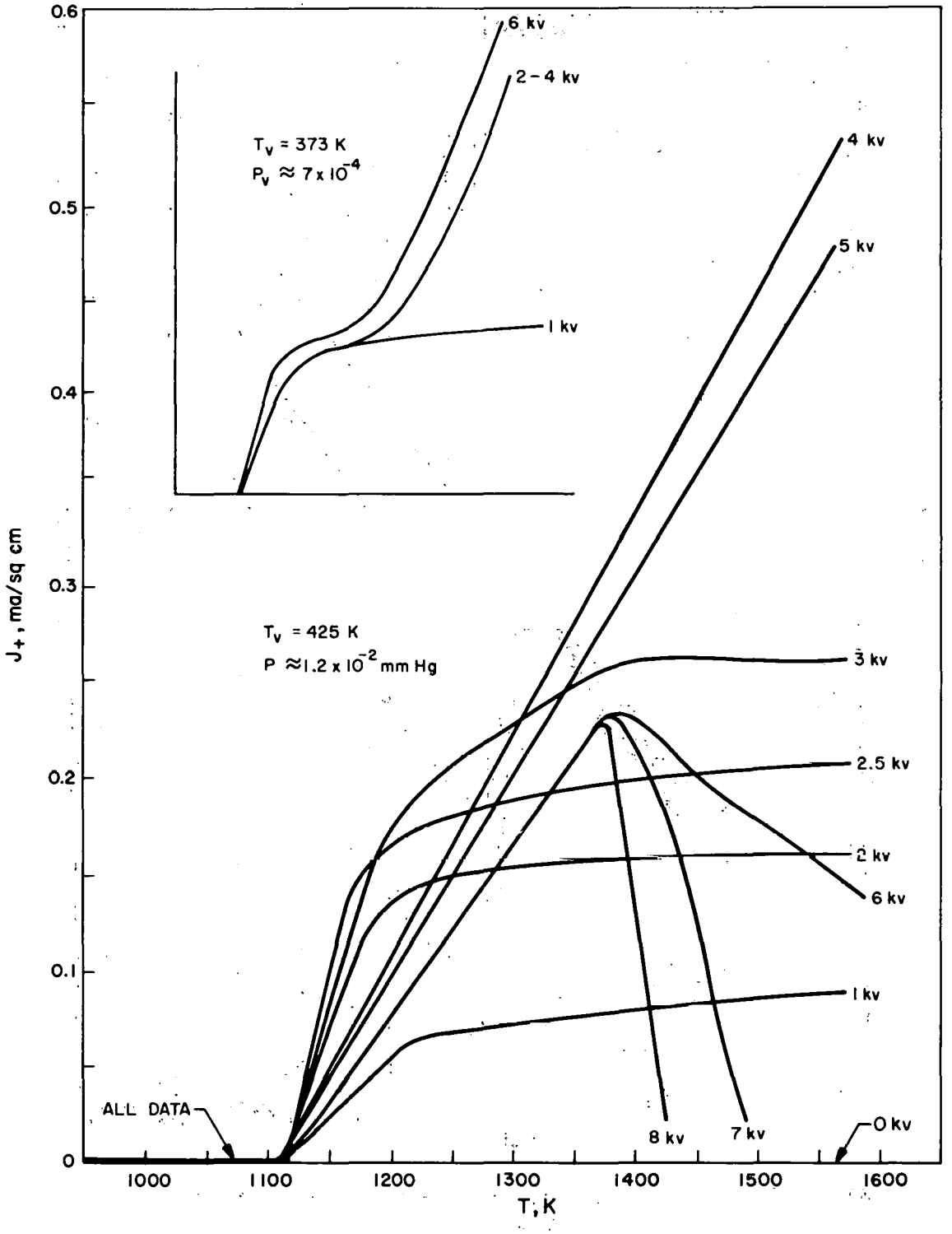

Figure 36. Ion Current Density vs Ionizer Temperature for Various Accelerating Voltages for 44- to 74-Micron Ionizer

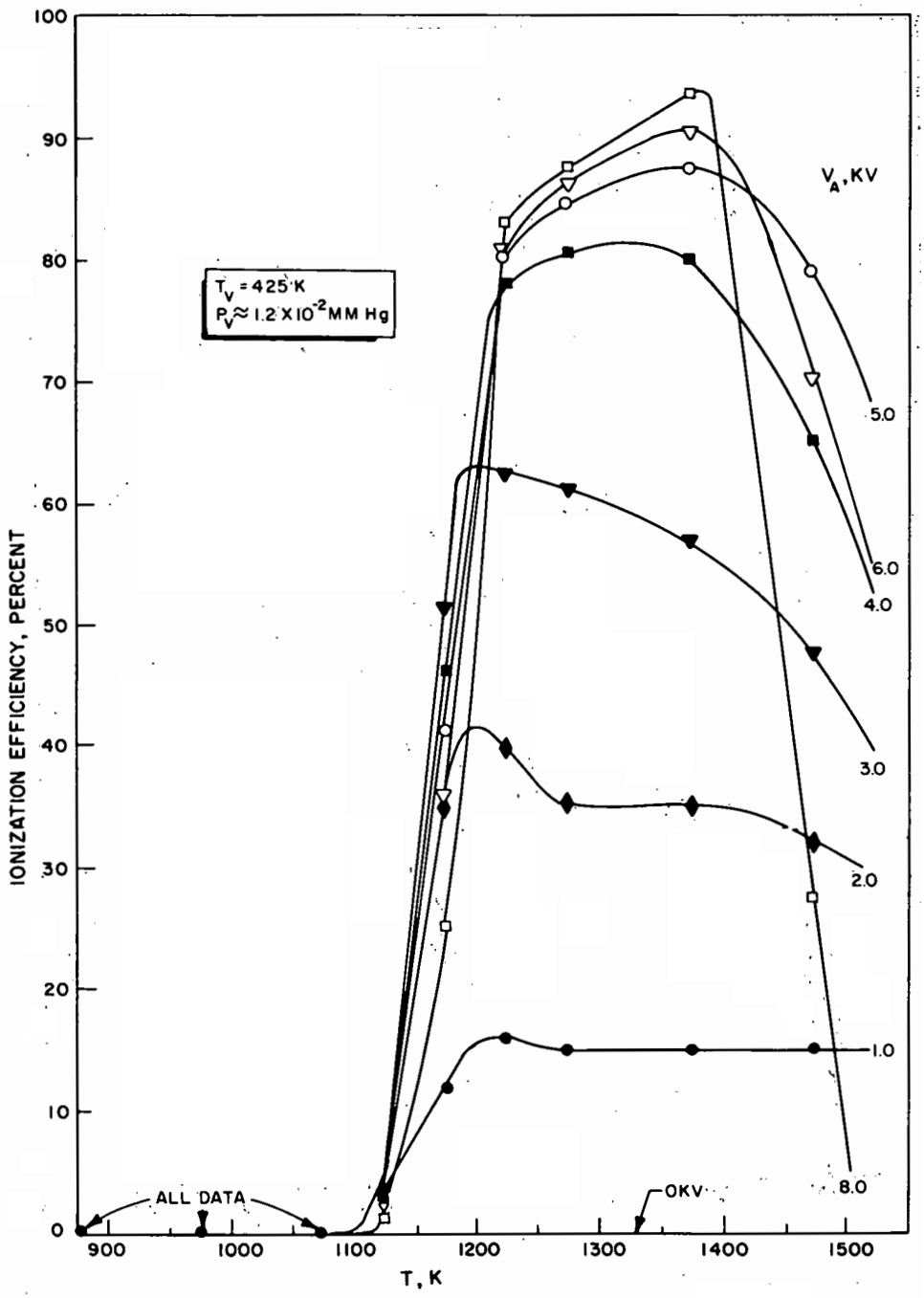

Figure 37. Ionization Efficiency vs Ionizer Temperature for Various Accelerating Voltages for 44- to 74-Micron Ionizer

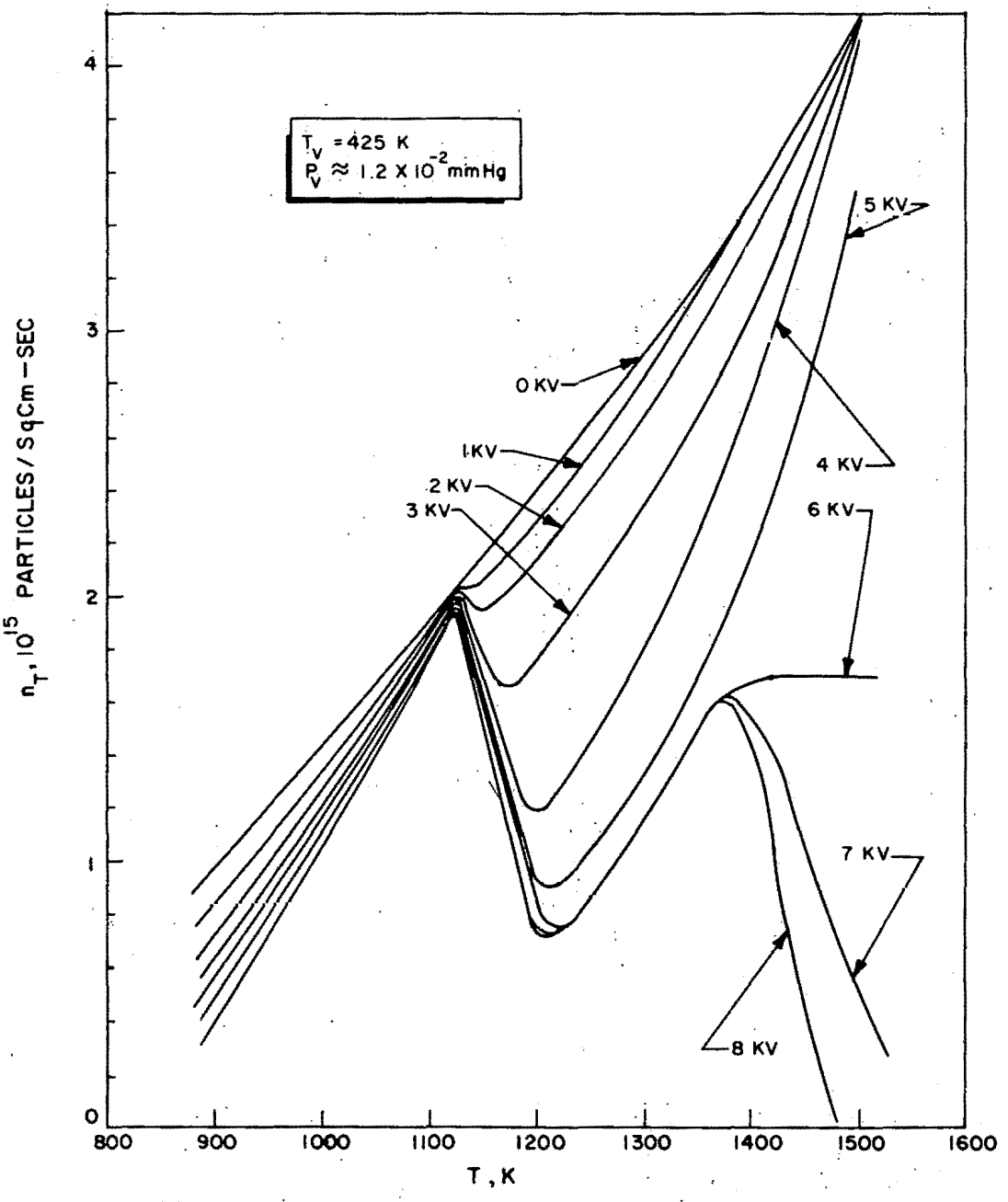

Figure 38. Total Particle Flux vs Ionizer Temperature for Various Accelerating Voltages for 44- to 74-Micron Ionizer

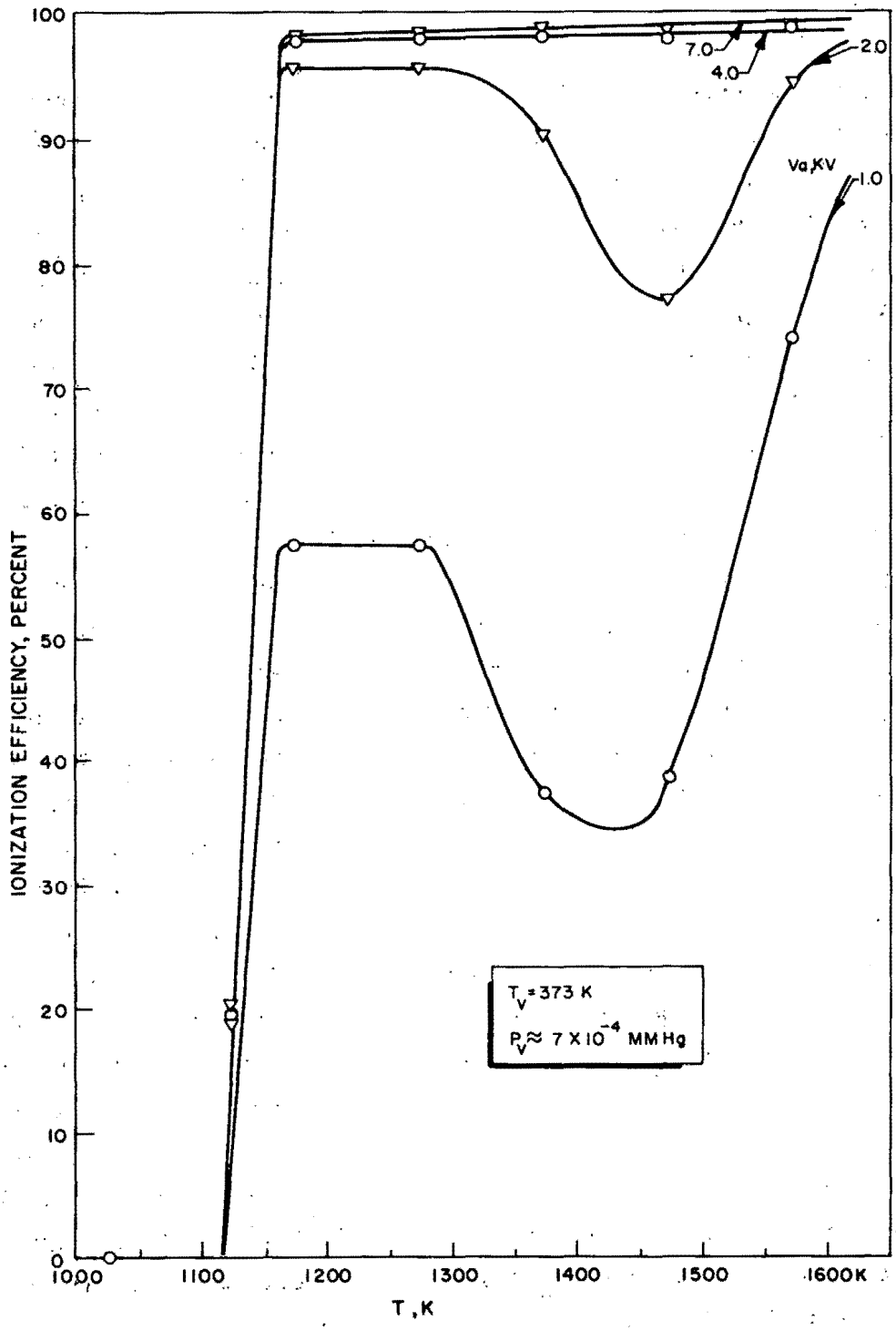

Figure 39. Ionization Efficiency vs Ionizer Temperature for Various Accelerating Voltages for 44- to 74-Micron Ionizer

The 1173 K data (Fig. 30) show the effect of low ionization efficiency because of being on the critical temperature slope. Figures 31 and 32 show the effects of higher ionizer temperatures (above the upper critical temperature). The shapes of the emission-limited regions in each case show a fairly constant ion current below T_{CU} (Fig. 30), a gradual decrease at 1273 K (Fig. 31), and a decrease followed by a rise at 1373 K. These shapes were commonly observed for all ionizers and can be compared to those of Fig. 9 for the 0.9-micron, Fig. 8 for the 12- to 18-micron, and Fig. 24 for the 5-micron ionizer. All of these curves show that J_T decrease in general with E, an observation unique to this largest-powder-size ionizer. The ionization efficiencies are also lower than for most other ionizers at comparable vapor pressures. This effect is not observed for the lower vapor pressure case (Fig. 39). It is concluded that the ionization efficiency for an ionizer of this large size powder will decrease even further with higher flowrates (vapor pressure). Figure 33 shows the unexpected effect at 1473 K where the ion current drops to essentially zero at 7.5 kv after having risen on the space-charge-limited curve to about 1/2 ma/sq cm at about 4.5 kv. The total flux drops to a low value, all of which is neutrals resulting in an ionization efficiency of essentially zero. This effect did not occur at the lower vapor pressure. The variation of the emitted neutral flux with ionizer temperature and the effect of increasing ion accelerating voltage are seen in Fig. 35 . The curve for V = 0 is just the cesium flowrate through the porous ionizer in the absence of any electric field and ion emission. The form of the curve is consistent with the arguments of section 5.6 and Eq. 37. The corresponding curve for the low vapor pressure case is shown as a dashed line in Fig. 29. The critical temperature also is evidenced in this type of plot. Figure 35 shows that for increasing V, n_o dips lower but eventually rises again somewhat more sharply than n_o at V = 0. In the 6-, 7-, and 8-kv cases, n_o reaches a minimum where it remains until some value of T, above which it increases as before. Apparently, the value of n_o and hence of β could be kept low at higher T by increasing the voltage still further.

Figure 36 shows corresponding plots of J_+ vs T at fixed values of V. For values of V less than the emission-limited voltage, the curves have the characteristic form observed for filament ionizers for which the maximum value of J_+ is fixed by the incident cesium flux (P_V) and is independent of T and V. This is not the case for porous ionizers; the flowrate is a function of both T and V (E), in addition to P_V.

Thus the curves for V > V (EL) continue to rise (n_o is also rising) almost linearly with T as seen for the 4- and 5-kv curves in Fig. 36. Up to this point, all such plots are similar for all of the ionizers studied in this work. However, for the 44- to 74-micron ionizer only, the forms of the 6-, 7-, and 8-kv curves of Fig. 36 were observed. All drop with increasing severity with V above about 1370 K. Corresponding plots for the low vapor pressure data which do not exhibit this effect and have the shape of the similar curves for the other ionizers are shown in the insert of Fig. 36. These curves are at constant V. If the value of J_+ at the space-charge, emission-limited knee is plotted vs T, a curve with a different shape is obtained, as seen in Fig. 29, which fits the form of Eq. 50.

The variations of the ionization efficiency with T at constant V are shown in Fig. 37. The effects of the critical temperature are again seen. The effects of both n_o and J_+ at high V and high T are combined in the effects of β.

If the curves for n_o and J_+ are added, a curve which shows the variation of the total flow of cesium through the ionizer with T and at various values of V results. This has been done in Fig. 38 for the 44- to 74-micron ionizer. For V up to 2 kv, the curves vary little from n_o at V = 0. From 2 to 5 kv, a decrease in total flux occurs as ion emission begins but recovery eventually ensues. For V = 6, 7, and 8 kv, a bimodal shape (unique to this ionizer) is exhibited.

THIS PAGE

WAS INTENTIONALLY

LEFT BLANK

6. REFERENCES

1. Hubach, R. A. and G. D. Seele: "Design of an Ion Rocket Research Device," ASD Technical Report 61-320, 1961.

2. Hubach, R. A. and G. D. Seele: "Properties of Porous Tungsten and Ionization of Cesium," American Rocket Society Paper No. 1780, 1961.

3. Adzumi, H.: "Flow of Gases Through a Porous Wall," Bulletin of the Chemical Society of Japan, Vol. 12, 1937, 304.

4. Kozeny, J.: Sitzungsberiche der Akademie der Wissenschaften in Wein, Vol. 136, 1927, 271.

5. Deryagin, B. V. et. al.: "Determination of the Specific Surface of Powders Used in the Production of Hard Alloys," Tsvethyye Metally, Vol. 11, 1959, 55.

6. Kraus, G., J. W. Ross, and L. A. Girifalco: "Surface Area Analysis by Means of Gas Flow Methods," Journal of Physical Chemistry, Vol. 57, 1953, 330.

7. Taylor, J. B. and I. Langmuir: Physical Review, Vol. 44, 1933, 423.

8. Wilson, R. G.: "Surface Ionization with Porous Ionizers," to be published.

9. Husmann, O. K.: "Experimental Evaluation of Porous Materials for Surface Ionization of Cesium and Potassium," American Rocket Society Paper No. 2359, 1962.

10. Shelton, H.: "Experiments on Atom and Ion Emission From Porous Tungsten," American Rocket Society Paper No. 2360, 1962.

11. Taylor, L. H. and H. H. Todd: "Ionizer Development and Surface Physics Studies," Interim Summary Report, Contract NAS8-1537, Electro-Optical Systems Report 1660-IR-1

12. Zandberg, E. Ya and N. I. Ionov: Soviet Physics Uspehki, Vol. 67 (2), 1959, 255.

13. Zandberg, E. Ya: J. Tech. Phys. (U.S.S.R.), Vol. 28, 1958, 2434, Soviet Physics "Technical Physics," 28 (3), 1958, 2233.

14. Zandberg, E. Ya: J. Tech. Phys. (U.S.S.R.), Vol. 27, 1957, 2583, Soviet Physics "Technical Physics," Vol. 27 (2), 1957, 2399.

15. Zandberg, E. Ya and N. I. Ionov: J. Tech. Phys. (U.S.S.R.), Vol. 28, 1958, 2444, Soviet Physics, "Technical Physics," Vol. 28 (3), 1958, 2243.

16. Morgulis, N. D.: Physics Z. Sowjetunion, Vol. 5, 1934, 221.

17. Copley, M. J. and T. E. Phipps: Physical Review, Vol. 48, 1935, 960.

18. Dobretsov, L. N.: Jour. Expt'l e Teoret. Phys. (U.S.S.R.), Vol. 6, 1936, 552.

19. Langmuir, I. and K. Blodgett: "Currents Limited by Space Charge Between Concentric Spheres," Physical Review, Vol. 24, 1924, 29.

20. Langmuir, I. and K. Blodgett: "Currents Limited by Space Charge Between Coaxial Cylinders," Physical Review, Vol. 22, 1923, 347-356.

21. Wilson, R. G., J. F. Hon, and F. Hai: "Experimental and Analytical Research on Ion Electrostatic Accelerating Techniques," ASD-TDR-62-164, AF33(616)-7622, Rocketdyne Report, R-3281, 1962.

22. Carman, P. C.: Flow of Gases Through Porous Media, Butterworth Scientific Publications, Academic Press, Inc., N. Y. 10, N. Y.

23. Taylor, J. W.: "Wetting by Liquid Metals," Progress in Nuclear Energy (AERE), Vol. 2, 1959, 398-416.

24. Proceedings of an International Conference on the Structure and Properties of Thin Films, Ed. C. A. Neugebauer, J. B. Newkirk, and D. A. Vermilyea; John Wiley and Sons, Inc., New York, N. Y., September 1959.

25. Frenkel, J.: Kinetic Theory of Liquids, Oxford University Press, 1947.

26. Knudsen, M.: Ann. Physik, Vol. 28, 1909, 75 and 999; Vol. 38, 1911, 389.

27. Weatherford, W. D., Jr., T. C. Tyler, and P. M. Ku: "Properties of Inorganic Energy Conversion and Heat Transfer Fluids for Space Applications," W.A.D.D. Technical Report 61-96, 1961.

28. Kuskevics, G., R. C. Speiser, R. M. Worlock, and D. Zuccaro: "Ionization, Emission, and Collision Processes in the Cesium Ion Engine," American Rocket Society Paper No. 2364, 1962.

29. Becker, J. A.: Physical Review, Vol. 28, 1926, 341.

30. Alterthum, H., K. Krebs, and R. Rompe: Zeit. Physik, Vol. 92, Vol. 92, 1934, 1.

31. Zandberg, E. Ya.: J. Tech. Phys., (U.S.S.R.), Vol. 27, 1957, 2583.